Doctoral Dissertation

A Study on Estimating Electrical Characteristics of Wave Source and Its Applications Using Electromagnetic Information in Near-Field

(波源近傍の電磁界情報を用いた電気特性の推定とその応用に関する研究)

Graduate School of Engineering

Yokohama National University

Yoshiki Sugimoto

杉本　義喜

Abstract

The demand for electromagnetic wave applications such as wireless communication has remained unchanged, and in recent years it has shown a further diversification aspect. It is expected that the spread of applications using electromagnetic waves will not cease, and we hope that electromagnetic waves will be used in a way that we cannot predict in the future. In an application using electromagnetic waves, grasping antenna characteristics as a radiation source or a receiving point is extremely important to understanding the total characteristics of entire system. Therefore, we can say that the technique of accurately measuring and evaluating the radiation performance of the antenna that the essential part of the use of electromagnetic waves, is a required technologies unchanged since the olden days.

In recent years, riding the tide of the trend of IoT, antennas are beginning to be installed in every electronic device in our immediate vicinity. In the future it is expected that all the devices will perform wireless communication, thus it is considered that a larger quantity of antennas will be manufactured. It is easy to imagine that the usage environment of the device will be further versatile according to this social transformation. Simple reduction technique of the time required for evaluating the antenna performance by speed up the measurement itself is certainly required, also is required to estimate the characteristics assuming various environments as the evaluation method of the manufacturing antenna.

Techniques for measuring the radiation performance of an electromagnetics such as an antenna have been widely studied so far, in the measurement; it is also economically desirable that electromagnetic waves can be measured in a small space with minimum disturbance of from the outside. A technique called near-field measurement is very useful for such a request. This technique measures the electromagnetic field in the region called the near-field among the field regions classified according to the relationship between the physical size of the source and the operating frequency wavelength. It is possible to calculate electric characteristics in a form according to the request by applying numerical processing to the acquired electromagnetic field, and it can be expected to be applied in a wide range of applications. In this dissertation focusing on this point, we consider numerical processing on the electromagnetic field acquired in the near-field region and estimate the desired electric characteristics of the source.

Moreover, we introduce the equivalent field principle and inverse problem analysis of electromagnetic waves based on the electromagnetic field acquired by near-field measurement for this dissertation. In equivalent principle, assuming an equivalent closed surface on the measurement surface of the electromagnetic field, replace the electromagnetic field exists on the surface with an equivalent electromagnetic current. An electromagnetic field outside of the measurement surface can be calculated by solving the Maxwell equation assuming the existence of each equivalent source in

the free space. In addition, if we assume objects other than the estimation source in this calculation space, we can also estimate the electromagnetic field taking account of the influence by them. The electromagnetic field on an arbitrary position and environment is obtained based on the electromagnetic field in the near-field region using this theorem. Also, the source distribution of arbitrary shape inside the measurement region can be visualized by solving the inverse problem of the electromagnetic field. It is possible to remove radiated waves from unnecessary portions if we use that, to expect applications such as acquiring only necessary electromagnetic field components. In this dissertation, we aim that to establish an electromagnetic field measurement method assuming various applications and measurement environments, by a combination of these methods.

Chapter 2 describes the handling technique of the electromagnetic field by the equivalent source theorem and the reconstruction method of the wave source distribution from the measured electromagnetic field by the inverse problem. This chapter is the introduction of the numerical methods in this dissertation, we discuss in after this chapter based on the introduced techniques.

Chapter 3 proposes a fast far-field estimation method of electrically long antenna in compact measurement space. The presented method estimates far-field pattern on orthogonal cut plane from the linear equivalent electric current and circular current distribution. The equivalent electric current data is measured in reactive near-field region using a small loop probe. In the proposed method, the linear equivalent current distribution is extended by simple numerical extrapolation formula for improves the accuracy of estimated far-field of the broadside direction. In the horizontal plane, the far-field pattern is calculated from circular equivalent electric and magnetic distribution approximating equivalent magnetic current with equivalent electric current. We confirmed the validity of the proposed method from the numerical simulation and measurements results. The noteworthy contribution of this chapter is that the proposed method was achieved the fast far-field estimation method by reduction of measurement data dimension. The method allowed directivity measurement accurately in a small space measurement in about a few minutes.

Chapter 4 proposes a super-fast far-field measurement method for linear array antenna using short length near-field distribution. The proposed method corrects the radiation field from reconstructed partial source, regenerates the near-field distribution the same size as the AUT aperture. The linear array antenna with various distributions was taken up as an example of numerical analysis and the effectiveness of this method was shown. It is shown that the estimated maximum directivity in the vertical plane was achieved within 0.25 dB errors with respect to the reference value. Furthermore, we applied this method to the measured near-field data of the base station antenna. In the case of the measurement area is 3/4 of the AUT aperture size, the estimation error was achieved within 0.15 dB, and in addition, the case of 1/2, the error was achieved within 0.5 dB. The noteworthy contribution of this chapter is possible to measure the far-field in the vertical plane of the linear array antenna by near field measurement in a quite small space. The proposed method was

achieved the fast far-field estimation method by reduction of measurement area.

Chapter 5 proposes a method for inverse separation estimation of source distribution using two electromagnetic field distributions. In this method, we can reconstruct the wave source distribution unique to each surface by measuring the electromagnetic field distribution around the wave source in two directions, setting two surfaces of the inner boundary surface and the outer boundary surface and solving the inverse problem. This method is applied to wave source distribution on rectangular coordinate plane and spherical surface, and the effectiveness of this method is clarified by numerical analysis and actual measurement. It is expected to realizing stable measurement under outdoor environment by applicable the proposed method in future.

Chapter 6 proposes a method to compensate the measurement errors caused by misalignment of the probe and its jig; further, this chapter proposes a far-field estimation method by phase resurrection that incorporates the compensation techniques. We have classified the cause of the positioning errors in measurement as random errors occurring at each measurement points due to minute misalignments of the probe; also we have classified depth errors occurring at each measurement surfaces as errors caused by improper setting of the probe jig. The random positioning error is eliminated by adding a low-pass filter in wavenumber space, and the depth positioning error is iteratively compensated based on the relative residual obtained in each plane. The validity of the proposed method is demonstrated by estimating the far-field patterns using the results from numerical simulation and is also demonstrated using measurements of probe-positioning errors. The noteworthy contribution of this chapter is a method that can self-correct errors that cannot avoid in near field measurements.

Chapter 7 proposes a far-field estimation method when an antenna is placed above the earth. The proposed method estimates far-field using current distribution on the antenna surface that is reconstructed from hemispherical near-field information. Matrix equation used in this paper becomes ill-posed problem by the partial missing of measurement area. In order to solve this problem, the proposed method regenerates the near-field in the missing area from the reconstructed source distribution, and to reconstructs the source again using regenerated near-field. Far-field of the antenna above the earth is estimated by assuming the image current below the earth derived from reconstructed electric current distribution on the antenna surface. From numerical calculations and experiments, the paper shows that the proposed method can accurately estimate far-field pattern above the earth from hemispherical near-field measured in the free space. The noteworthy of this chapter is that brought a method to accurately estimate the behavior of the antenna in a practical environment.

Chapter 8 is a summary and conclusion of this dissertation.

Chapters 3 and 4 mainly describe a method of shortening the measurement time directly by reducing the measurement amount of the near-field measurement. Chapters 5 and 6 mention a

method for removing numerical disturbance in an environment in which strong interference waves are incident and a solution to reduce the measurement information error peculiar to a method for acquiring plural measurement planes. Section 7 shows a method to improve estimation accuracy of source reconstruction in measurement environment with large physical restriction and estimation method of radiation performance considering practical use environment. Throughout this dissertation, we aggregate a solution to the disadvantage of measurement environment caused by various factors and estimation method of antenna performance assuming various usage environments.

Contents

1 Introduction

1.1 Background

Although 150 years had passed since prediction of electromagnetic waves by Maxwell [1], the mankind desire for utilization of electromagnetic waves has been continues to develop rather than decline. In response to above, the development of applied technology of electromagnetic waves has been remarkable, and electromagnetic waves are used for various applications in wide-range fields. Antennas that serve as entrances and exits of electromagnetic waves are used in a wide range of environments, and in recent years the IoT is introduced familiar and also communications in very close area of the human body have been drawing attention. We can easily imagine that a massive amount of antennas will be manufactured in the near future and will be installed in all kinds of equipment.

It is necessary to test absolutely the performance of the manufactured antennas before use/implementing, because antennas are not the just making fun toys. Antennas which are an interface between a space and a high-frequency circuit are evaluation subjects for which radiation characteristics are particularly important. As a method of measurement the electromagnetic field, it is desirable to be able to measure and evaluate the performance of the antenna as accurately as possible; in addition it is also required to output a stable test result under any circumstances. When a massive amount of antennas are to be manufactured, a high-speed method to measure electromagnetic field and evaluate its performance is indispensable. Furthermore, the measurement system often cannot build the practical use environment, thus it is also required to estimate the operating condition of the antenna under different environments using the measurement field as a reference.

An issue to be noted in evaluating the radiation performance of the antenna is the case where the physical size is very large (electrically large) as compared with the wavelength of the measurement frequency. The radiation characteristics in the region generally called the far-field area are the subject of discussion, when characterizing the radiation performance of the antenna. A criteria of the far-field region is generally defined as a region in which the measurement distance L from the AUT (Antenna Under Test) is $L>2D^2/\lambda$ when the physical aperture size of the measured antenna is D and the wavelength of the measurement frequency is λ [2]. The radiation electromagnetic field from the source in region far from this criterion is assumed to be the plane wave, and the electromagnetic field pattern does not change depending on the distance between the source and the observation point. The open site measurement technique is often chosen when measuring an electrically large aperture antenna, because it is difficult to satisfy the far-field condition indoors [3]. A far-field in a single plane can be easily obtained simply by rotating the AUT thus the far-field of the cut plane can be acquired at high speed, if a sufficient measurement distance

is secured. On the other hand, the spatially required cost is enormous and measurement results are influenced by the weather, we cannot help but say that the stable measuring technique. In addition, it is essential the scattering wave reduction, since reflected waves from the earth arrive at the receiving antenna. This problem can be solved to some extent by devising measures such as slant range measurement [4], however it is necessary to lift the AUT to a higher place as the measuring distance becomes longer, which is not economic. The compact range [5] is a method to solve such a problem, and it is possible to measure in an anechoic chamber. In this method, a reflection mirror is placed near the AUT and the reflected wave from the reflection mirror is measured with a probe. The far-field criteria is pseudo satisfied by forcing the reflected wave to be the plane wave by the reflecting mirror, and the far-field pattern can be estimated in a physical small space. However, the reflecting mirror is big as to occupy the anechoic chamber; the technique is inferior from the viewpoint of economical cost such as hindering the use of anechoic chamber in other applications.

1.2 Brief Overview of Near-Field Measurements

We describe near-field measurement techniques and its characteristic. The near field region of the antenna to be measured is defined by the electrical size determined by the physical size of the AUT and the measurement frequency. As described above, when the aperture diameter of the AUT is D and the wavelength of the measurement frequency is λ. The region where the measurement distance L from the AUT is $L>2D^2/\lambda$ is defined as a far field and the region of $L\leqq 2D^2/\lambda$ is defined as a near-field [2]. In the near-field measurements, electromagnetic field is measured in the near-field region, and characterizing the AUT performance based on the measured information [6]. The near-field measurements are almost performed in an anechoic chamber, because the output characteristics are obtained by numerical processing based on the electromagnetic field acquired in a small scale measurement area. The measurement operator does not need to secure the huge measurement space, and does not have to worry about disturbances by weather and interference waves. It is unnecessary to apply for a radio license for measurement and also there is no possibility that the measurement device will occupy the anechoic chamber. Thus, near-field measurements have various advantages.

In the near-field measurements fundamentally, the electromagnetic field is acquired by move a measurement probe against the AUT, there are several types of scanning methods of the probe as shown Figure 1.1. It can be classified into plane scan [7], cylinder scan [8], and spherical scan [9] largely depending on the scanning method, and there is not much to be adopted, but there are also polar planar scan [10], spiral spherical scan [11], and cube-shaped scan including AUT [12], [13]. In this dissertation, the planar scan, the cylindrical scan and the spherical scan widely used in general are taken as measurement systems of the near-field. The scanning method of the probe is basically selected according to the radiation characteristics presumed from the shape of AUT, because the

degree of convergence of the electromagnetic energy of the source is proportional to the size of the AUT projected to the observation direction.

Almost radiation energy concentrates to normal direction of aperture plane when the AUT has 2 dimensional aperture, the planar scan technique can be recover most of its radiant energy. The planar scanning is suitable to measure pencil beam antennas. On the contrary, it is inappropriate for measurement of a low gain antenna that radiates electric power in all directions. In the planar measurement, the probe is scanned with two axes and the near-field is measured while the position of AUT is completely fixed. The planar scanning has an advantage that is easy to place the AUT, and the state of the cable connected to AUT does not change during the measurement and can be measured stably.

The cylindrical measurements are often adopted for an antenna that has aperture in one-dimensional direction such as fan beam antenna. In the cylindrical measurements, it is common that a jig has an operation axis in the rotation direction and the probe has the linear operation axis. It is sometimes referred as a measurement method that combines the advantages and disadvantages of planar scanning and spherical scanning. In addition it is possible to make the small measurement system relative to the physical scale of AUT, suitable for scale-down of the measurement setup. In planar and cylinder scanning, the truncation error becomes a problem since finite truncation of the measurement area necessarily occurs due to the restrictions on facilities [14]. Therefore, the measurement region must be set while always considering the radiation characteristics of AUT.

The spherical scanning has less electromagnetic field leakage, and accurate measurement such as radiation efficiency is possible because it can be measure the full-spherical near-field including the AUT. It is common to acquire electromagnetic field by fixing the probe and rotating the AUT. A measuring system may be constructed in which the AUT is placed on a jig having a rotation axis in the azimuth direction and the probe is scanned in the zenith angle direction in the case of measure a physically large AUT. Also there is a measurement system for measure a physically small scale AUT in which the AUT is fixed and the probe is scanned by the robot arm [15]. It can be said that it is the most excellent measurement system if it ignores the physical and economical cost not only is it suitable for measurement of low gain antennas but also high gain antennas can be measured without problems. However to construct the spherical measurement system is not easy. It is necessary to pay attention to wiring of the cable and placement stability of the AUT, and also there is a difficulty in the arrangement of the AUT since it is necessary to rotate the AUT complicatedly. In addition, only hemispherical near-field can be acquired, when the AUT is physically big because the AUT cannot be rotate. The computational cost when performing far-field transformation from the measured near-field is also enormous compared to the planar measurement system and the cylindrical measurement system.

There are various advantages and disadvantages in each scanning system of the near-field

measurement as described above, it is essential to form an appropriate measurement setup according to the measurement environment and characteristics to be acquired. it is necessary to supplement the lack of measurement information by numerical processing, when an optimum measurement system cannot be constructed due to some circumstances such as economic cost or measurement space.

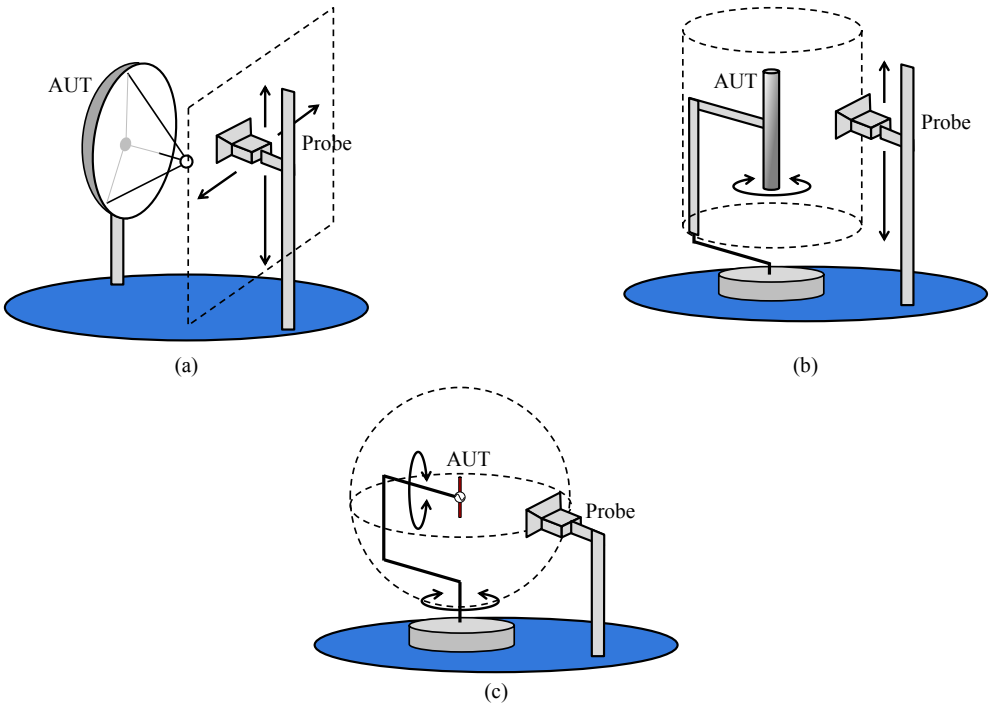

Figure 1.1: Various measurement domains in near-field measurement. (a) presents the planar scanning domain, the probe can be scan in orthogonal directions in general planar domain. (b) presents the cylindrical scanning domain. In general cylindrical method can rotate the AUT and the probe moves in the longitudinal direction. (c) presents the spherical scanning domain. The AUT rotates in the orthogonal angle direction is simple configuration.

1.3 Objectives

As mentioned above, the environment in which the electromagnetic field measurement is performed, the required estimation result, and the application are various. In some cases, measurement system does not satisfy the generally required measurement requirements. Thus, measurement operator having to estimate performance based on insufficient electromagnetic field information. In order to cope such situation, it is necessary to flexibly convert the measuring electromagnetic field and to apply appropriate numerical processing for obtain desired information. In this dissertation, we focus on the near-field measurement of electromagnetic source, and we aim to realize various required

electric performance measurements by applying forward and inverse spatiotemporal transformation processing of electromagnetic.

1.4 Organization of the Dissertation

This dissertation is organized by 8 chapters as shown in Figure 1.2. In this chapter, we introduced the background surrounding measurement of electromagnetic field and the point of problem.

Chapter 2 describes the handling of the electromagnetic field in the free space by the equivalent source theorem and the reconstruction method of the wave source distribution from the measured electromagnetic field by the inverse problem.

Chapter 3 proposes a fast far-field estimation method of electrically long antenna in compact measurement space. The presented method estimates far-field pattern on orthogonal cut plane from the linear equivalent electric current and circular current distribution. The equivalent electric current data is measured in reactive near-field region using a small loop probe. In the proposed method, the linear equivalent current distribution is extended by simple numerical extrapolation formula for improves the accuracy of estimated far-field of the broadside direction. In the horizontal plane, the far-field pattern is calculated from circular equivalent electric and magnetic distribution approximating equivalent magnetic current with equivalent electric current. We confirmed the validity of the proposed method from the numerical simulation and measurements results. The method allows directivity measurement accurately in a small space measurement in about a few minutes.

Chapter 4 proposes a super-fast estimation method of radiation performance for electrically long antenna. In this chapter, the measurement area is considered as shorter than the aperture size of an AUT. The proposed method in this chapter based on radiation field from partial equivalent source distribution. The partial source is obtained by solve inverse problem, near-field distribution the same size of the AUT aperture is regenerated by compensate the partial source. Near-field distribution under unmeasured area is acquired virtually. We confirm that the developed work is effectively for measurement of various kinds of linear array antennas and from numerical simulation, and from the measured electric field distribution, the presented method is suitable as an ultrahigh speed measurement method for the base station antenna for mobile communications.

Chapter 5 proposes a method for inverse separation estimation of source distribution using two electromagnetic field distributions. In this method, we can reconstruct the wave source distribution unique to each surface by measuring the electromagnetic field distribution around the wave source in two directions, setting two surfaces of the inner boundary surface and the outer boundary surface and solving the inverse problem. This method is applied to wave source distribution on rectangular coordinate plane and spherical surface, and the effectiveness of this method is clarified by numerical analysis and actual measurement.

Chapter 6 proposes a method to compensate the measurement errors caused by misalignment of the probe and its jig; further, this chapter proposes a far-field estimation method by phase resurrection that incorporates the compensation techniques. We have classified the cause of the positioning errors in measurement as random errors occurring at each measurement points due to minute misalignments of the probe; also we have classified depth errors occurring at each measurement surfaces as errors caused by improper setting of the probe jig. The random positioning error is eliminated by adding a low-pass filter in wavenumber space, and the depth positioning error is iteratively compensated based on the relative residual obtained in each plane. The validity of the proposed method is demonstrated by estimating the far-field patterns using the results from numerical simulation and is also demonstrated using measurements of probe-positioning errors.

Chapter 7 proposes a far-field estimation method when an antenna is placed above the earth. The proposed method estimates far-field using current distribution on the antenna surface that is reconstructed from hemispherical near-field information. Matrix equation used in this paper becomes ill-posed problem by the partial missing of measurement area. In order to solve this problem, the proposed method regenerates the near-field in the missing area from the reconstructed source distribution, and to reconstructs the source again using regenerated near-field. Far-field of the antenna above the earth is estimated by assuming the image current below the earth derived from reconstructed electric current distribution on the antenna surface. From numerical calculations and experiments, the paper shows that the proposed method can accurately estimate far-field pattern above the earth from hemispherical near-field measured in the free space.

Chapter 8 is a summary and conclusion of this dissertation.

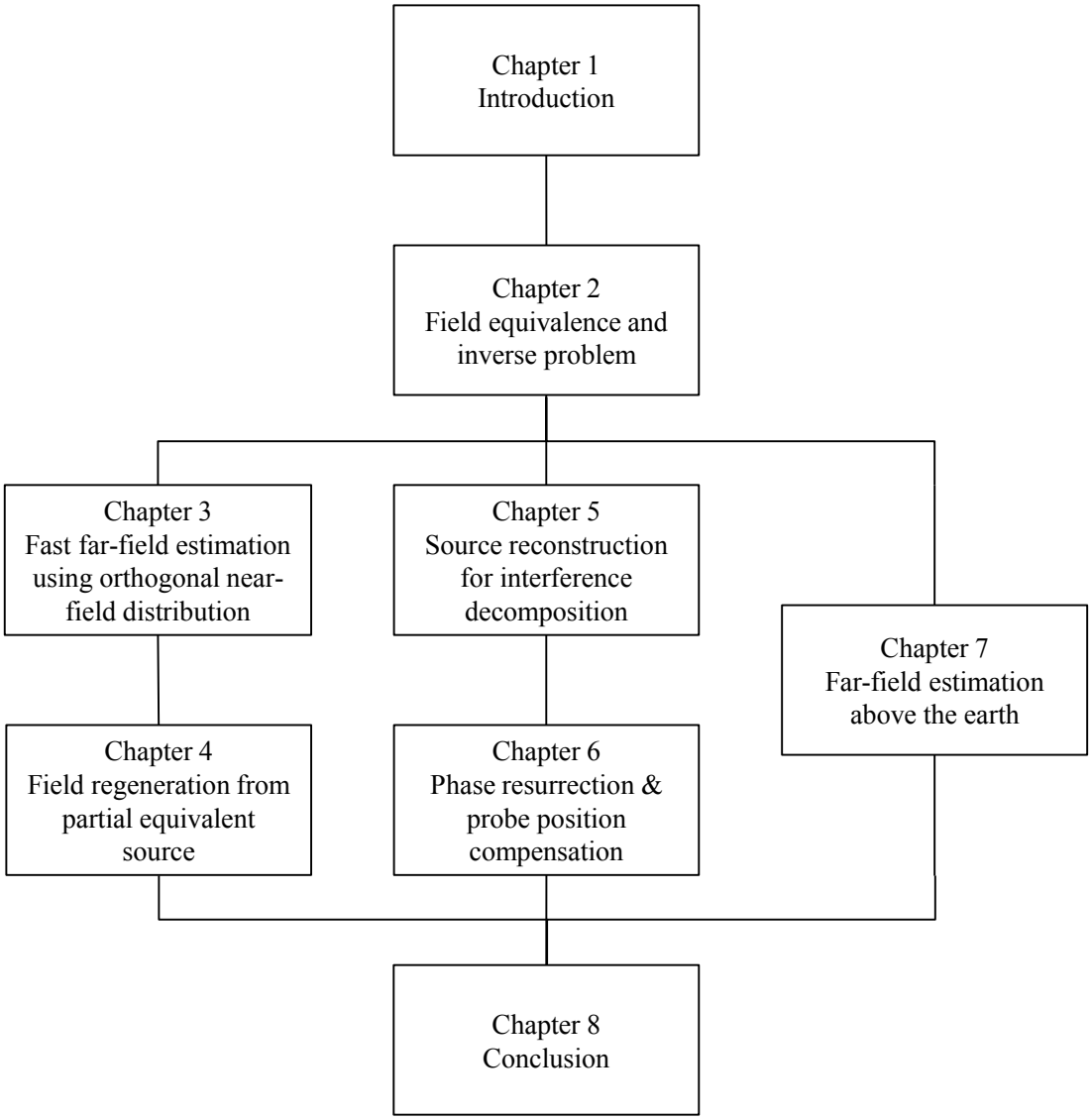

Figure 1.2: Overview of the dissertation.

Reference

[1] J. C. Maxwell, "A dynamical theory of the electromagnetic field," *Phis. Trans. R. Soc. London,* 155, pp. 459-512, Jan. 1865.

[2] D. Slater, *Near-field antenna measurements*, Artech House, 1991.

[3] F. J. C. Fácila, S. Burgos, F. Martin and M. S. Casteñer, "New reflection suppression method in antenna measurement systems based on diagnostic techniques," *IEEE Trans., Antennas and Propag*., vol. 59, no. 3, pp. 941-949, March 2011.

[4] P. W. Arnold, "The slant antenna range," *IEEE Trans., Antennas and Propag*., vol. AP-14, no. 5, pp. 658-659, Sept. 1966.

[5] M. W. Shields and A. J. Fenn, "A new compact range facility for antenna and radar target measurements," *Lincoln Lab. Journal*, vol. 16, no. 2, 2007.

[6] A. D. Yaghjian, "An overview of near-field antenna measurements," *IEEE Trans., Antennas and Propag*., vol. AP-34, no. 1, pp. 30-45, Jan. 1986.

[7] T. P. Sakar and A. Taaghol, "Near-field to near/far-field transformation for arbitrary near-field geometry utilizing an equivalent electric current and MoM," *IEEE Trans., Antennas and Propag*., vol. 47, no. 3, pp. 566-573. March 1999.

[8] J. A. Hansen, "On cylindrical near-field scanning techniques," *IEEE Trans., Antennas and Propag*., vol. AP-28, no. 2, pp. 231-234, March 1980.

[9] F. D' Agostino, F. Ferrara, C. Gennarelli, R. Guerriero and M. Migliozzi, "Spherical near-field-far-field transformation for quasi-planar antennas from irregularly spaced data," *Journal of Electromagn. Analysis and Applications*, no. 4, pp. 147-155, Apr. 2012.

[10] S. Blanchm R. G. Yaccarino, J. Romeu and Y. R. Samii, "Near-field for far-field transformation of bi-polar measurements by equivalent magnetic current approach," *Prop. 1996 IEEE International Symposium on Antennas and Propag. (AP-S)*, July 1996.

[11] F. D' Agostino, F. Ferrara, J. A. Fordham, Cl Gennarelli, R. Guerriero and M. Migliozzi "An experimental validation of the near-field – far-field transformation with spherical spiral scan," *IEEE Antennas and Propag., Magazine*, vol. 55, no. 3, pp. 228-235, June 2013.

[12] X. Gao, J. Fan, Y. Zhang, H. Kajbaf and D. Pommerenke, "Far-field prediction using only magnetic near-field scanning for EMI test," *IEEE Trans., Electromag. Compatibility*, vol. 56, no. 6, pp. 1335-1343, Dec. 2014.

[13] K. Sarabandi, J. Choi, A. Sabet and K. Sabet, "Pattern and gain characterization using nonintrusive very-near-field electro-optical measurements over arbitrary closed surfaces," IEEE Trans., Antennas and Propag., vol. 65, no. 2, pp. 489-497, Feb. 2017.

[14] A. C. Newell, "Error analysis techniques for planar near-field measurements," *IEEE Trans., Antennas and Propag*., vol. 36, no. 6, pp. 754-768, June 1988.

[15] M. Allman, D. Novotny, S. Sandwith, A. Curtin and J. Gordon, "Serial-robotic arm-joint

characterization measurements for antenna metrology," *2017 Antenna Measurement Techniques Association (AMTA)*, Oct. 2017.

2 Field Equivalence Principle and Inverse Problem

2.1 Introduction

This chapter considers to perform numerical processing to electromagnetic field obtain from near-field measurements. We introduce the field equivalence principle, and to brief a method of handling an electromagnetic field as an equivalent electromagnetic wave source existing on an equivalent surface. Following this introduction, the inverse problem of electromagnetic waves is taken up as a method for estimating wave source distribution inside of measurement surface. Electromagnetic field distribution inside the measurement surface can be inverse estimated by solve integral equation that the constructed between a measured near-field and an equivalent source.

2.2 Field Equivalence Principle

In the case where there is an electromagnetic wave source or scattering source in the free space, if we know the current distribution on the wave source surface, it is possible to directly obtain the radiation field and the scattering field from these. It is very difficult to directly measure real current distribution because of the current distribution is changes if the probe contacts to electromagnetic source. Therefore we introduce an equivalent source according to the field equivalence principle [1].

Let us consider a closed surface S including an electromagnetic source in the free space as shown in Figure 2.1. According to Love's equivalence principle, we assume the null field in the surface S and by remove the internal source, then we can replace the electromagnetic field on the surface with an equivalent electromagnetic currents [2].

$$\begin{aligned} \boldsymbol{J} &= \hat{\mathbf{n}} \times \boldsymbol{H} \\ \boldsymbol{M} &= \boldsymbol{E} \times \hat{\mathbf{n}}, \end{aligned} \tag{2.1}$$

where $\hat{\mathbf{n}}$ is the normal unit vector in surface outward direction. If we want to consider an incident wave from outside region of the surface S, to replace the normal vector in outward direction with the normal vector in inside direction.

An electromagnetic field outside the surface S can be obtained by substituting the equivalent currents that acquired above mentioned for the Maxwell's equation that considering an electric current source and a magnetic current source [3]. By using this principle, it is possible to consider the electromagnetic field outside of the measurement surface by assuming the closed surface S on a probe scanning surface and replacing the measurement electromagnetic field with the equivalent electromagnetic currents. Even if the shape of the wave source is unknown, there is an advantage that an external electromagnetic field can be considered.

Where both of the electric field and the magnetic field information are obtained as measured

values, it was only necessary to consider the radiation field according to the Love's principle; however it is difficult to measure both of the electromagnetic fields in actual measurement systems. Besides not only the measurement amount of the near-field increases to twice the electric field and the magnetic field but also two kinds of the electric field probe and the magnetic field probe have to be introduced for measurement system. Furthermore, numerical processing must be performed between both EM probes taking into consideration the difference in the amount of mutual coupling between AUT and probe. Hence we introduce the Schelkunoff's equivalence principle as shown in Figure 2.2 [4], [5]. Schelkunoff's theorem assumes a Perfect Electric Conductor (PEC) or a Perfect Magnetic Conductor (PMC) as a medium of the closed surface. According to the image theory, when *S* is replaced by PEC, the radiation due to the equivalent current becomes 0, and when it is replaced with PMC, the radiation due to the equivalent magnetic current becomes 0. Using this, when the surface *S* is replaced with PEC, we regard the equivalent current on S is 0, while when it is replaced by PMC, we regard the equivalent magnetic current is 0 and the outside electromagnetic field is calculated. Since the equivalent electric current or the equivalent magnetic current on the surface can be ignored, it is possible to calculate the outside radiation field by measuring either the electric or magnetic field.

In this method, we must to regard the electromagnetic field inside the *S* as 0 in any case when considering the radiation field from the surface S to the outside. In the case of planar scanning domain, since the inside of the measurement surface is an unmeasured area in the near-field measurement, it is unnecessary to define the area that becomes the *S* internal direction in calculating the outside field. Since the measurement system and theoretical compatibility are well matched and the outside field of *S* has good agreement with the theoretical value, the planar measurement system is suitable for introducing Schelkunoff's theorem [6]. In the case of cylindrical or spherical scanning domains, we have to pay attention to the handling of the surface internal electromagnetic field in calculating the *S* internal direction. Since only equivalent current or equivalent magnetic current is assumed on the surface *S*, an electromagnetic field is also generated in the direction penetrating *S* by radiation from the equivalent source in the process of calculation. This is contradict to the theory that the internal electromagnetic field is 0, thus countermeasure which to numerically canceling the radiation in the surface inward direction, approximating the equivalent magnetic current with the equivalent electric current, or approximating the equivalent electric current with the equivalent magnetic current is necessary.

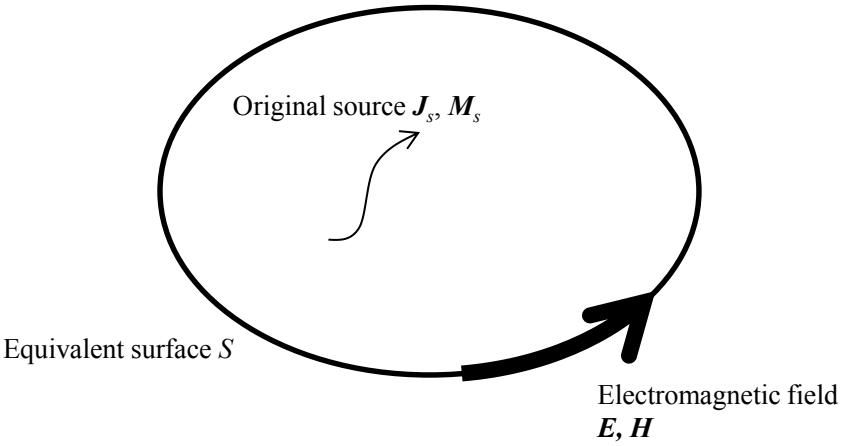

(a) The original problem of near-field and original source.

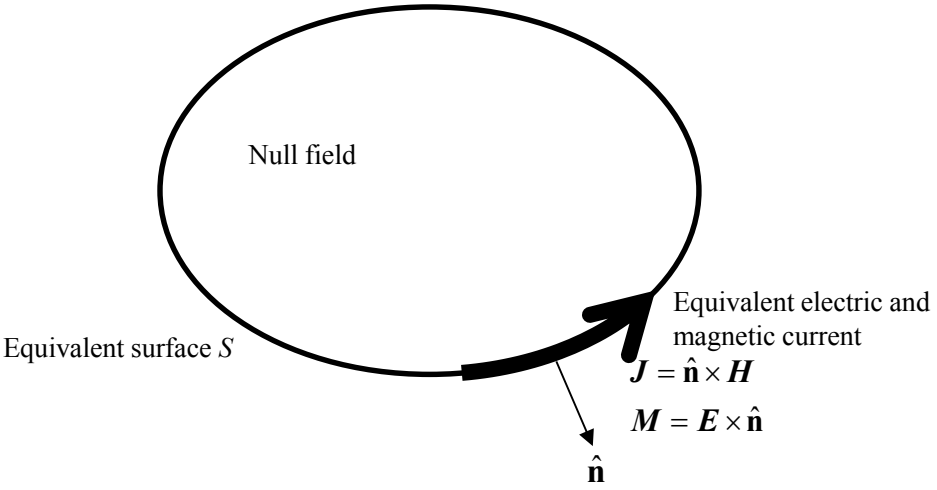

(b) Field equivalence for the external region.

Figure 2.1: Field equivalence principle on equivalent surface including source.

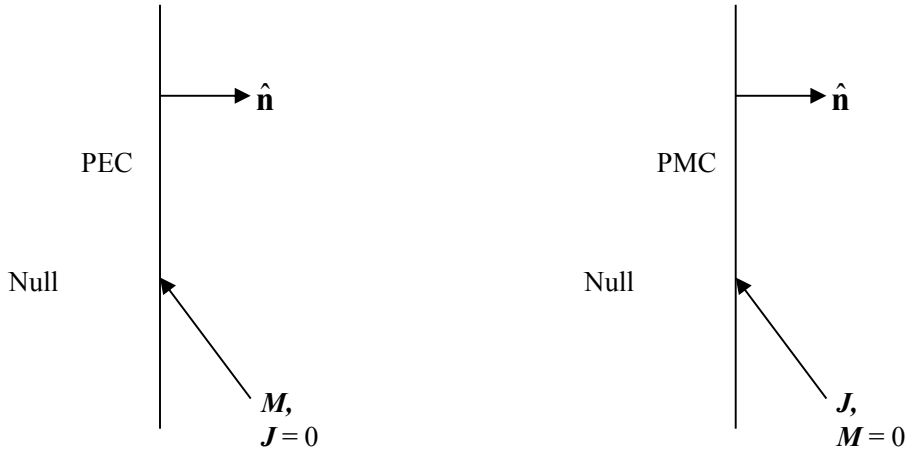

(a) Equivalent magnetic current approach. (b) Equivalent electric current approach.

Figure 2.2: Field equivalence introducing Schelknoff's theorem.

2.3 Inverse Problem

In the previous section, the method of obtaining the electromagnetic field outside the measurement surface from the electromagnetic field acquired by the near-field measurement has been described. In some cases the electromagnetic field information inside the measurement region is required. If we can know the electromagnetic field at an arbitrary point inside the measurement region from the electromagnetic field around the radiation source, it is possible to diagnose the internal electrical operating condition and the failure point. There is an advantage that the structure of the source can be adjusted for obtain the desired radiation field by acquire the radiation field from only a part of the electromagnetic current of the source, this usefulness is very large. Therefore, we introduce the inverse problem of electromagnetic waves as mathematical procedure [7]-[9].

To begin with, let us consider an arbitrary closed surface S as shown in Figure 2.3, and we replace the electromagnetic field on the S with an equivalent electromagnetic current $\boldsymbol{J}$, $\boldsymbol{M}$ according to the field equivalence principle. If S is presented in the free space and there are no interference sources or scattering sources on the outside of S, electromagnetic fields $\boldsymbol{E}(\mathbf{r})$ and $\boldsymbol{H}(\mathbf{r})$ at arbitrary points $\mathbf{r}$ are given as radiation waves from $\mathbf{r}'$ as follows.

$$\begin{aligned}\boldsymbol{E}(\mathbf{r}) &= -jk_0\eta\int_S\left\{\boldsymbol{J}(\mathbf{r}')+\frac{1}{k_0^2}\nabla\nabla\cdot\boldsymbol{J}(\mathbf{r}')\right\}G(\mathbf{r},\mathbf{r}')dS \\ &\quad -\int_S\nabla\times\boldsymbol{M}(\mathbf{r}')G(\mathbf{r},\mathbf{r}')dS\end{aligned} \tag{2.3}$$

$$\begin{aligned}\boldsymbol{H}(\mathbf{r}) &= \int_S\nabla\times\boldsymbol{J}(\mathbf{r}')G(\mathbf{r},\mathbf{r})dS \\ &\quad -\frac{jk_0}{\eta}\int_S\left\{\boldsymbol{M}(\mathbf{r}')+\frac{1}{k_0^2}\nabla\nabla\cdot\boldsymbol{M}(\mathbf{r}')\right\}G(\mathbf{r},\mathbf{r}')dS\end{aligned} \tag{2.4}$$

$$G(\mathbf{r},\mathbf{r}') = \frac{e^{-jk_0|\mathbf{r}-\mathbf{r}'|}}{4\pi|\mathbf{r}-\mathbf{r}'|}. \tag{2.5}$$

Where η is the characteristic impedance of the free space, and the k_0 is the wavenumber of the free space.

These integral equations are separated as components of equivalent current on the *S*, and an operator matrix from **r** to **r'**. Assuming that the electric field component is used as the measurement value of the near-field, the (2.3) is transformed into a suitable form for numerical calculation, and the following matrix equation is obtained.

$$\begin{bmatrix} E_1 \\ \vdots \\ E_m \end{bmatrix} = \begin{bmatrix} A_{j,11} & \cdots & A_{j,1n} \\ \vdots & \ddots & \vdots \\ A_{j,m1} & \cdots & A_{j,mn} \end{bmatrix} \begin{bmatrix} J_1 \\ \vdots \\ J_n \end{bmatrix}. \tag{2.6}$$

The unknown electromagnetic current vector is derived by solve the given matrix equation. In this paper reconstructs the internal source information using radiation wave from internal region of the surface *S*. Although if scattering wave can be measured the electromagnetic wave incident from outside region, this technology can also be applied to radio wave tomography [10].

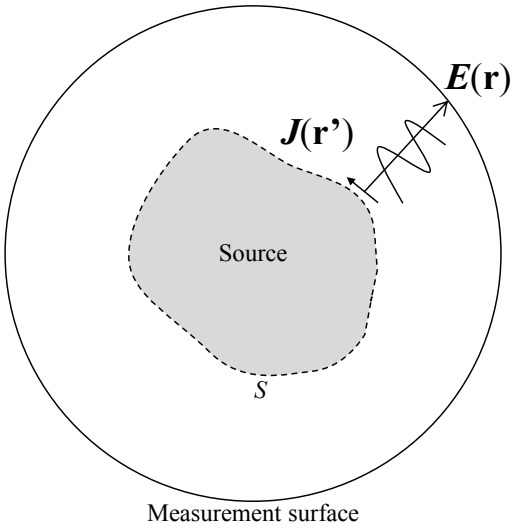

Figure 2.3: Source on the equivalent surface and inverse problem by measurement electromagnetic field.

2.4 Summary

In this chapter, we described the near-field measurement method of the electromagnetic source and numerical processing for measurement information. We introduced the equivalence principle, and showed how to calculate the electromagnetic field outside the measurement area. In addition, the inverse problem of electromagnetic wave is introduced, and the source reconstruction method inside the measurement region using it was described.

Reference

[1] S. R. Rengarajan and Y. Rahmat-Samii, “The field equivalence priciple: Illustration of the establishment of the non-intuitive null fields,” *IEEE Antenna Propag. Mag*., vol. 42, no. 4, pp.122-128, Aug. 2000.

[2] A. E. H. Love, “The integration of equations of propagation of electric waves,” *Phil Trans. Roy. Soc. London, Ser. A*, 197, 1901.

[3] R. E. Collin, *Field theory of guided waves*, Piscataway, NJ, IEEE Press, 1991.

[4] S. A. Schelkunoff, “Some equivalence theorems of electromagnetics and their application to radiation problems,” *Bell System Technical Journal*, 15, 1936, pp. 92-112.

[5] S. A. Schelkunoff, “Kirchhoff's formula its vector analogue and other field equivalence theorems,” *Communications in Pure and Applied Mathematics*, 4, 1951, pp. 43-59.

[6] P. Petre and T. K. Sarkar, “Planar near-field to far-field transformation using an equivalent magnetic current approach,” *IEEE Trans., Antennas and Propag*., vol.40, no.11, pp.1348-1356, Nov. 1992.

[7] Y. Álvarez, M. Rodríguez, F. L. Heras and M. M. Hernando, “On the use of the source reconstruction method for estimating radiated EMI in electronic circuits,” *IEEE Trans., Instrum. Meas*., vol. 59, no. 12, pp.3174-3183, Dec. 2010.

[8] J. L. A. Quijano and G. Vecchi, “Improved-accuracy source reconstruction on arbitrary 3-D surfaces,” *IEEE Antennas and Wireless Propag. Lett*., vol. 8, pp. 1046-1049, Sept. 2009.

[9] Y. Álvarez, F. L. Heras and M. R. Pino, “Reconstruction of equivalent currents distribution over arbitrary three-dimensional surfaces based on integral equation algorithms,” *IEEE Trans., Antennas and Propag*., vol. 55, no. 12, pp. 3460-3468, Dec. 2007.

[10] F. Cakoni, D. Calton and P. Monk, “Qualitative methods in inverse electromagnetic scattering theory,” *IEEE Antenna and Propag. Magazine*, vol. 59, no. 5, pp. 24-33, Oct. 2017.

3 A Fast Far-Field Estimation Method by Compact Single Cut Near-Field Measurement for Electrically Long Antenna

3.1 Introduction

Simple and accurate measurement method for base station antenna is necessary because the number of base stations installed is increasing due to the rapid development of the mobile communications. Far-field is one of the most important characteristics to evaluate the base station antenna performance. Long distance between the antenna and the probe is required for measurement because it needs to satisfy the far-field criteria of electrically large aperture antennas [1], [2].It is difficult to measure the far-field and its directivity of a base station antenna in a widely used anechoic chamber for handset antenna measurements, because it has an electrically long aperture constructed by multiple elements [3], [4].

The near-field measurement technique is an effective method to characterizing far-field of an antenna under test (AUT) [5]. The cylindrical near-field measurement is most usual adopted technique for a base station antenna; it is suitable to transform a fan beam pattern. Reducing the time of measurement and calculation an antenna is a big demand for near-field measurements [6]. There is some presented method resolve this problem. Multi-probe measurement is one of a simple technique for resolve this problem [7]. Measurement time is reduced drastically by introduce to equipment a large number of probes. Another one is single cut near-field to far-field transformation. Processing time achieved be minimized by limiting the measurement data and the estimate plane.
In literature [6], [8], it is shown to reconstruct far-field accurately by circular one cut measurements and cylindrical modes transformation. However in most cases, it is not easy to rotate the AUT in order to measure the broadside directivity of the long aperture AUT. The cylindrical setup is requires smaller measurement space in long antenna measurement than the spherical setup, for it is rotate an AUT just only in azimuthal direction. The cylindrical one-cut near-field measurement is most suitable for obtaining quickly the far-field of base station antenna in the compact anechoic chamber.

The cylindrical scanning system has a defect to cause by its mechanical structure, which is a finite truncation of longitudinal direction. In the cylindrical systems it is impossible to acquire an infinitely long data in the endfire direction, thus an estimable angle of far-field pattern is limited. In order to avoid this problem, there is only numerical extrapolation as in [9]. Valid angle of far-field is increased in [9]; however the measurement length of cylinder is desirable which it can be reduced to at least the same length of the AUT. If the measurement is to be performed longer than the AUT length, the apparatus becomes overly complicated. In particular, in the case of single cut measurement, since complicated numerical processing cannot be performed from small quantity of acquired data, there is a need to extrapolate the assumed value as simple as possible.

In this chapter, we propose a rapid far-field estimation method by single cut and short length near-field measurement for electrically long array antenna. The proposed method to estimate the far-field is based on equivalent line electric current, which is measured in reactive near-field using a small loop probe for minimize disturbance of electromagnetic field in the vicinity of AUT. The equivalent currents are measured on a line in front of and a circle around the AUT. The far-field pattern of each plane is estimated from the extended linear distribution and the circular distribution applied 1-D integral equation, the measurement time and the equipment can be kept very small. The spherical far-field is approximated from the product of the far-field of each cut plane and its maximum directivity can be estimated. A priority of the proposed method is a fast measurement speed and a small scale of measurement space.

The section is organized as follows. 3.2 describes the estimation theory and the simple extrapolation method. Numerically test and its accuracy evaluation are indicated in section 3.3. Section 3.4 validates the proposed method from measured near-field data. Finally, conclusions are drawn in section 3.5.

3.2 Method

The proposed method follows the near-field to far-field transformation method based on equivalent current method [10], [11]. The equivalent current theorem assumes arbitrary surface enclosing the AUT. This approach can obtain the radiation field outside the closed surface if the equivalent current on the surface is determined by measurement. An equivalent electric current $\boldsymbol{J}$ and an equivalent magnetic current $\boldsymbol{M}$ on the closed surface are obtained from the electromagnetic field on the closed surface as

$$\begin{aligned} \boldsymbol{J} &= \hat{\mathbf{n}} \times \boldsymbol{H} \\ \boldsymbol{M} &= \boldsymbol{E} \times \hat{\mathbf{n}} \end{aligned} \tag{3.1}$$

where $\hat{\mathbf{n}}$, $\boldsymbol{H}$, and $\boldsymbol{E}$ are outward normal vector of AUT, magnetic field and electric field. In order to obtain radiation field on an arbitrary point, $\boldsymbol{J}$ and $\boldsymbol{M}$ are necessary. However to measure both of electric field and magnetic field, the measurement equipment will be complicated. The radiation field outside the closed surface is determined from either the electric current distribution or magnetic current if we can consider the radiation field internal the closed surface is zero, closed surface is replaced as perfect magnetic conductor or perfect electric conductor and introduce Schelkunoff's theorem, the radiation field can be obtained from either $\boldsymbol{J}$ or $\boldsymbol{M}$ [11]-[15]. The proposed method estimates far-field using only equivalent electric current distribution. To get the equivalent current using small loop probe with few electromagnetic field disturbance. The electrical size of the probe is enough small, disturbance can be kept few; hence we measure the equivalent current close to the

AUT. For simplify the estimation technique, we assume the equivalent electric currents as infinitesimal dipole group to calculate far-field pattern.

Geometry of near-field measurement is shown in Figure 3.1. Longitudinal direction of the AUT is set parallel in *z*-axis direction. The vertical plane far-field pattern is estimated from the linear current distribution parallel to the longitudinal direction of the AUT [16]. We need to calculate only in the electromagnetic field in the region where $x > 0$, we place a perfect magnetic conductor in front of the AUT extending to infinity in the *y* and *z* directions on the *yz* plane. Therefore, the actual equivalent current distribution on the closed surface is given as $\boldsymbol{J'} = 2\,\hat{\mathbf{n}} \times \boldsymbol{H}$ according to image theory [11].

We assume each current are small dipole, far-field is calculated the same as a linear array antenna [17] as follows:

$$\begin{aligned} E(\theta,\phi=0^\circ) &= E_\theta(\theta)\hat{\boldsymbol{\theta}} + E_\phi(\theta)\hat{\boldsymbol{\phi}} \\ &= \eta\sin(\theta)\sum_{m=1}^{M} J_z'(m)e^{(jk0z_m\cos\theta)}\hat{\boldsymbol{\theta}} \\ &\quad + \eta\sum_{m=1}^{M} J_y'(m)e^{(jk0z_m\cos\theta)}\hat{\boldsymbol{\phi}} \end{aligned} \tag{3.2}$$

where η is the characteristic impedance in free space, subscription means a polarization, J_z(m) and J_y(m) is the acquired complex current and z_m is its position on the *z*-direction and k_0 is the wavenumber in free space.

In order to measure in as compact area as possible, the measurement length of the linear current distribution is assumed to be equal to the length of the AUT as a precondition. Valid angle in broadside region is to zero according to the definition [9], the far-field pattern in vertical plane cannot be estimated accurately. Truncation error reduction method was denoted as in [9], although it requires a longer measurement than the length of the AUT, and complex reconstruction algorithm.

Thus the method is insufficient to reduction of estimation time, it is necessary to apply a simpler extrapolation method. The section view of the linear current sampling and extrapolation scheme is shown in Figure 3.2. As previously mentioned, the actual measurement area is the same length of the AUT l_M, the upper and the lower data is extended using the data of the measured edge point $J(l_\mathrm{M}/2)$, where $(l_\mathrm{M}/2)$ means coordinate position on *z*-axis. The extended currents is approximated from the amplitude inversely proportional to distance and the phase rotation corresponding to distance as

$$J\left(\frac{l_\mathrm{M}}{2}+\Delta z\right) = J\left(\frac{l_\mathrm{M}}{2}\right)A_{\Delta z}e^{(-jk_0d_{\Delta z})} \tag{3.3}$$

and

$$
\begin{aligned}
A_{\Delta z} &= \frac{d^2 + \left(\frac{l_{\mathrm{M}}}{2}\right)^2}{d^2 + \left(\frac{l_{\mathrm{M}}}{2} + \Delta z\right)^2} \\
d_{\Delta z} &= \sqrt{d^2 + \Delta z^2} - d
\end{aligned}
\tag{3.4}
$$

This correction factor utilizes the nature that the amplitude sharply decreases and the phase constant rotates uniformly out of the aperture area in very near-field region. In the case of the extrapolated length is too long beyond necessity, the proportion of reliable data decreases, we need to limit the approximate length. Whatever the case, since the amount of measured data should not be less than the amount of extrapolated data, the extrapolation length l_{E} is limited as $2l_{\mathrm{E}} < l_{\mathrm{M}}$. It is confirmed that far-field can be estimated accurately with this extrapolation length in many numerical calculations. Extend the linear equivalent current distribution as twice as the actual measurement length; it is possible to extend the valid angle to

$$
\theta_{\mathrm{ex}} = \tan^{-1}\left(\frac{l_{\mathrm{E}}}{d}\right). \tag{3.5}
$$

It can reduce the error in the vertical plane due to the finite truncation of the linear current distribution. When extrapolation is not performed, the valid angle θ_{ex} is 0° and it is difficult to obtain accurately the pattern in the vertical plane.

The far-field in horizontal plane is calculated from the circular current distribution around the AUT. If we know both of equivalent electric current and equivalent magnetic current on the closed surface S, electromagnetic field inside the closed surface due to the radiation from the $\boldsymbol{J}$ and $\boldsymbol{M}$ becomes zero because of obtain the poynting vector. From the Maxwell's equations, the electric field as

$$
\begin{aligned}
\boldsymbol{E} &= j\omega\mu\boldsymbol{A}_j + \frac{1}{j\omega\varepsilon}\nabla\nabla\cdot\boldsymbol{A}_j \\
&\quad -\nabla\times\boldsymbol{A}_m
\end{aligned}
\tag{3.6}
$$

where $\boldsymbol{A}_j$ and $\boldsymbol{A}_m$ are the electric and the magnetic vector potential defined as

$$
\begin{aligned}
\boldsymbol{A}_j &= \int_S \boldsymbol{J}(\mathbf{r}')G(\mathbf{r},\mathbf{r}')dS, \\
\boldsymbol{A}_m &= \int_S \boldsymbol{M}(\mathbf{r}')G(\mathbf{r},\mathbf{r}')dS
\end{aligned}
\tag{3.7}
$$

and

$$G(\mathbf{r},\mathbf{r}') = \frac{e^{-jk_0|\mathbf{r}-\mathbf{r}'|}}{4\pi|\mathbf{r}-\mathbf{r}'|}. \tag{3.8}$$

The proposed method uses only electric current. If calculated as above, the electromagnetic field inside the closed surface by equivalent current does not become zero. In other words, perfect magnetic conductor cannot be assumed on the closed surface. Therefore in (7), we approximate $\boldsymbol{M}$ with $\eta\boldsymbol{J}$. Originally $\boldsymbol{M} = \eta\boldsymbol{J}$ does not hold in very near-field region. Since the AUT has a width in the *y*-axis direction, the distance between the AUT and the probe is sufficiently separated around main radiation direction when performing circular scan. In this paper, we assuming that the distance from AUT center to circular scan line are farther than wavelength. This is sufficient compared with the far-field criterion of an infinitesimal dipole. Thus the assumption holds well practical. Based on these the horizontal plane far-field is calculated as follows;

$$\begin{aligned} E(\theta = 90^\circ, \phi) &= E_\theta(\phi)\hat{\boldsymbol{\theta}} + E_\phi(\phi)\hat{\boldsymbol{\phi}} \\ &= \eta\sum_{n=1}^{N}\left(1 + \hat{\boldsymbol{\phi}}\cdot\hat{\boldsymbol{\phi}}_{\boldsymbol{n}}\right)J_z(n)e^{\left(jk_0 d_\phi\right)}\hat{\boldsymbol{\theta}} \\ &\quad + \eta\sum_{n=1}^{N}\left(1 + \hat{\boldsymbol{\phi}}\cdot\hat{\boldsymbol{\phi}}_{\boldsymbol{n}}\right)J_\phi(n)e^{\left(jk_0 d_\phi\right)}\hat{\boldsymbol{\phi}} \end{aligned} \tag{3.9}$$

And

$$d_\phi = x_n\cos\phi + y_n\sin\phi \tag{3.10}$$

where N is the total number of equivalent currents on the circle, x_n and y_n are the coordinate points on *x*- and *y*-axis, respectively and, ϕ_n is the azimuth angle of each equivalent current. $\hat{\boldsymbol{\phi}}$ is unit vector of ϕ direction and $\hat{\boldsymbol{\phi}}_{\boldsymbol{n}}$ is the position vector of each sampling points. The derivation is described in the appendix.

By using the orthogonal cut planes obtained as described above, the spherical far-field pattern is approximated as

$$E_p(\theta,\phi) = E_p\left(\theta, \phi = 0^\circ\right)E_p\left(\theta = 0^\circ, \phi\right). \tag{3.11}$$

The horizontal far-field pattern of electrically long antenna does not change significantly depending on the change of the zenith angle. Therefore, the approximation of (9) holds well accuracy with respect to the long aperture antenna. Error in vertical plane is derived from estimated normalized vertical plane pattern as

$$Error(\theta) = \frac{\left| FF_{Ref.}(\theta) - FF_{Est.}(\theta) \right|}{\left| FF_{Ref.}(\theta_0) \right|} \tag{3.12}$$

where $FF_{Ref.}(\theta_0)$ is maximum value of estimated far-field in vertical plane. We discuss the improved amount in vertical plane using mean value of (12) in valid angle area. We evaluate the total accuracy by the maximum directivity. The directivity in the maximum radiation direction (θ_0, ϕ_0) is given by

$$D(\theta_0, \phi_0) = \frac{4\pi \left| E(\theta_0, \phi_0) \right|^2}{\int_0^{2\pi} \int_0^{\pi} \left| E(\theta, \phi) \right|^2 \sin\theta d\theta d\phi}. \tag{3.13}$$

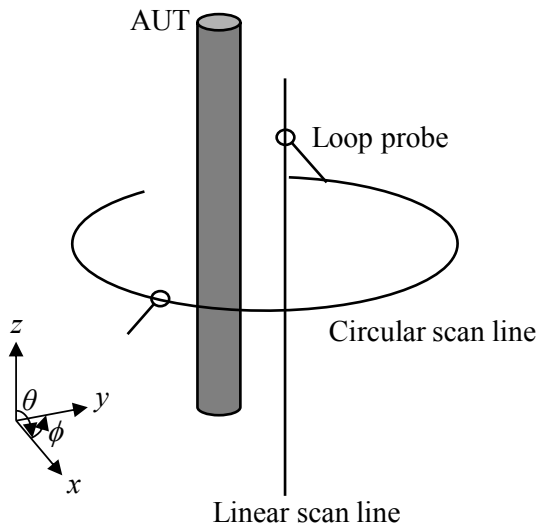

Figure 3.1: Measurement setup of equivalent electric current in each single cut plane.

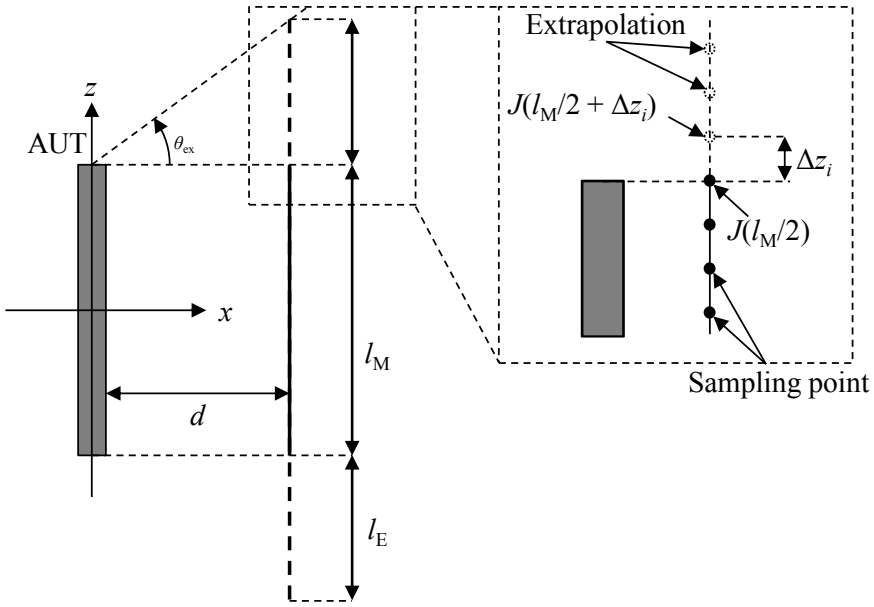

Figure 3.2: Geometry of source extrapolation in vertical plane.

3.3 Simulation

We demonstrate some numerical results by simulation of a long aperture linear array antenna. We used a 4 elements patch linear array as an AUT (at a frequency of 3 GHz), its excitation is uniform and it is arranged parallel to the z-axis direction. The AUT has a rectangular aperture of the height is 2λ and the width is λ. Line current distribution is sampled at an interval of 0.1λ right above the front of AUT and circular current distribution is sampled at an interval of 5° on the center of AUT. The actual sampling length of the linear current distribution is the same as the length of the AUT, and total length is extended as twice as the length of the AUT according to (3). Although the sampling points are set densely here, it suffices if the interval meets the sampling theorem [5]. Therefore, the sampling interval can be shortened to a slightly shorter than a half wavelength.

The estimated far-field in the vertical plane from a near-field data in very close region of the AUT is shown in Figure 3.3. The distance between the AUT and the sampling line is 0.2λ. The co-polarization of the AUT is θ direction and sampled current direction is parallel to z-axis. The solid line is reference far-field pattern calculated from FEKO [19]. In the case of Figure 3.3, the estimated pattern of the truncated and the extrapolated are almost no difference. When the measurement distance is very close, a lack of the data in the endfire direction is not a big problem. However in many cases, due to the mechanical reason it is physically impossible to deploy a probe to the very close range of the AUT. In particular, when evaluating characteristics with radomes, it can be inferred that the distance between the probe and AUT is about half wavelength apart. The amount of data in the endfire direction is decreased as the distance of the linear current distribution is increase; as a result the estimation accuracy in the vertical plane far-field is degraded. The far-field pattern

estimated from near-field in valid angle region is shown in Figure 3.4, when the measurement position $d = \lambda$. As can be seen from Fig. 4 (a), the far-field obtained from the truncated near-field has a mismatch with the reference pattern in not only the side lobes but also the main beam. In the case of a realistic measurement distance, missing data in the endfire direction cannot be avoided, the mismatch of the estimated pattern occurs. This pattern discrepancy is improved by the data extension; the valid angle of this sampling case is expanded to ±45° from ±0° without data extrapolation according to (5). It can be seen that the estimated pattern based on the extended data has good agreement with the reference far-field. This is apparent from Fig. 4 (b) mean value of the error in the valid angle region is improved more than 6 dB. The extrapolated current distribution is shown in Figure 3.5. Although the extrapolation well reproduces the exact current distribution for both amplitude and phase, it can be seen that when $|z|$ is sufficiently large, the extrapolated value is approximated larger than the exact amplitude. The true current decreases according to sum of the $1/r$ and $1/r^2$ terms depending on the distance from the AUT. However, since (3) decreases only with $1/r$ with the measurement end as a starting point, an error from the exact value occurs at a portion where $|z|$ is sufficiently large. If the extrapolated length is infinite, the radiation level around polar direction becomes hypertrophied by the reason, we introduced (4) as a limitation. As we can see from the pattern in vertical plane, the method can estimate even electrical tilt pattern. Figure 3.6 shows the estimation results of the far-field in the case of the AUT radiating horizontal polarization. The AUT is 4 elements linear array the same as vertical polarization case; it is constructed by patch elements which is radiating horizontal polarization. Even in horizontally polarization, the far-field pattern in the vertical plane can be accurately estimated by the proposed method, and particularly good agreement is obtain in the estimation result by extrapolating the near-field data. It was numerically demonstrated that proposed method can accurately estimate the far-field in the vertical plane.

The horizontal plane pattern of the AUT estimated according to (9) is shown in Figure 3.7. The difference in line type indicates the difference in sampling radius r from the AUT center. The estimation accuracy in the horizontal plane is wrong, when the sampling position of the scanning circle is too close to the AUT. The accuracy deterioration of the proposed method occurs from imperfection of the integral equation in near-field region. If the scan radius is sufficiently large, almost the same pattern as the far-field is obtained, thus the estimation accuracy improves. In order to accurately estimate the pattern in the horizontal plane, it is desirable to provide an distance larger than about 0.5λ between the edge in the horizontal plane of the AUT and the scan circle.

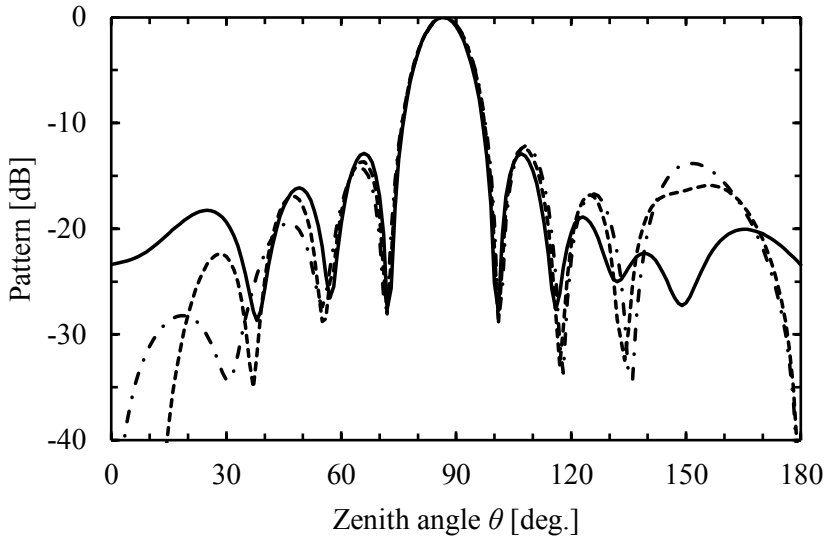

Figure 3.3: Estimated vertical plane far-field sampled in very close area, probe distance $d = 0.2\lambda$ (solid: reference; chain: truncated; dotted: extrapolated).

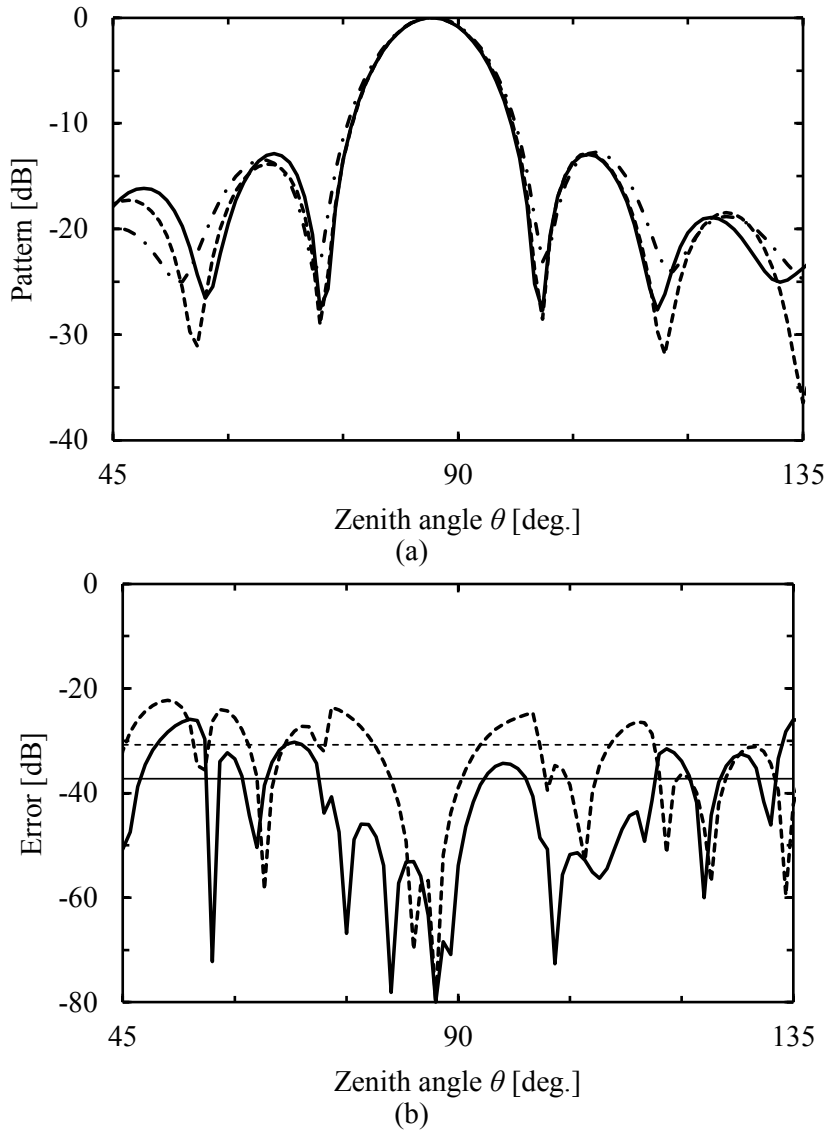

Figure 3.4: Estimated results of E_θ in vertical plane, probe distance $d = \lambda$. (a) is the far-field pattern (solid: reference; chain: truncated; dotted: extrapolated). (b) is the relative error (solid: extrapolated; dotted: truncated). The horizontal lines are its mean value

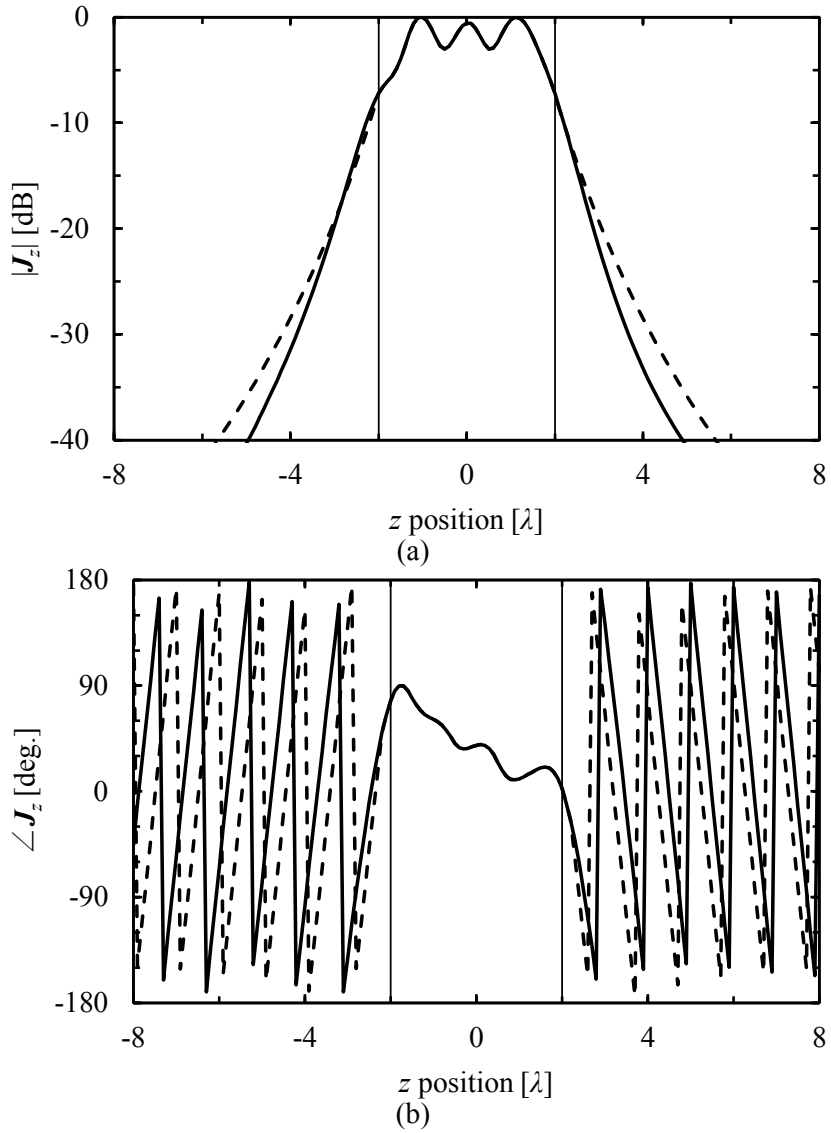

Figure 3.5: Extrapolated equivalent current. (a) is amplitude (solid: reference; dotted: extrapolated). (b) is the phase (solid: reference; dotted: extrapolated). The vertical lines are its edge position of the AUT.

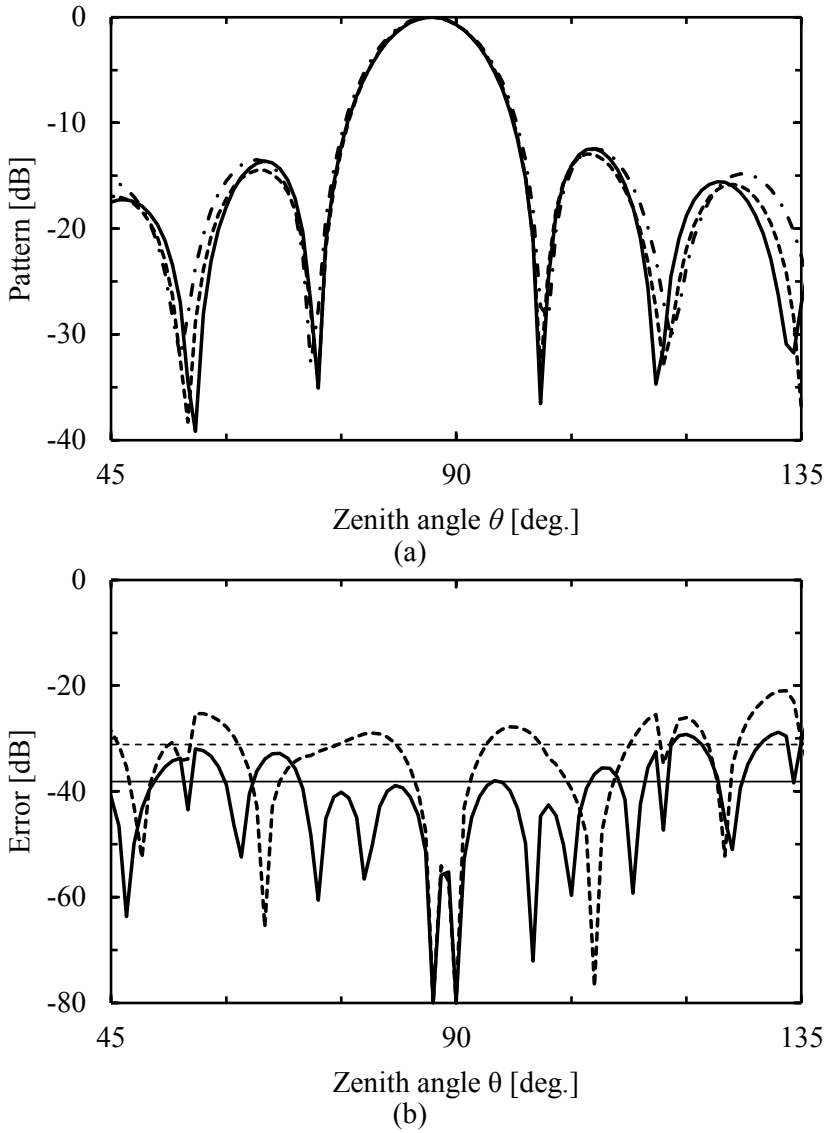

Figure 3.6: Estimated results of E_ϕ in vertical plane, probe distance $d = \lambda$. (a) is the far-field pattern (solid: reference; chain: truncated; dotted: extrapolated). (b) is the relative error (solid: extrapolated; dotted: truncated). The horizontal lines are its mean value.

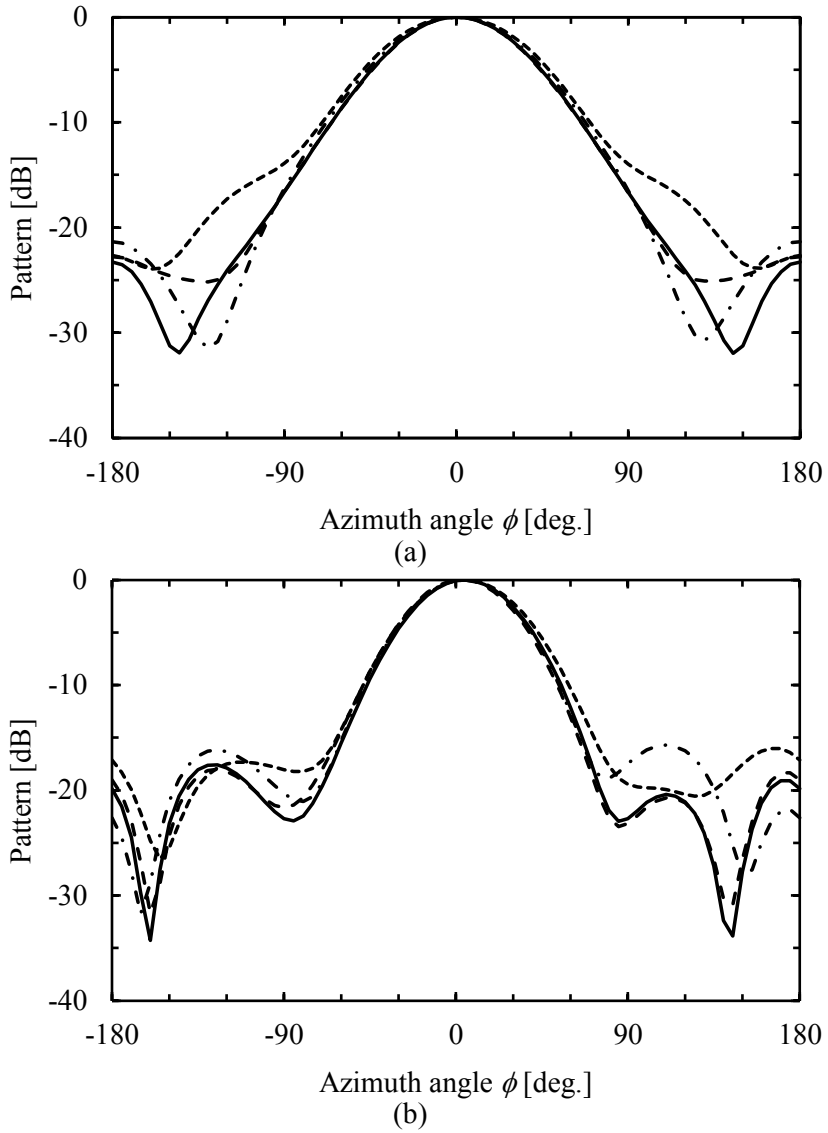

Figure 3.7: Far-field pattern in horizontal plane (solid: reference; dotted: $r = 0.6\lambda$; chain: $r = 1.0\mathrm{r}\lambda$; break: $r = 2.0\lambda$;). (a) is E_θ of vertical polarized AUT. (b) is E_ϕ of horizontal polarized AUT.

3.4 Experiment

This section shows estimation results using measured equivalent current in very near-field area. A measurement overview of a base station antenna in an anechoic chamber is shown in Figure 3.8. The measurement of the current distribution was performed in a small anechoic chamber. As shown in the previous section, since the proposed method can estimate the far-field using the equivalent current in the very near-field region of AUT, a large-scale anechoic chamber is unnecessary for near-field measurement. An outer diameter of the probe is 12 mm, and the electrical size of the probe

is about 0.1λ at 2.69 GHz. The AUT is configured by 8 radiation elements placed on co-linear line and the polarization is slanted at 45°. The scanning probe is tilted at 45° from the vertical axis of the AUT. Measurement specifications of the current distribution are shown in Table 3.1, where measurement length is 2155 mm for 900 MHz band AUT and 834 mm for 2.6 GHz band AUT; these are the same length as each AUT physical length. Measurement distance of the linear current distribution is set to 100 mm, where it is an approach limit of the probe jig. All measurements of the current distribution were performed in very near-field area of the AUT. The probe scans in a straight line above the AUT, and the AUT is held by jig which can rotate in the circumferential direction. Compared to the cylindrical scan, the measurement time of the proposed method is extremely small, and the time required for the measurement was about 3 minutes.

Estimation results from the measured data are shown in Figure 3.9 and Figure 3.10. Measurement frequency is at 0.79GHz and 2.69GHz. Solid lines are reference far-field pattern by cylindrical near-field measurement [20] as reference pattern. The estimated pattern can reproduce the main lobe, especially when used the extrapolated near-field data, the sidelobe also matches well. The proposed method is able to well represent the reference horizontal plane far-field ±90° around the main beam. There is a supporting metal pillar behind the AUT; the pattern in the backward direction is disturbed by the reflection wave from there. Since the objective of the proposed method is to obtain directivity in maximum direction fast and accurately, the error of the behind direction with small radiation intensity does not become a problem. Table 3.2 shows estimation error of the maximum directivity. The directivity of the AUT can be accurately estimated at any frequency, the maximum error is within 0.2 dB. Relative errors of measurement results in the vertical plane are shown in Figure 3.11. In valid angle area, the relative errors of the extrapolated cases are improved against to the truncated. The mean values and their improved values are shown in Table 3.3. The improvement by the proposed simple extrapolation method is obvious, at least the average error can be improved by 3 dB or more. It was shown that the far-field of electrically long antennas can be estimated fast and accurately by measurement in the minimum space.

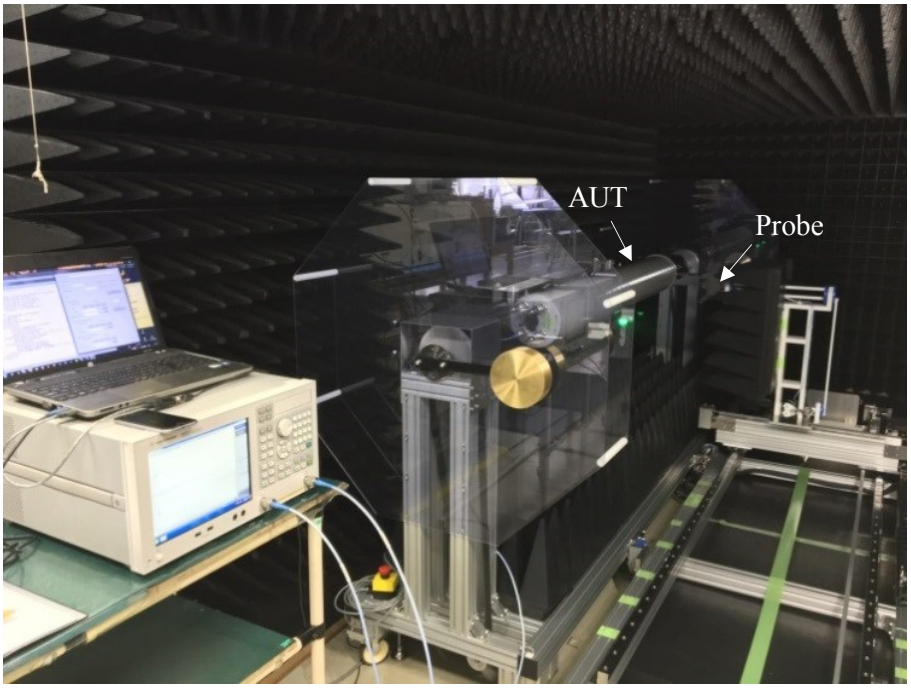

Figure 3.8: Measurement overview.

Table 3.1 Measurement Specifications

900 MHz sector antenna	1D measurement	Length	2155 mm (6.90λ)
		Distance	100 mm (0.32λ)
		Interval	33 mm (0.11λ)
	Circular measurement	Radius	660 mm (2.11λ)
		Step	2° (0.07λ)
	Fresnel region		> 3500 mm
	Far-field		> 29700 mm
2.6 GHz sector antenna	1D measurement	Length	834 mm (7.75λ)
		Distance	100 mm (0.90λ)
		Interval	11 mm (0.10λ)
	Circular measurement	Radius	300 mm (2.69λ)
		Step	1° (0.05λ)
	Fresnel region		> 1390 mm
	Far-field		> 12056 mm

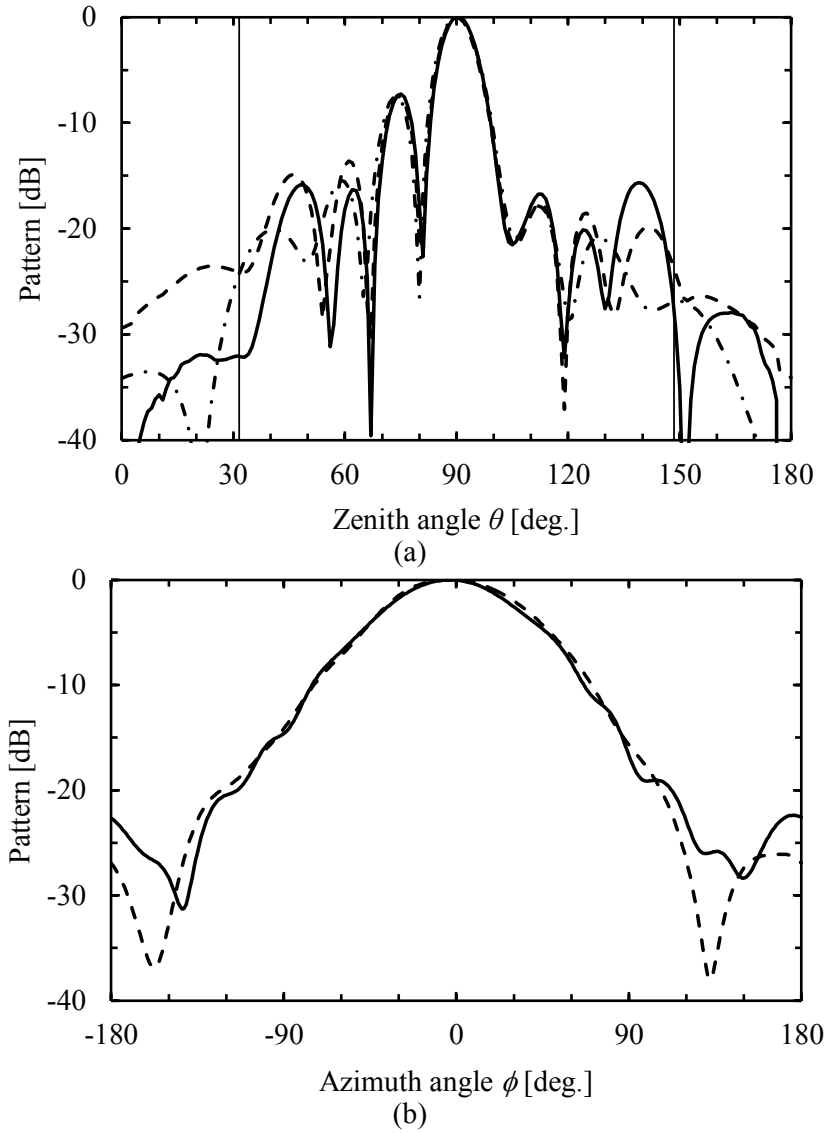

Figure 3.9: Measurement result at 0.79 GHz. (a) is vertical plane (solid: reference; chain: truncated; dotted: extrapolated), vertical lines are valid angle after data extension. (b) is horizontal plane (solid: reference; dotted: estimated).

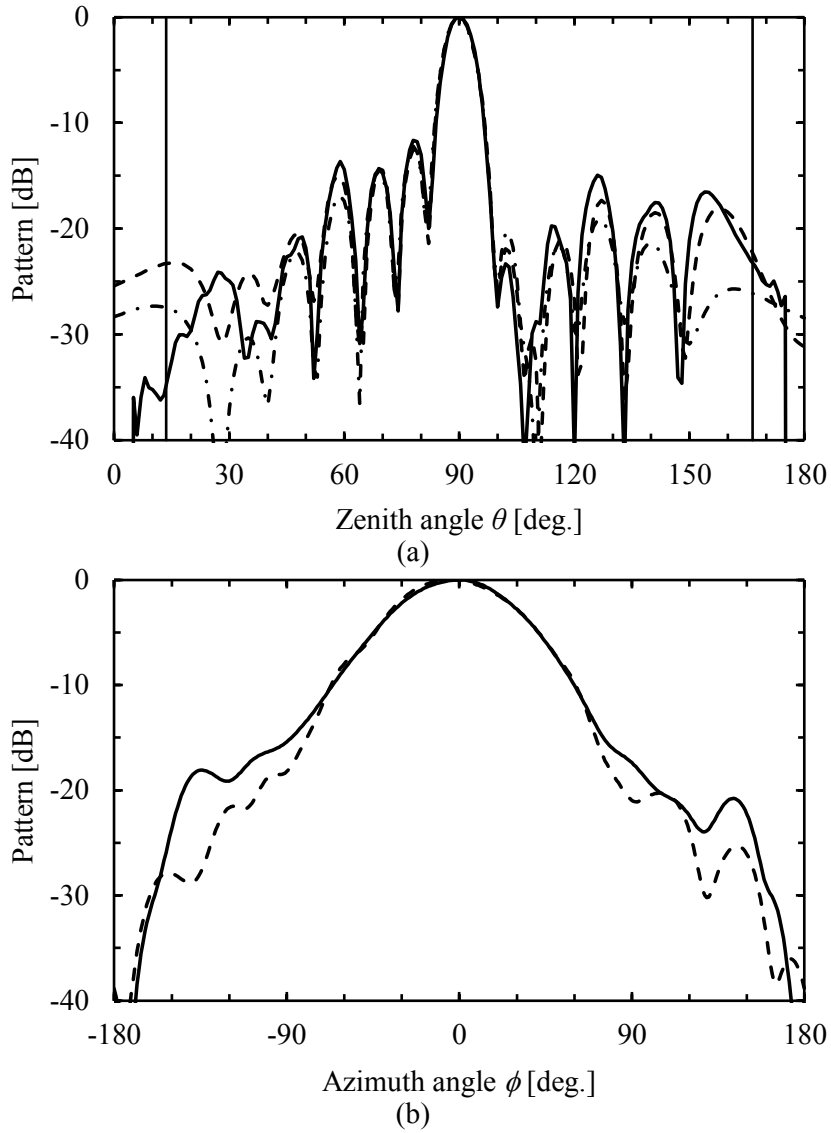

Figure 3.10: Measurement result at 2.69 GHz. (a) is vertical plane (solid: reference; chain: truncated; dotted: extrapolated), vertical lines are valid angle after data extension. (b) is horizontal plane (solid: reference; dotted: estimated).

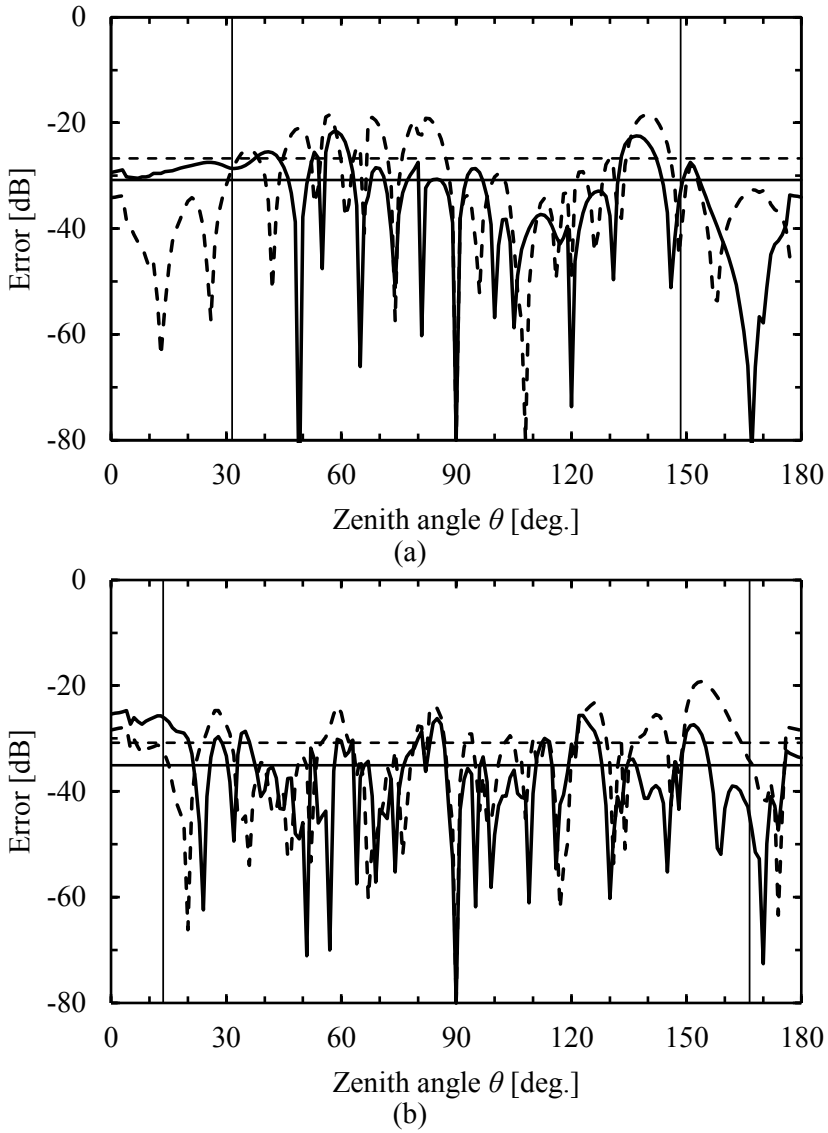

Figure 3.11: Relative error in vertical plane (solid: extrapolated; dotted: truncated), vertical lines are valid angle, horizontal lines are its mean value. (a) is AUT at 0.79 GHz. (b) is AUT at 2.69 GHz.

Table 3.2 Estimated directivity and error

Frequency [GHz]	Reference [dBi]	Estimated [dBi]	Error [dB]
0.79	16.15	16.23	0.08
0.81	16.47	16.59	0.12
0.89	16.88	16.99	0.11
0.96	17.18	17.29	0.11
2.49	17.51	17.64	0.13
2.59	17.70	17.79	0.09
2.69	18.00	18.08	0.08

Table 3.3 Mean error in vertical plane

Frequency [GHz]	Truncated [dB]	Extrapolated [dB]	Improved [dB]
0.79	-26.75	-30.83	4.08
0.81	-25.88	-29.46	3.58
0.89	-26.36	-30.46	4.10
0.96	-27.31	-32.94	5.63
2.49	-32.12	-37.43	5.31
2.59	-29.81	-35.22	5.41
2.69	-30.84	-35.07	4.23

3.5 Summary

A fast method to estimate far-field pattern of electrically long aperture antennas by orthogonal single cut measurement in compact space was proposed. A method to estimate the far-field pattern of long aperture array antenna by simple measurement has been proposed. The method is based on the equivalent electric current approach and using orthogonal linear and circular current distribution. In the proposed method, the equivalent current in the vertical plane with insufficient measured length is extrapolated numerically and the estimation accuracy of the far-field in vertical plane is improved. The proposed method can be possible to measure the near-field with a physical minimum measurement space by using a small loop probe with small electromagnetic disturbance. From the numerical examples, the proposed method demonstrated it can estimate the far-field using equivalent electrical current data sampled in very near-field area. We verified the validity of the calculation by using the measured equivalent current distribution. Since the maximum directivity can be estimated with an error within 0.2 dB, it is indicated that proposed method is effective to fast and compact far-field estimation of electrically long antennas.

Reference

[1] T. Uno and S. Adachi, “Rante distance requirements for large antenna measurements,” *IEEE Trans., Antennas and Propag.*, vol. 37, no. 6, pp.707-720, June 1989.

[2] D. Slater, *Near-field antenna measurements*, Artech House, 1991.

[3] K. Fujimoto and J. R. James, *Mobile Antenna Systems Handbook*, Artech House, 1994.

[4] H. Arai and K. Cho, “Cellular and PHS base station antenna system,” *IEICE Trans., Commun*., vol. E86-B, no. 3, pp. 980-992, March 2003.

[5] A. D. Yaghjian, “An overview of near-field antenna measurements,” *IEEE Trans., Antennas and Propag*., vol. AP-34, no. 1, pp. 30-45, Jan. 1986.

[6] R. Conelius, T. Salmerón-Ruiz, F. Saccardi, L. Foged, D. Heberling and M. Sierra-Caste¥~ner, “A comparison of different methods for fast single-cut near-to far-field transformation,” *IEEE Antennas and Propag. Magazine*, vol. 56, no. 2, pp. 252-261, Apr. 2014.

[7] L. J. Forged, G. Barone and F. Saccardi, “Antenna measurement systems using multi-probe technology,” *2015 IEEE International Conference on Antenna Measurements & Applications (2015 CAMA)*, Dec. 2015.

[8] T. Salmerón-Ruiz, M. Sierra-Casteñer, F. Saccardi, S. Burgos, F. J. Cano-Fácila and Lars. J. Foged, “A fast single cut spherical near-field-to-far-field transformation using cylindrical modes,” *European Conference on Antennas and Propagation (EuCap 2014)*, pp. 2476-2480, Apr. 2014.

[9] J. C. Bolomey, O. M. Bucci, L. Casavola, G. D'Elia, M. D. Migliore and A. Ziyyat, “Reduction of truncation error in near-field measurement of antennas of base-station mobile communication systems,” *IEEE Trans., Antennas and Propag*., vol. 52, no. 2, pp. 593-602, Feb. 2004.

[10] P. Petre and T. K. Sarkar, “Planar near-field to far-field transformation using an equivalent magnetic current approach,” *IEEE Trans., Antennas and Propag*., vol.40, no.11, pp.1348-1356, Nov. 1992.

[11] T. P. Sakar and A. Taaghol, “Near-field to near/far-field transformation for arbitrary near-field geometry utilizing an equivalent electric current and MoM,” *IEEE Trans., Antennas and Propag*., vol. 47, no. 3, pp. 566-573. March 1999.

[12] Y. Álvarez, M. Rodríguez, F. L. Heras and M. M. Hernando, “On the use of the source reconstruction method for estimating radiated EMI in electronic circuits,” *IEEE Trans., Instrum. Meas*., vol. 59, no. 12, pp.3174-3183, Dec. 2010.

[13] W. J. Zhao, H. B. Park, M. Tan, H. H. Park, E. X. Liu, E. Song and E. P. Li, “Far-field prediction from amplitude-only near-field measurements using equivalent electric currents,” *2012 IEEE International Symposium on Electromagnetic Compatibility (EMC 2012)*, pp. 590-593, Aug. 2012.

[14] X. Gao, J. Fan, Y. Zhang, H. Kajbaf and D. Pommerenke, “Far-field prediction using only magnetic near-field scanning for EMI test,” *IEEE Trans., Antennas and Propag*.}, vol. 56, no. 6, pp. 1335-1343, Dec. 2014.

[15] K. Sarabandi J. Choi, A. Sabet and K. Sabet, “Pattern and gain characterization using nonintrustive very-near-field electro-optical measurements over arbitrary closed surfaces,” *IEEE Trans., Electromagn. Compat*., vol. 65, no. 2, pp. 489-497, Feb. 2017.

[16] E. Ohashi and H. Arai, “Estimation method of directivity on array antennas by using 1D electric current distribution,” *International Symposium on Antennas and Propagation (ISAP 2014)*, pp. 291-292, Dec. 2014.

[17] J. Litva, T. K. Y. Lo, *Digital beamforming in wireless communications*, Artech House, 1996.

[18] R. Yamaguchi, Y. Kimura, K. Komiya and K. Cho, “A far-field measurement method for large size antenna by using synthetic aperture antenna,” *European Conference on Antennas and Propagation (EuCap 2009)*, pp. 1730-1733, March 2009.

[19] FEKO Suite 7.1, http://www.feko.info/

[20] J. A. Hansen, “On cylindrical near-field scanning techniques,” *IEEE Trans., Antennas and Propag*., vol. AP-28, no. 2, pp. 231-234, March 1980.

4 A Fast Far-Field Estimation Method Using Imaginary Cylindrical Near-Field by Reconstructed Partial Source

4.1 Introduction

Near-field measurement technique has a great advantage the view point to reduce the cost of the measurement equipment and environment when to measure and evaluate an antenna radiation performance [1]. In particularly, it has become widely used for manufactured antenna evaluation with the development of the mobile communications. Among them, a planar and cylindrical measurement system is frequently adopted as the base station antenna measurement system they because suitable for electrically large aperture antenna measurements [2]. Reduction of the measurement space and shortening of measurement time in the antenna measurements are general essential desires from of old [3]. Recently, in order to measure antenna performance at high speed, a method to estimate antenna characteristics using only single cut plane has also attracted attention [4]. This method can dramatically reduce the time cost required for measurement because the dimensions of information required for measurement and numerical processing are reduced. It is also known that by scanning a large number of probes, it is possible to boldly reduce the probe scanning time and shorten the total measurement time [5], [6].

In the cylindrical [7], [8] or planar [9] near-field measurements, physically large antennas are often apply as an Antenna Under Test (AUT), thus how to measure in a small space is also an important subject. In addition, it is basically necessary to decide the sampling interval of near-field satisfying the Nyquist sampling theorem, reducing the number of measurement points by increasing the measurement interval is numerically limited. Therefore, reduction the number of measurement points by shrinking the measurement area is directly effective for shortening the time required for measurement and numerical processing. However, we cannot ignore the error caused by finite truncation of measurement area in the cylindrical and planar measurement domains [10]. Accurate near-field measurements request that to perform the measurement in a sufficiently large space respect to the size of AUT, it will be strong restriction on economic cost. In order to efficiently test the base station antenna where huge amounts will be produced in the future, we are asked to measure near-field information in an area as small as possible, and evaluate the radiation performance at high speed with practical enough accuracy.

A method using the conjugate gradient method based on the equivalent magnetic current approach has been proposed as a reduction technique to improve the truncation error in finite area measurement system [11]. It is shown that the high accurate far-field pattern can be obtained in wide angle region by calculate far-field using reconstructed magnetic currents on an aperture plane from measured electric field. It should also be noted that another truncation reduction technique has been

recently developed [12], [13]. In these methods, the distribution outside the measurement region is extrapolated using coefficients obtained from Shannon-Whittaker's interpolation formula; it is applicable with cylindrical and planar domains [14]. Although a far-field with a high accuracy was achieved in an extremely wide angle range, the study of the application kinds of the AUT is insufficient. Further, what is common to these methods is that the measurement region is configured larger than the aperture length of the AUT. It is common sense to set the measurement region to be larger than the aperture of the AUT in the near-field measurement. If the measurement region is smaller than the AUT aperture, an enormous error occurs which cannot be said that it is said a simple truncation error. Conversely, if the far-field can be estimated using the near-field data of the measurement region shorter than the AUT length, the measurement time of the array antenna can be drastically shortened and also the measurement requested space can be reduced.

In this chapter, we will take a cylindrical near-field measurement domain and to consider the case where the measurement length is shorter than the AUT aperture length. We assuming as the precondition that a linear array antenna is constituted by a one-dimensional array of elements of the same shape, and also use the fact that the radiation field from each element has high correlation. Radiation field is regenerated from the partial equivalent source reconstructed using measured near-field, and the radiation field under the unmeasured area is corrected based on the radiation field distribution under the measurement area. By calculate the summation of the measured near-field and corrected field under unmeasured area, the near-field distribution that the same length as the AUT aperture length is reincarnated from measurement distribution shorter than the AUT length.

This chapter is organized as follows. 4.2 defines measurement domain and typical measurement scenario. Following above, we describe the method of near-field reincarnation using partial equivalent source distribution. 4.3 evaluates the effectiveness of the proposed method by numerical simulations. In this section, a typical dipole array of vertical/horizontal polarization, a beam tilt array, a cosine distributed linear array antenna, and an array antenna including faults in a part of constituent elements are taken up as AUT, and we show that the proposed method performs effectively and the main beam can be accurately estimated. In 4.4, the proposed method is applied to base station antenna measurements, In 4.4, the proposed method is applied to base station antenna measurements, and it is shown that the maximum directivity in the vertical plane can be estimated sufficiently accurate for practical use when the actual measurement length is 3/4 of the AUT length or 1/2, respectively. The conclusions are provided in 4.5.

4.2 Method

Before explaining the proposed method, we define the measurement domain to be handled in this chapter and the features of the AUT. This chapter assumes long linear array antenna in one-dimension as shown in Figure 4.1 as the AUT. The AUT is placed on the z-axis. The AUT is

formed by linearly arranging a multiple radiating elements and the physical shape and feeding position of each element are made the same. In other words, when paying attention the radiation field from each element, its amplitude and the relative phase patterns are considered to have high correlation among all the elements. In designing the base station antenna, this assumption holds generally widely because of it is difficult to calculate theoretically the far-field from the array factor, and there is a drawback in economic using different shape antenna for each array element. Let us consider that to measure the near-field distribution around the AUT cylindrically. We must to finite discontinue the measurement in *z*-axis direction by mechanical restriction, the truncation error is occurring by this factor. In this chapter, it is assumed that this measurement cylinder is shorter than the AUT length due to such constraints. Let us suppose the cylindrical equivalent surface *C* containing the AUT inside the measurement cylinder, the electromagnetic field on the equivalent surface is replaced as equivalent current [14]

$$\begin{aligned} \boldsymbol{J} &= \hat{\mathbf{n}} \times \boldsymbol{H} \\ \boldsymbol{M} &= \boldsymbol{E} \times \hat{\mathbf{n}} \end{aligned}, \tag{4.1}$$

Where we assuming a perfect electrical conductor as the medium of the equivalent surface and assuming that the electromagnetic field inside the surface is 0, only the equivalent magnetic current exists on the equivalent cylinder and is given as follows [15],

$$\boldsymbol{M} = 2\boldsymbol{E} \times \hat{\mathbf{n}} . \tag{4.2}$$

Electric field on the measurement cylinder *C*' is supposed as radiation from the equivalent magnetic current, the following equation is given as

$$\boldsymbol{E}(\mathbf{r}) = -2\int_C \nabla \times \boldsymbol{M}(\mathbf{r}')G(\mathbf{r},\mathbf{r}')dC \tag{4.3}$$

$$G(\mathbf{r},\mathbf{r}') = \frac{e^{-jk_0|\mathbf{r}-\mathbf{r}'|}}{4\pi|\mathbf{r}-\mathbf{r}'|}. \tag{4.4}$$

According to (4.3) the following matrix equation is obtained

$$\begin{bmatrix} E_1 \\ \vdots \\ E_m \end{bmatrix} = \begin{bmatrix} A_{11} & \cdots & A_{1n} \\ \vdots & \ddots & \vdots \\ A_{m1} & \cdots & A_{mn} \end{bmatrix} \begin{bmatrix} M_1 \\ \vdots \\ M_n \end{bmatrix}. \tag{4.5}$$

Therefore, the equivalent current distribution can be reconstructed by solve (4.4).

Next, for reduction of the measurement time and simplify the calculation, we consider only one-dimensional electric field distribution along the z-axis direction and reconstruct the linear equivalent magnetic current distribution along the z-axis direction. Ignoring the pattern fluctuation in the azimuth direction and considering it as omnidirectional in the horizontal plane, the electric field distribution on the measurement line *L'* is considered as the radiation from the equivalent magnetic current source on the equivalent line *L* as follows

$$\boldsymbol{E}(\mathbf{r}) = -4\pi d \int_L \nabla \times \boldsymbol{M}(\mathbf{r}')G(\mathbf{r},\mathbf{r}')dL \tag{4.6}$$

Naturally, (4.6) does not hold under actual measurement environment, because AUT has directivity in the horizontal plane. However, taking the product of the coefficient matrix of the equation (4.6) and the equivalent magnetic current distribution, the measured value on the measurement line can be regenerated. In the proposed method, the distribution of the non-measurement edge part is regenerated by correcting the near-field distribution calculated from the reconstructed magnetic current distribution. The subject of discussion is only the distribution in the vertical plane, thus we ignore the variation in the horizontal plane and consider only the vertical plane. Although this assumption holds because we improving only the estimation accuracy of the far-field, it does not hold if antenna diagnosis is performed using the reconstructed source. It is necessary strictly setting the cylindrical surface.

Next step, we consider to expand the near-field on the measurement line against to *z*-axis direction. The z positive region in *zx* cut plane of the measurement system is shown in Figure 4.2, the AUT, measurement line, and equivalent line are presented. The measurement line is shorter than the AUT length; on the other hand, the reconstruction line is the same length as the AUT aperture length. We focus on electric field on the measurement line radiated by a part of equivalent magnetic current. In $z_2 \leqq z \leqq z_3$ region is defined as L_D and also $z_1 \leqq z \leqq z_2$ region is defined as L_A. The maximum length of the AUT is $2z_3$ and measurement length is $2z_2$, and then $z_3 - z_2 = z_2 - z_1$. The radiation field on the measurement line from $\boldsymbol{M} \in L_D$ reconstructed by (4.6) is lead as

$$\boldsymbol{E}_D(\mathbf{r}) = -4\pi d \int_{z_2}^{z_3} \nabla \times \boldsymbol{M}(\mathbf{r}')G(\mathbf{r},\mathbf{r}')dz \tag{4.7}$$

(4.6) is equal to calculating the radiation component from $\boldsymbol{M} \in L_D$. A characteristically pattern is represented on the *L'*. The radiation component from $\boldsymbol{M} \in L_D$ on *L'* is accurately reproduced in $|z| \leqq z_2$ (i.e. under measured area), however in $|z| > z_2$ (i.e. under non-measured area) a distribution with a

remarkably smaller amplitude than the exact amplitude is reconstructed. It causing by the electric field above the L_D assumed as 0 in the stage of reconstruction of equivalent magnetic current. Further, radiation to measurement line from $\boldsymbol{M} \in L_A$ find similarly

$$\boldsymbol{E}_A(\mathbf{r}) = -4\pi d \int_{z_1}^{z_2} \nabla \times \boldsymbol{M}(\mathbf{r}') G(\mathbf{r}, \mathbf{r}') dz \tag{4.8}$$

The radiation field from the partial source generates accurate electric field in $|z| \leqq z_2$. More specifically, the radiation component $\boldsymbol{E} \in L'_A$ from $\boldsymbol{M} \in L_A$ in the region $z_1 \leqq z \leqq z_2$ can reconstruct the true value. Here, following approximation is established from high correlation between radiation elements as mentioned first.

$$E(z) \in L'_D \approx E(z_2) \in L'_D \frac{E(z - z_2 + z_1) \in L'_A}{E(z_1) \in L'_A} \tag{4.9}$$

This approximation is based on the fact that the radiation in the front direction from $\boldsymbol{M} \in L_A$ has high correlation with the radiation in front direction from $\boldsymbol{M} \in L_D$ and that $\boldsymbol{E} \in L'_D$ at z_2 can be obtained accurately. In order to collapse this approximation, it is necessary to configure the AUT with elements of different shape intentionally or to adopt unequally spaced array as the AUT configuration. Both of these are lead increasing manufacturing cost, this approximation formula is well satisfactory in practice. Finally calculating the sum of the measured electric field distribution and the regenerated electric field distribution under non-measured area, it is possible to reincarnate the electric field which is the same length as the AUT aperture from the measurement electric field distribution shorter than the AUT aperture.

The far-field in the vertical plane of the AUT is estimated by applying the near-field far-field transformation using the linear electric field distribution expanded using the proposed method. The length of the measurement area that can be expanded by this method is same as the AUT length. The valid angle in the vertical plane is 0°, and we cannot obtain strict far-field including sidelobe. However, it is possible to accurately estimate the maximum directivity and the main beam pattern which is most important for the performance evaluation of the base station antenna, because of the distribution within the AUT aperture region is obtained. From this fact, the proposed method is suitable for evaluating radiation performance at very high speed in a small scale measurement region. It is desirable to perform precise near-field measurement again for its AUT and to evaluate the accurate radiation characteristics if clear deficiencies are found from the estimated far-field by the proposed method.

We emphasis to radiation accuracy of estimated mainbeam, the far-field pattern in $\theta = 90° \pm 30°$.

The directivity in vertical plane of this region is adopted as the criteria for evaluation as

$$D(\theta_0,\phi_0)=\frac{2\pi\left|E(\theta_0,\phi_0)\right|}{\int_0^{2\pi}\int_{\frac{1}{3}\pi}^{\frac{2}{3}\pi}\left|E(\theta,\phi)\right|\sin\theta d\theta d\phi}. \tag{7.10}$$

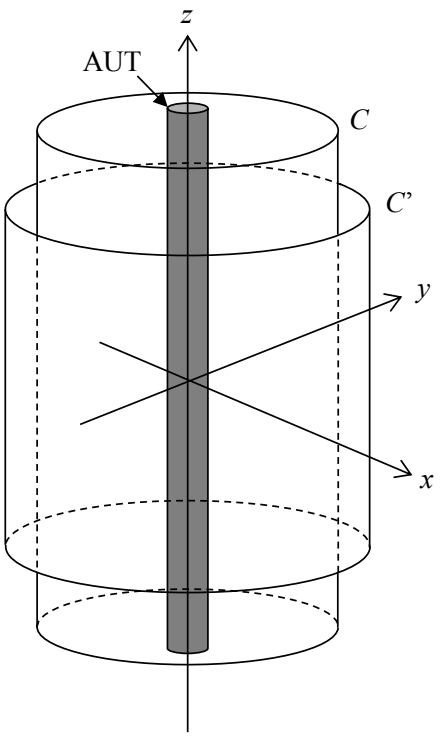

Figure 4.1: Short length cylindrical measurement and reconstruction cylinder.

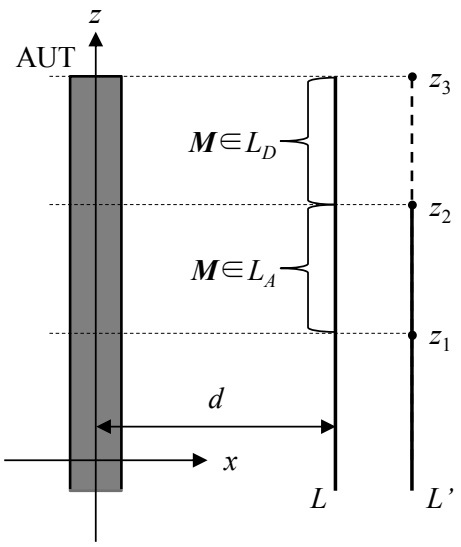

Figure 4.2: Partial source on reconstruction line

4.3 Simulation

4.3.1 Vertical and Horizontal Polarization Dipole Array

In this section, we show the effectiveness of the proposed method and its application range by numerical simulation. As a first study, we adopt a dipole array as an AUT. The AUT is configured from 8 elements dipole and the all elements are uniformly excited. Calculation frequency is 3 GHz and the length of the AUT is 8λ. The AUT is placed as Figure 4.1. Electric field distribution as length of $-3\lambda \leqq z \leqq 3\lambda$ is obtained at location 9λ from the AUT for x-axis direction. A reconstruction line as length of $-4\lambda \leqq z \leqq 4\lambda$ is set at the location of λ for the -x direction from the measurement line. Paying attention to z positive region, z_1 is $z = 2\lambda$, z_2 is $z = 3\lambda$, and z_3 is $z = 4\lambda$, also the L_A means $3\lambda \leqq z \leqq 4\lambda$ and L_D means $3\lambda \leqq z \leqq 4\lambda$. It means the measurement area has been cut as 1/4 against to the size of AUT. The interval of the sampling points is constant as 0.1λ.

We simulate the case of z-axis polarized dipole is arranged. Electric field distribution that was regenerated from $\boldsymbol{M} \in L_A$ and $\boldsymbol{M} \in L_D$ is shown in Figure 4.3. The radiation $z_2 \leqq z \leqq z_3$ from $\boldsymbol{M} \in L_D$ in reconstructed near-field is largely depressed. This is recovered by corrects according to the proposed method. The reincarnated near-field distribution on the measurement line obtained by adding the calculated field distribution is shown in Figure 4.4. For comparison, an example of uncorrected radiation field is also presented. When correction is not performed, computed field is smaller than the exact amplitude under non-measurement area. The phase distribution is also disagreement with the exact distribution such as it monotonically rotates to the lagging phase starting from the measurement edge. This is because the computation assumes L_D region is no radiation

source area. The proposed method corrects these degradation both amplitude and phase and improves the reproduction accuracy of the exact distribution. It means that the proposed method executing effectively.

Results of the estimated far-field using regenerated near-field distribution as mentioned are shown in Figure 4.5. It can be seen that the main beam width wider than the exact pattern when without regeneration of the radiation field, because the original measurement length is shorter than the AUT length. Along with this, the maximum directivity in the vertical plane is calculated as greatly reduced. The accuracy of estimation is improved by using the proposed method, and correct main beam is reproduced. This method cannot expand to the same length as the AUT aperture; in addition the reincarnated distribution is approximated value. Therefore, although it is impossible to strictly reproduce around the sidelobes, the maximum directivity that most important for evaluating the characteristics of the base station antenna can be accurately estimated.

Figure 4.6 shows the estimated far-field when the AUT is composed by horizontal polarized dipoles. The measurement scenario is the same as the case of the vertical polarization AUT. Improvement of the mainbeam pattern estimation accuracy can be confirmed as in the vertical AUT case. From these, the polarization independence of the proposed method was shown.

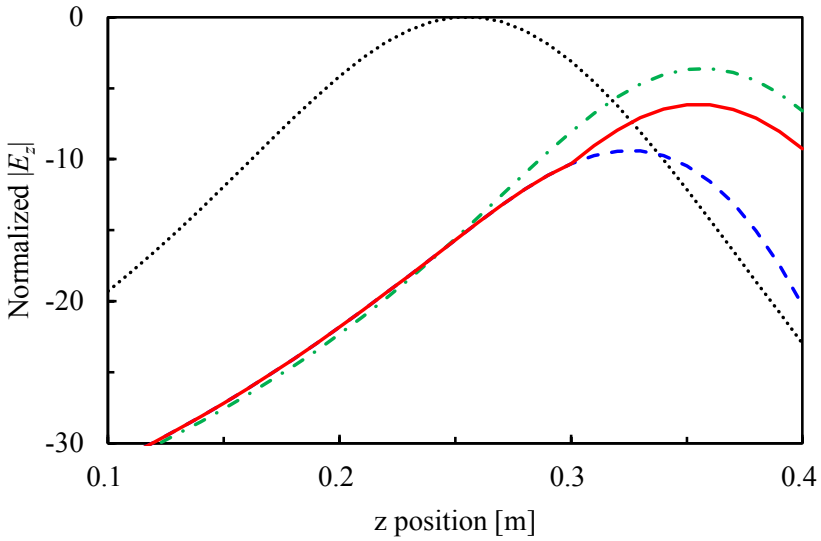

Figure 4.3: Radiation field from partial source. The solid line represents compensated field, the break line represents radiation from partial source under unmeasured area, the chain line is its exact radiation field and the dotted line represents the radiation field from partial source under measured area.

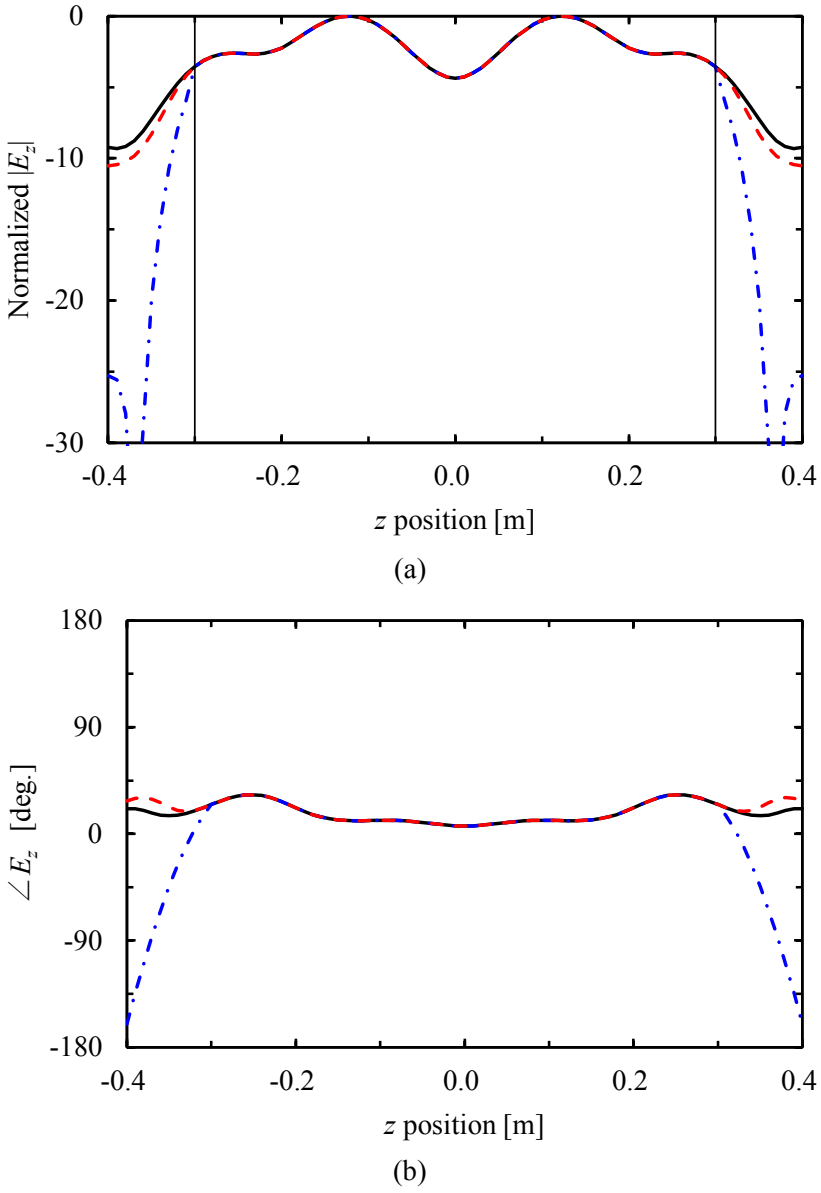

Figure 4.4: Electrical field distribution on the measurement line. The solid line represents the exact distribution, the dotted line represents the supplemented field and the chain line represents the non-supplemented field.

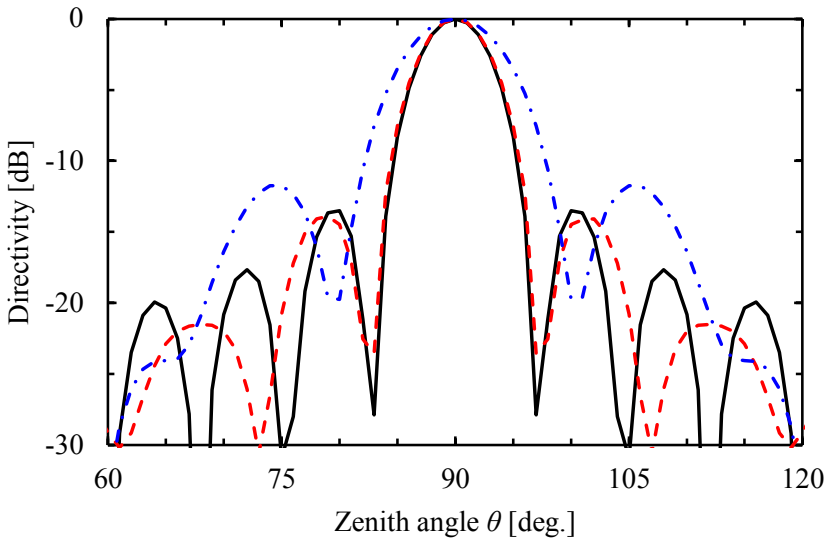

Figure 4.5: Estimated vertical cut far-field of vertical polarization array. The solid line represents the exact pattern, the dotted line represents the pattern using proposed technique, and the chain line represents the conventional method.

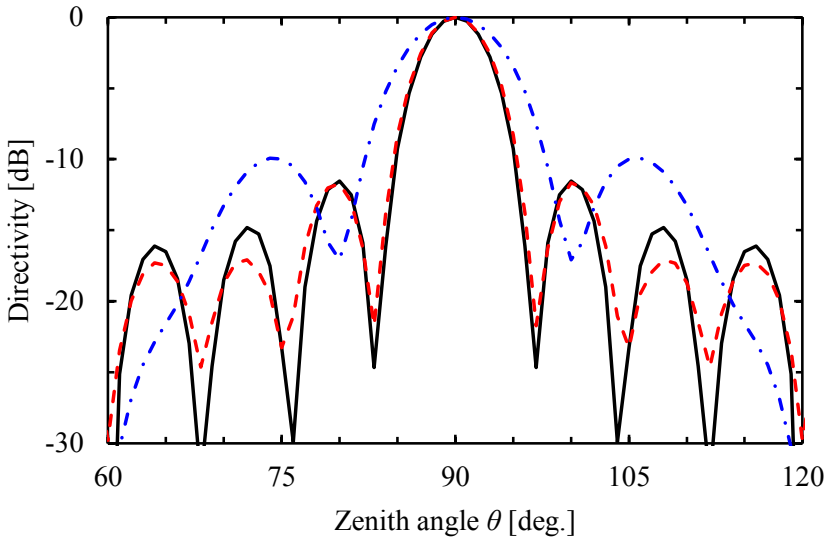

Figure 4.6: Estimated vertical cut far-field of horizontal polarization array. The solid line represents the exact pattern, the dotted line represents the pattern using proposed technique, and the chain line represents the conventional method.

4.3.2 Patch Array

A patch array antenna is used as next AUT. Slant polarized patch antennas are arranged in the z-axis direction and acquire the electric field distribution at the position of 6λ distance from the AUT for the x-axis direction. The sampling length is $-2\lambda \leqq z \leqq 2\lambda$, a reconstruction line of $-4\lambda \leqq z \leqq 4\lambda$ is set at a position of -0.5λ in the x-axis direction from the measurement position. In this case, the measurement length is cut as 1/2 of the AUT aperture. The sampling interval is constant as 0.1λ. The estimated far-field in vertical plane is shown in Figure 4.7. The beam width is estimated to be quite wider than the reference pattern when without using the proposed method, since it is equivalent to the case that the AUT aperture size is only half of the actual aperture. The maximum directivity also calculated far from the exact value. This problem is solved by using the proposed method, the mainbeam is produced accurately. From this, it was confirmed that this method performs effectively even if the radiation pattern of the AUT is asymmetrical in the horizontal plane.

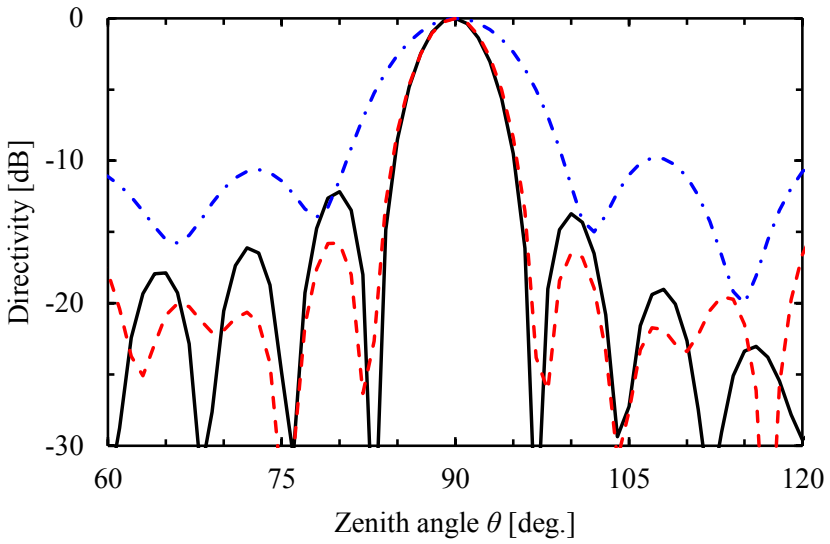

Figure 4.7: Estimated vertical cut far-field of patch array. The solid line represents the exact pattern, the dotted line represents the pattern using proposed technique, and the chain line represents the conventional method.

4.3.3 Beam-Tilt Array

A beam tilt array antenna is adopted as the AUT. Slant polarization dipole antenna is used as the radiating element, and the maximum radiation direction is tilted by 5° by the feeding phase gradient of each element. The excited amplitude is uniformly. Measurement location is $x = 5\lambda$, the measurement length is $-3\lambda \leqq z \leqq 3\lambda$, and the size of the AUT aperture is $-4\lambda \leqq z \leqq 4\lambda$. The sampling interval is constant as 0.2λ. The estimated far-field in vertical plane is shown in Figure 4.8.

Obviously, the proposed method effectively performs for beam tilt antenna. Nulls are filled; it is because the near-field that should be acquired in cylindrical shape is obtained linearly.

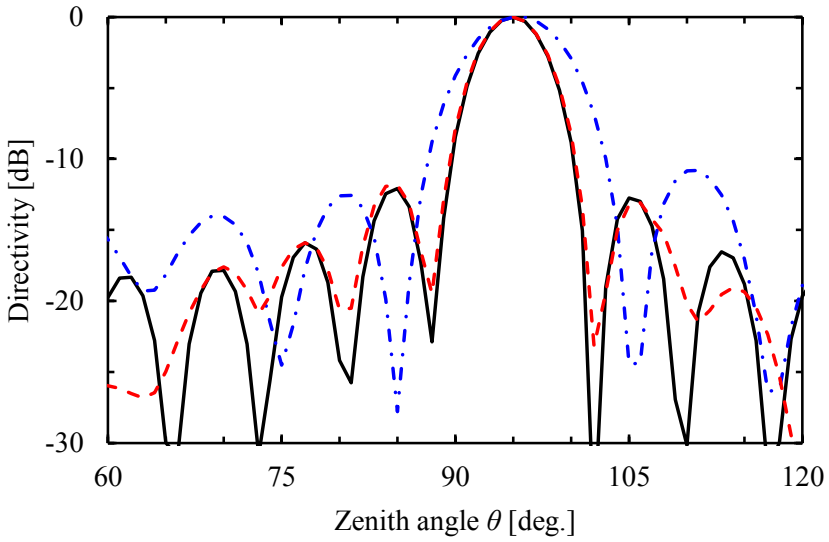

Figure 4.8: Estimated vertical cut far-field of beam-tilt array. The solid line represents the exact pattern, the dotted line represents the pattern using proposed technique, and the chain line represents the conventional method.

4.3.4 Taper Excitation Array

An example of an AUT in which the sidelobe is suppressed with the feeding amplitude of the array element as a cosine distribution is shown. The measurement specification is the same as the beam tilt antenna case. The estimated far-field in vertical plane is shown in Figure 4.9. We can see that the proposed method is effectively performed even if the excitation amplitude is tapered. When the feeding amplitude at the AUT end is small, the effect of truncation error is small. However, even in this case, we can see that the estimation accuracy should be improved by using the proposed method.

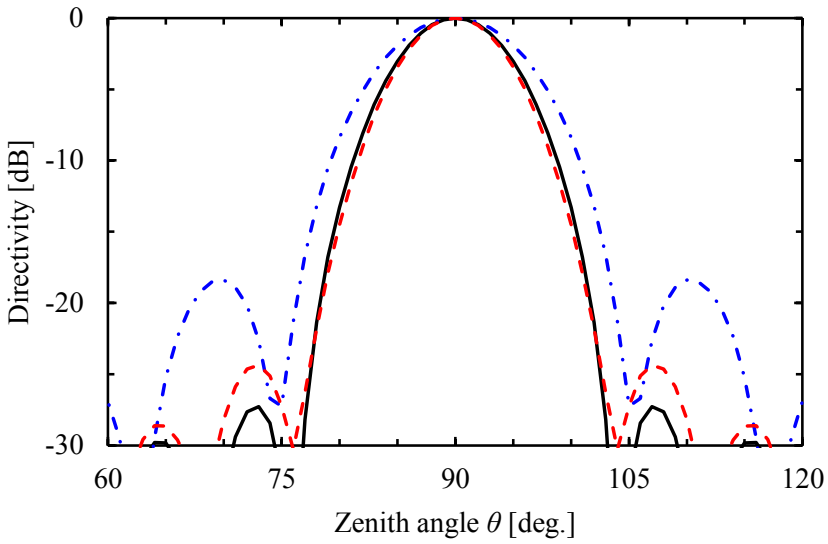

Figure 4.9: Estimated vertical cut far-field of taper excited array. The solid line represents the exact pattern, the dotted line represents the pattern using proposed technique, and the chain line represents the conventional method.

4.3.5 Antenna Diagnostics

The final numerical example is the case of a broken element is used in the AUT. The AUT is composed from the array of slant polarization dipole. Two elements at the positive edge of the z-axis are terminated at 50 Ω, and other elements are fed with uniform amplitude and phase. The distance between the AUT and measurement location is 6 λ , the measurement length is $-2\lambda \leqq z \leqq 2\lambda$, and the size of the AUT aperture is $-4\lambda \leqq z \leqq 4$. That is, the actually measured area is only above the element that is not terminated. The estimated far-field is shown in Figure 7.10. Figure 7.10 also presents the far-field in the case of all elements is excited uniformly. The proposed method can estimate the far-field pattern when the elements are terminated. From this fact, it is possible to recognize the fault of the AUT correctly even by using the near field extended by the proposed method.

Table 4.1 shows the maximum directivities of the AUT adopted above. The error of the maximum directivity in the vertical plane is achieving within 0.25 dB in each case. In the horizontal polarization case and the beam tilt case, the estimation accuracy is slightly degraded because the correlation between radiation elements is reduced due to mutual coupling of elements. The effective valid angle will reduced as the distance between the measurement surface and the AUT becomes larger, and when the cut amount of the measurement region is large, the error increasing. It is better to measure with a long measuring length and to measure in close to AUT as much as possible.

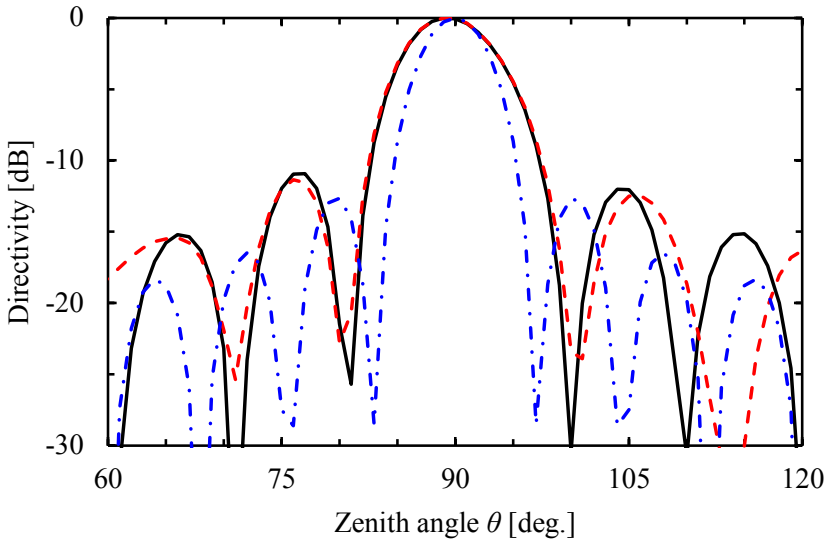

Figure 4.10: Estimated vertical cut far-field of loaded array. The solid line represents the exact pattern, the dotted line represents the pattern using proposed technique, and the chain line represents the exact pattern of full-excited array case.

Table 7.1 Estimated directivity in vertical cut plane.

	Reference [dB]	Estimated [dB]	Difference [dB]
V-pol.	13.14	12.98	0.16
H-pol.	12.27	12.03	0.24
Patch	13.13	13.31	0.18
Tilt	12.45	12.22	0.23
Taper	11.70	11.80	0.10
Load	10.52	10.35	0.17

4.4 Experiment

Following numerical evaluation in previous section, we confirm the validity of calculation. As an AUT, a base station antenna for mobile communications is used. The polarization is slant. The distance between the AUT and near-field measurement location is 100 mm. The estimated far field when the measured length of the near field is 3/4 and 1/2 of the AUT length are shown in Figure 4.11. The far-field cannot be determined correctly as in the past numerical calculation when not using the proposed method. The proposed method certainly solves this problem; the main beam is reproduced accurately. The measurement area of 3/4 cut case is larger than the 1/2 cut case, we can see that its estimation accuracy of the far-field is better and the first side lobe can be accurately reproduced. If the evaluation item is only main beam shape, we can reduce the measurement length shorter than the

half of the AUT length. In order to accurately estimate between first side lobes, it should to be measure in longer than 3/4 of the AUT length. Table 4.2 shows the maximum directivity in vertical plane of these cases. For obtaining the accuracy within 0.15 dB, it should be set the measurement length longer than the 3/4 of the AUT length. On the other hand, if the error allowed up to 0.5 dB, we can reduce the measurement area by half of the AUT length.

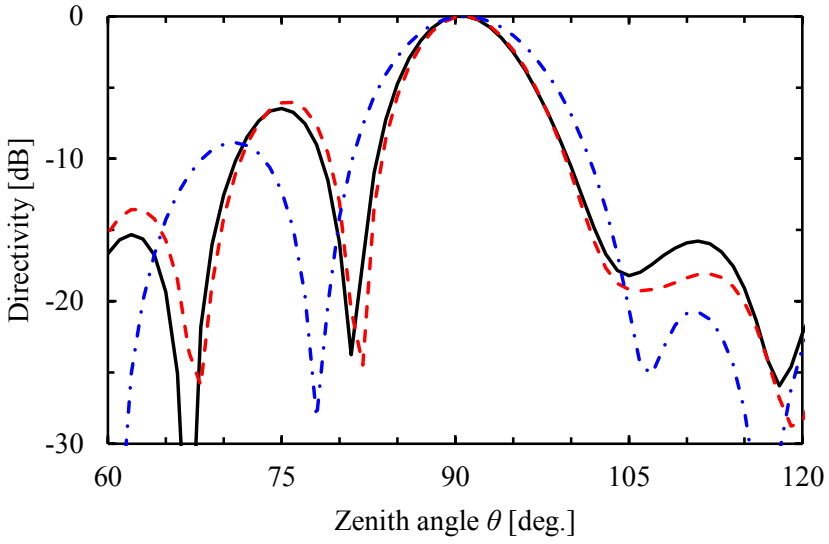

(a)

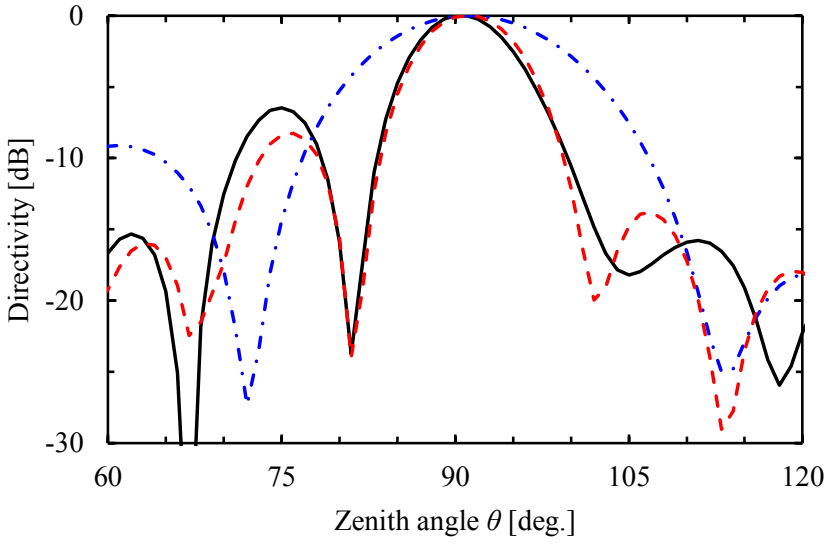

(b)

Figure 4.11: Estimated vertical cut far-field from measured near-field data. The solid line represents the exact pattern, the dotted line represents the pattern using proposed technique, and the chain line represents the conventional method.

Table 7.2 Estimated directivity using measured data.

	Frequency [GHz]	Reference [dB]	Estimated [dB]	Difference [dB]
Quarter cut	0.79	9.15	9.27	0.12
	0.81	9.79	9.90	0.11
	0.96	10.40	10.49	0.09
Half cur	0.79	9.15	9.56	0.41
	0.81	9.79	10.12	0.33
	0.96	10.40	10.79	0.39

4.5 Summary

This chapter proposed the super-fast far-field measurement method for linear array antenna using short length near-field distribution. The proposed method corrects the radiation field from reconstructed partial source, regenerates the near-field distribution the same size as the AUT aperture. The linear array antenna with various distributions was taken up as an example of numerical analysis and the effectiveness of this method was shown. It is shown that the estimated maximum directivity in the vertical plane was achieved within 0.25 dB errors with respect to the reference value. Furthermore, we applied this method to the measured near-field data of the base station antenna. In the case of the measurement area is 3/4 of the AUT aperture size, the estimation error was achieved within 0.15 dB, and in addition, the case of 1/2, the error was achieved within 0.5 dB. It is possible to measure the far-field in the vertical plane of the linear array antenna by near field measurement in a quite small space. From the application of the proposed method, it can be expected to dramatically shorten the measurement time required for measuring the radiation performance of electrically large aperture array antenna.

Reference

[1] A. D. Yaghjian, “An overview of near-field antenna measurements,” *IEEE Trans., Antennas and Propag*., vol. AP-34, no. 1, pp. 30-45, Jan. 1986.

[2] F. L. Heras, M. R. Pino, S. Loredo, Y. Alvarez and T. K. Sarkar, “Evaluating near-field radiation patterns of commercial antennas,” *IEEE Trans., Antennas and Propag*., vol. 54, no. 8, pp. 2198-2207, Aug. 2006.

[3] D. Slater, *Near-field antenna measurements*, Artech House, 1991.

[4] R. Cornelius, T. S. Ruiz, F. Saccardi, L. Foged, D. Heberling and M. S. Castañer, “A comparison of different methods for fast sigle-cut near-to-far-field transformation,” *IEEE Antennas and Propag. Magazine*, vol. 56, no. 2, Apr. 2014.

[5] J. C. Bolomey, B. J. Cown, G. Fine, L. Jofre, M. Mostafavi, D. P.icard, J. P. Estrada, P. G. Friederich and F. L. Cain, “Rapid near-field antenna testing via arrays of modulated scattering probes,” *IEEE Trans., Antennas and Propag*., vol. 36, no. 6, pp.804-814, June. 1988.

[6] L. J. Foged, L. Scialacqua, P. Noren and F. Herbiniére, “Fast measurements and diagnostics on radar antennas using compact cylindrical NF range,” *Proc*. *European Conference on Antennas and Propag. (EuCap 2013)*, pp.2930-2933, Apr. 2013.

[7] W. M. Leach Jr and D. T. Paris, “Probe compensated near-field measurements on a cylinder,” *IEEE Trans., Antennas and Propag*., vol. AP-21, no. 4, pp.435-445, July 1973.

[8] J. A. Hansen, “On cylindrical near-field scanning techniques,” *IEEE Trans., Antennas and Propag*., vol. AP-28, no. 2, pp.231-234, Mar. 1980.

[9] A. C. Newell, “Error analysis techniques for planar near-field measurements,” *IEEE Trans., Antennas and Propag*., vol. 36, no. 6, pp. 754-768, June 1988.

[10] P. Petre and T. K . Sarkar, “Planar near-field to far-field transformation using an equivalent magnetic current approach,” *IEEE Trans., Antennas and Propag*., vol. 40, no. 11, pp. 1348-1356, Nov. 1992.

[11] O. M. Bucci, G. D’Eila and M. D. Migliore, “A new strategy to reduce the truncation error in near-field/far-field transformations,” *Radio Sci*., vol. 35, no. 1, pp. 3-17, Jan.-Feb. 2000.

[12] O. M. Bucci and M. D. Migliore, “A new method for avoiding the truncation error in near-field antennas measurements,” *IEEE Trans., Antennas and Propag*., vol. 54, no. 10, pp. 2940-2952, Oct. 2006.

[13] J. C. Bolomey, O. M. Bucci, L. Casavola, G. D’Eila, M. D. Migliore and A. Ziyyat, “Reduction of truncation error in near-field measurements of antennas of base-station mobile communication systems,” *IEEE Trans., Antennas and Propag*., vol. 52, no. 2, pp. 593-602, Feb. 2004.

[14] S. R. Rengarajan and Y. R. Samii, “The field equivalence principle: Illustration of the establishment of the non-intuitive null fields,” *IEEE Antennas and Propag. Magazine*, vol. 42,

no. 4, pp.122-128, Aug. 2000.

[15] T. K. Sarkar and A. Taaghol, “Near-field to near/far-field transformation for arbitrary near-field geometry utilizing an equivalent electric current and MOM,” *IEEE Trans., Antennas and Propag*., vol. 47, no. 3, pp. 566-573, Mar. 1999.

5 A Method of Decomposition Inverse Estimation for Surface Current Under Interference Wave Conditions Using Dual Surface Electromagnetic Field

5.1 Introduction

Source reconstruction method by inverse problem is an effective technique for antenna diagnostics or visualizing electromagnetic field, because we can know analytically electromagnetic field derived from a wave source if we know an electromagnetic distribution in finite area. This method assumes a equivalent source on the finite area as a estimation target. Its equivalent source distribution is estimated inversely by solve a boundary integral equation composed from the source distribution and electromagnetic field around the source [1]. Inverse problem analysis falls into ill-posed problem depending on measurement and estimation conditions, it has been pointed out it may not be obtained accurate solution [2], [3], Inverse problem analysis has been pointed out it may not be obtained accurate solution, because it falls into ill-posed problem depending on measurement and estimation conditions. However an arbitrary shape surface including the source can be set as the estimated area and the equivalent electromagnetic current on the surface and very near-field can be estimated [4]. Making the best use of this, source reconstruction is expected not only measurement of antenna characteristics but also identification of unnecessary radiation point in EMC test and use as electromagnetic field imaging method [5], [6].

In the inverse problem analysis, the boundary integral equation of the measurement electromagnetic field is solved to obtain the internal source distribution. However, when electromagnetic waves from the outside of the measurement area are contaminated in the measuring electromagnetic field, external incident waves are also false recognized as radiation from the internal wave source, the distribution is inversely estimated, and it becomes impossible to obtain a correct solution. It is known that if the noise mixed in the measurement data is a complicated distribution such as random noise, even if the noise is sufficiently smaller than the radiation field, it causes a great error in the estimation result [7]. Reduction for the effects from the interference and reflection waves is one of the most important subjects for not only inverse problem but also in general electromagnetic field measurement.

The most common and effective technique for eliminate external incident wave in electromagnetic field measurements are to measure the electromagnetic field in an anechoic chamber. Interference and reflection waves contaminating measurement field can be reduce if electromagnetic wave can be measure in an anechoic chamber in which the wall is completely shielded and the absorption characteristics of the wall absorber are guaranteed. However a huge anechoic chamber is

required to measure a physically large antenna and to reconstruct including a big object such as cars and aircraft. Also, even if measurement in anechoic chamber, it is impossible to make the reflected wave completely zero, we must to remove the disturbance from outside by some processing. A means to reducing incident waves from direction other than the internal source by use a directional antenna such as horn antenna as measurement probe is basic technique. There is a drawback with this method, the coupling between the source and the probe becomes a problem, since an electrically large antenna is used as the probe [8]. In order to acquire the external field intensity as small as possible with respect to the internal field amplitude, it is desirable to measure the electromagnetic field in the close to the internal source using an electrically small probe, and to eliminate external fields by numerical processing. If the information on the interference wave is known to some extent, it can be remove the outside field by numerical process in k-field [9], [10]. However, considering the actual measurement environment, it is not easy to know the interference wave information in advance because interference waves are incident from all directions, and it is conceivable that interference waves are incident from the same direction as AUT. Thus a method to eliminate the external field component without any prior information on the interference wave is required.

This chapter is organized as follows. 5.2 mentions a problem of source reconstruction method under interference conditions, and proposes a method of decomposition inverse estimation for surface current using dual surface electromagnetic field distribution mixed internal radiation wave and external incident wave. 5.3 shows the numerical results of dual surface reconstruction method for orthogonal axis coordination and spherical coordination. The reconstructed equivalent source distributions with dual surface reconstruction are illuminated in 5.4. 5.5 concludes this chapter.

5.2 Method

Let us consider an arbitrary shape surface S surrounding an unknown source as shown in Figure 5.1. We replace electromagnetic field on the surface S as equivalent electromagnetic source by introducing equivalent principle [11].

$$\begin{aligned} \boldsymbol{J} &= \hat{\mathbf{n}} \times \boldsymbol{H} \\ \boldsymbol{M} &= \boldsymbol{E} \times \hat{\mathbf{n}} \end{aligned} \tag{5.1}$$

where $\hat{\mathbf{n}}$ is the unit normal vector of S. The surface S is present in the free space and no interference source or scattering source exists outside of the S. Magnetic field $\boldsymbol{H}_1(\mathbf{r})$ on an arbitrary point $\mathbf{r}$ outside from the S is derived by radiation from the equivalent source $\boldsymbol{J}_1(\mathbf{r'})$, $\boldsymbol{M}_1(\mathbf{r'})$ as given as [12]

$$\begin{aligned}\boldsymbol{H}_1(\mathbf{r}) &= \int_{S'} \nabla \times \boldsymbol{J}_1(\mathbf{r}')G(\mathbf{r},\mathbf{r})dS' \\ &\quad -\frac{jk_0}{\eta}\int_{S'}\left\{\boldsymbol{M}_1(\mathbf{r}')+\frac{1}{k_0^2}\nabla\nabla\cdot\boldsymbol{M}_1(\mathbf{r}')\right\}G(\mathbf{r},\mathbf{r}')dS'\end{aligned} \tag{5.2}$$

$$G(\mathbf{r},\mathbf{r}')=\frac{e^{-jk_0|\mathbf{r}-\mathbf{r}'|}}{4\pi|\mathbf{r}-\mathbf{r}'|}. \tag{5.3}$$

Where **r'** is position vector of an arbitrary point on the S, η is characteristic impedance of the free space and k_0 is the wavenumber.

Here, assuming that magnetic distribution outside of the surface is known by measurement, (5.2) can be rewrite to a form of linear equation using coefficient matrix of Green's function $\boldsymbol{A}_1$ and unknown equivalent source vector $\boldsymbol{J}_1$ as

$$\boldsymbol{H}_1 = \boldsymbol{A}_1\boldsymbol{J}_1 \tag{5.4}$$

And we can obtain equivalent current distribution by solving this for $\boldsymbol{J}_1$.

In the next step, we consider about case of interference waves are incident to the measurement distribution. Assuming that there is some scattering or interference source on **r"** of the outside of the measurement surface, there is an equivalent source $\boldsymbol{J}_2$(**r"**) and $\boldsymbol{M}_2$(**r"**) are exist on the surface *S"*. The actually obtained magnetic field distribution $\boldsymbol{H}_1$**'**(**r**) can be expressed as follows if we assuming that the radiation field from these equivalent electromagnetic currents is measured simultaneously on the measurement surface,

$$\begin{aligned}\boldsymbol{H}_1'(\mathbf{r}) &= \left[\int_{S'} \nabla \times \boldsymbol{J}_1(\mathbf{r}')G(\mathbf{r},\mathbf{r}')dS' \right.\\ &\quad \left. -\frac{jk_0}{\eta}\int_{S'}\left\{\boldsymbol{M}_1(\mathbf{r}')+\frac{1}{k_0^2}\nabla\nabla\cdot\boldsymbol{M}_1(\mathbf{r}')\right\}G(\mathbf{r},\mathbf{r}')dS'\right] \\ &\quad +\left[\int_{S''} \nabla \times \boldsymbol{J}_2(\mathbf{r}'')G(\mathbf{r},\mathbf{r}'')dS'' \right.\\ &\quad \left. -\frac{jk_0}{\eta}\int_{S'}\left\{\boldsymbol{M}_2(\mathbf{r}'')+\frac{1}{k_0^2}\nabla\nabla\cdot\boldsymbol{M}_2(\mathbf{r}'')\right\}G(\mathbf{r},\mathbf{r}'')dS''\right]\end{aligned} \tag{5.5}$$

If we denote (5.5) as a linear equation as (5.4) with $\boldsymbol{A}_2$ for the Green's function on *S"* and $\boldsymbol{J}_2$ as the external wave source vector, as follows

$$\boldsymbol{H}_1' = \boldsymbol{A}_1\boldsymbol{J}_1 + \boldsymbol{A}_2\boldsymbol{J}_2 \tag{5.6}$$

However, obviously this linear equation is undetermined problem for unknown source vector $\boldsymbol{J}_1$ and $\boldsymbol{J}_2$, thus we cannot obtain the exact solution even if solving (5.6) when the surface *S'* and *S"* are set as estimation surfaces. On the other example, we assume only the inner surface *S'* as the estimation surface and solving (5.6) for $\boldsymbol{J}_1$. The obtained resolution is as

$$\boldsymbol{A}_1^{-1}\boldsymbol{H}_1^{'} = \boldsymbol{A}_1^{-1}\boldsymbol{A}_1\boldsymbol{J}_1 + \boldsymbol{A}_1^{-1}\boldsymbol{A}_2\boldsymbol{J}_2 \tag{5.7}$$

Distribution of $\boldsymbol{A}_2\boldsymbol{J}_2$ projected on the *S'* in addition to $\boldsymbol{J}_1$ is reconstructed on the *S'*. Especially, if $\boldsymbol{J}_2$ is complex distribution, this is a numerical divergence factor in the process of solving the equation, a fatal error is occurring.

It is necessary to increase the number of equations in order to acquire separately the internal and external fields from the measurement field and to obtain only the inherent distribution of each plane. Therefore, let us consider measuring two electromagnetic fields $\boldsymbol{H}\in s_{1\mathrm{R}}$, $\boldsymbol{H}\in s_{2\mathrm{R}}$ between the inner surface $s_{1\mathrm{R}}$ and the outer surface $s_{2\mathrm{R}}$, which are surfaces to be estimated as shown in Figure 5.2. We define $\boldsymbol{J}_1$ is the equivalent current vector on the inner source and $\boldsymbol{J}_2$ is the equivalent current vector on the outer surface as the unknown vector and let the measured magnetic field vector in the measurement planes $s_{1\mathrm{M}}$ and $s_{2\mathrm{M}}$ are $\boldsymbol{H}\in s_{1\mathrm{M/2M}}$ as known vector. When these are formulated with the propagation coefficient matrix given by the Green's function from the estimated surface $s_{m\mathrm{R}}$ to the measured surface $s_{n\mathrm{M}}$ as $\boldsymbol{A}_{mn}$, the following linear simultaneous equations can be formed.

$$\begin{cases} \boldsymbol{H} \in s_{1\mathrm{M}} &= \boldsymbol{A}_{11}\boldsymbol{J}_1 + \boldsymbol{A}_{21}\boldsymbol{J}_2 \\ \boldsymbol{H} \in s_{2\mathrm{M}} &= \boldsymbol{A}_{12}\boldsymbol{J}_1 + \boldsymbol{A}_{22}\boldsymbol{J}_2 \end{cases}. \tag{5.8}$$

The above equation is a necessary and sufficient condition, it is possible to decompose and inverse estimate the respective equivalent surface current distributions $\boldsymbol{J}_{1/2}$ of the respective surfaces from the contaminated field $\boldsymbol{H}\in s_{1\mathrm{M/2M}}$ by solving (5.8) as a partial matrix equation as follows;

$$\begin{bmatrix} \boldsymbol{H} \in s_{1\mathrm{M}} \\ \boldsymbol{H} \in s_{2\mathrm{M}} \end{bmatrix} = \begin{bmatrix} \boldsymbol{A}_{11} & \boldsymbol{A}_{21} \\ \boldsymbol{A}_{12} & \boldsymbol{A}_{22} \end{bmatrix} \begin{bmatrix} \boldsymbol{J}_1 \\ \boldsymbol{J}_2 \end{bmatrix} \tag{5.9}$$

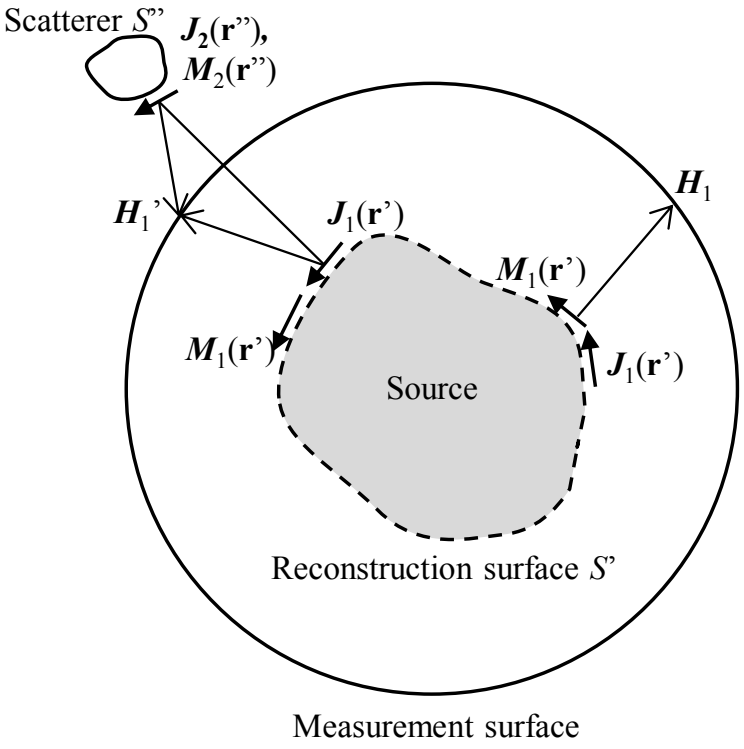

Figure 5.1: Radiation from equivalent currents and interference by a scatterer.

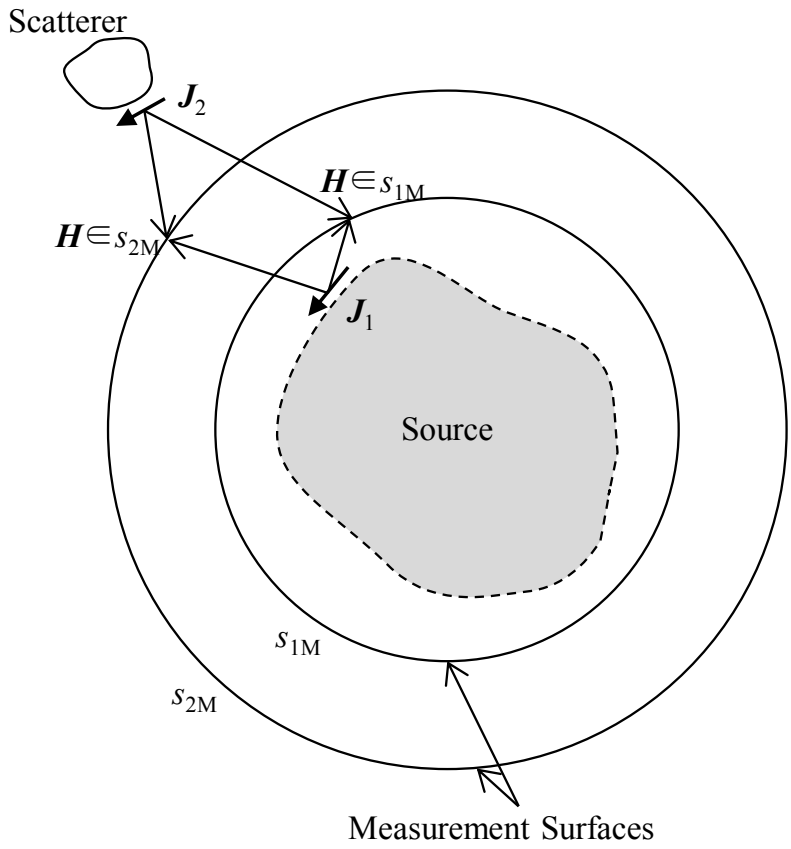

Figure 5.2: Decomposition reconstruction by dual surface measurements.

5.3 Simulation

5.3.1 Planar Measurements

For the first example of numerical simulation, we apply the proposed method to equivalent source distribution in Cartesian coordinates and to clearly the effectiveness of the proposed method. A half wavelength dipole antenna parallel to the z axis direction is placed on the origin as shown in Figure 5.3, and feeding as 1V with the center of the element. Linear half wavelength scatterers (#1, #2) made by the perfect electric conductor is arranged on a plane parallel to the yz-axis, which the distance from the dipole source in the x-axis direction of these dipoles are positive λ. λ is the wavelength of the calculation frequency. In this coordinates systems, measurement planes parallel to the yz-axis are set on the position of $x = 0.4\lambda$, 0.6λ, they are called as s_{1M} and s_{2M} in order from the origin direction. Further as the reconstruction plane of equivalent source, s_{1R} is placed on the $x = 0.2\lambda$, and s_{2R} is placed on the $x = 0.8\lambda$. At the Cartesian coordinates system, the truncation error by finite area measurement in the y- and z-axis direction is reflected in both of the measurement and reconstruction surfaces. If the measurement surface is too large with respect to the estimation surface,

radiation from outside the estimation surface will be reconstructed in the reconstruction source. On the other hand, if the measurement surface is too small relative to the estimation surface, equivalent source cannot be reconstructed accurately. In this chapter, the sizes of the all planes are assumed to be the same, and each measurement plane and estimation plane are set as sizes of $-2\lambda \le y \le 2\lambda$ and $-2\lambda \le z \le 2\lambda$. A sampling interval of the measurement and estimation surface in the y- and z-axis direction is constant as $\Delta y = \Delta z = 0.1\lambda$. We adopt the CGNR [14]-[16] as a matrix equation solver, from the fact of the method is general used as matrix solver in inverse problem analysis [1], [13], and to inverse estimate the source distribution on the reconstruction planes.

Reconstruction results of equivalent electric current amplitude under interference conditions that the only reflection wave is arrived from the outside direction are shown in Figure 5.4. The dipole of #1 and #2 are parasitic. The horizontal and vertical axes mean y- and z-axis, and the brightness of the color in the figure represents the logarithmic representation of the equivalent surface current amplitude A/m. Figure 5.4(a) presents an exact distribution derived using MOM, (b) is a reconstructed result using synthetic magnetic field on s_{1M}, and (c) is a reconstruction result on the s_{1R} and s_{2R} by using magnetic field of 2 surfaces on the s_{1M} and s_{2M} according to the proposed method. Although only J_z is shown in the figure, in the process of solving the matrix equation, J_y is also included in the matrix equation. In Figure 5.4(b), the equivalent current other than the dipole source on the origin appears on the estimated surface, whereas in Figure 5.4 (c) the source distribution almost similar to the reference distribution. It is found that only the internal field component is extracted and the inverse estimation of the internal wave source distribution is performed.

For the next example, we consider the case of the strong interference wave is contaminated to the measurement magnetic field. Strong interference wave incidents to s_{1M} and s_{2M} by feed the dipole of #1 and #2 as 1V. Where the dipoles #1 and #2 are fed the same amplitude and phase as the dipole on the origin, this condition means that the intensity of the external incident field is set to be larger than the internal radiation field by about 3 dB. The reconstruction results of source distribution under the condition are shown in Figure 5.5. Figure 5.5 (a) and (b) present the reference distribution on the s_{1R} and s_{2R}, (c), (d) present reconstructed distribution using only distribution on the s1M, and (e), (f) present reconstructed results according to the proposed method. If using only s_{1M} as measurement surface, radiation waves from the #1 and #2 are appear on the s_{1R}, whereas radiation wave from the dipole on the origin contaminates on the s_{2R}. When using single surface distribution, the reconstructed distributions differ greatly from the reference distributions and it is impossible to reconstruct accurately source distribution unique to each surface. Each distribution can accurately reproduce the reference distribution by the proposed method. Even when interference wave incidents from the outside stronger than the radiation wave from internal source, it is clear that unique distribution both of planes can be decomposed and estimated the respective inherent surface

distribution separately. Incidentally, in this chapter assumes the random noise free environment, when noise other than interference wave occurs randomly in the measurement field, SNR of at least 20 dB is require to accurately reconstruct the internal source distribution. However, since the dynamic range assumed for general near-field measurements [18] or inverse problem analysis is superior to 30 dB [19], we consider the random noise is sufficiently reduced in the proposed method.

Here, SIR is defined as following equation using internal radiation fields $S(s_{1M})$, $S(s_{2M})$ on the s_{1M} and s_{2M} and external incident fields $I(s_{1M})$, $I(s_{2M})$,

$$SIR = \frac{S(s_{1M}) + S(s_{2M})}{I(s_{1M}) + I(s_{2M})}. \tag{5.10}$$

We make clear numerically a relationship between equivalent source estimation accuracy and noise level by relative 2-norm [4] error using reference source distribution $\boldsymbol{J}_1$(Ref.) and estimated source distribution on $\boldsymbol{J}_1$(Est.) the s_{1R}.

$$Norm \quad error = \frac{\left\| \boldsymbol{J}_1(Ref.) - \boldsymbol{J}_1(Est.) \right\|_2}{\left\| \boldsymbol{J}_1(Ref.) \right\|_2} \tag{5.11}$$

The relation between noise level vs estimation error is shown in Figure 5.6. The SIR is changed by feeding voltage of the #1 and #2. The chained horizontal line represents the interference wave free condition. In the case of Figure 5.4, the SIR is about 21 dB, and the case of Figure 5.6 is about -5 dB. It is found that the estimation accuracy almost agrees with the reconstruction result in the free space if SIR $\geq$ 0 dB and the effectiveness of the proposed method are numerically obvious.

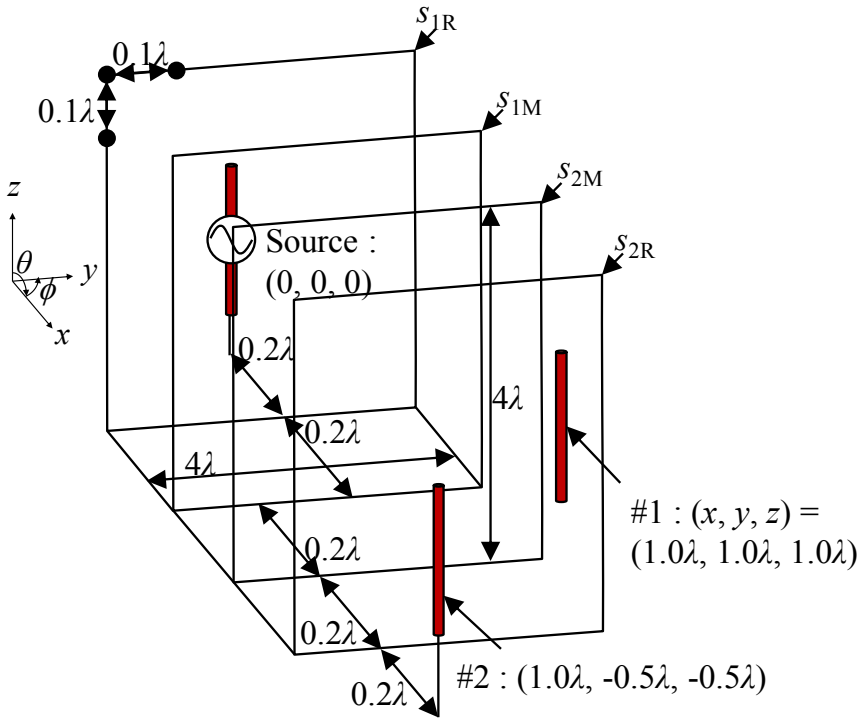

Figure 5.3: Source arrangement in Cartesian coordinates plane.

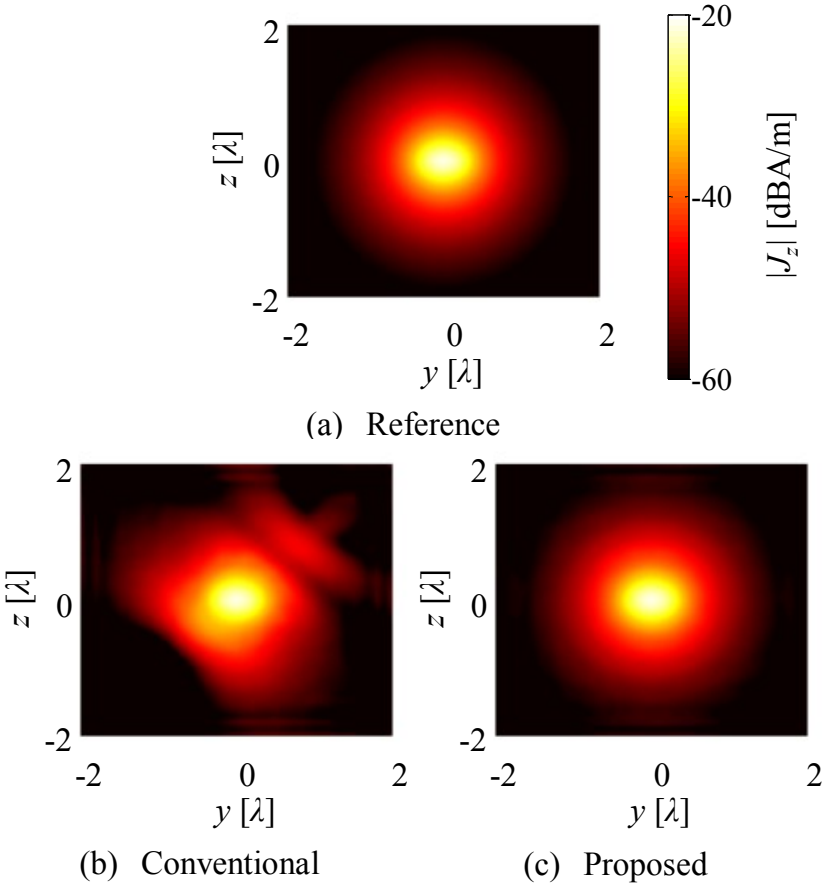

Figure 5.4: Elimination of reflection waves in Cartesian coordinates plane.

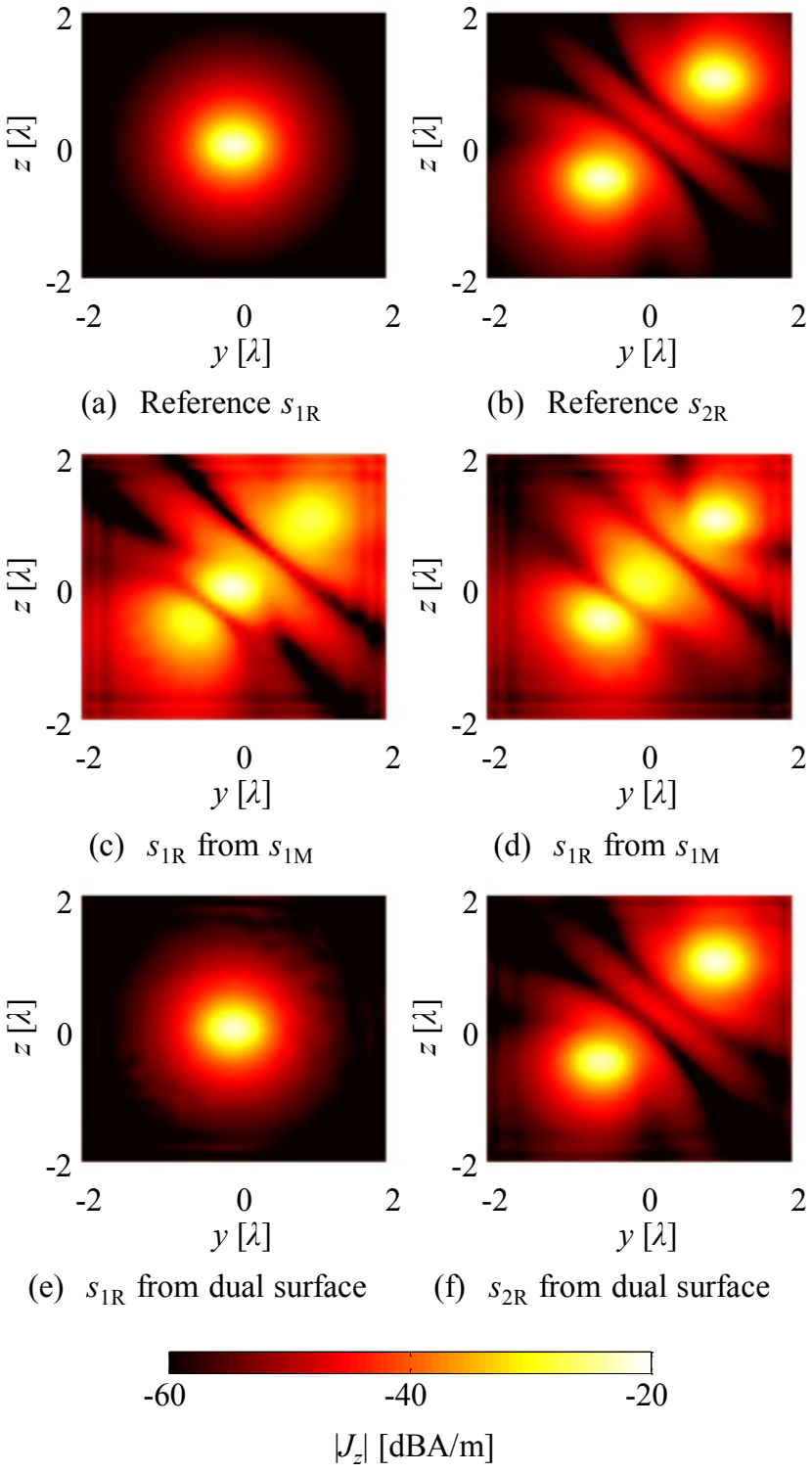

Figure 5.5: Decomposition inverse estimation in interference conditions.

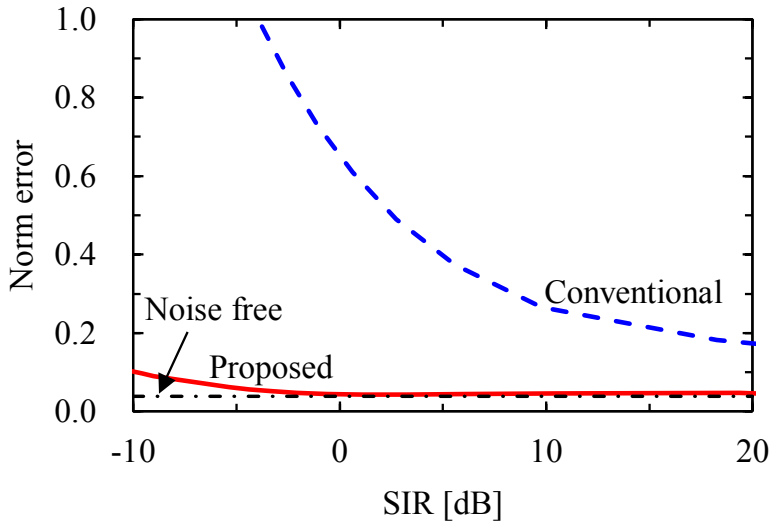

Figure 5.6: Relation between SIR and orm error norm in Cartesian coordination.

5.3.2 Spherical Measurements

For the next simulation, we apply the proposed method to spherical equivalent source distribution. A half wavelength dipole antenna parallel to the z-axis direction is placed on the coordinates origin as internal source shown in Figure 5.7. As the same as the case of Cartesian coordinates system, the source is fed as 1V. Reconstruction sphere s_{1R} of radius 1.0λ and s_{2R} of radius 2.5λ are set, and measurement sphere s_{1M} of radius 1.5$\lambda$and s_{2M} of radius 2.0$\lambda$are set between these spheres. Magnetic field distribution is sampled on the measurement spheres. Sampling interval of all spheres is the same as $\Delta\theta = \Delta\phi = 10°$. In the outside region of s_{2R}, half wavelength linear perfect electrical conductors (#1~#4) are placed parallel to the z-axis direction as scatterer. Scattering waves and interference waves by the scatterers are acquired on the each plane at the same time as the radiation wave from the internal source. The target solution is to reconstruct only the radiation field of the internal source on the internal reconstruction sphere s_{1R} by eliminate external incident wave from scatterers.

Inverse reconstruction results are shown in Figure 5.8. These figures present spherical distribution expanded as planer, the horizontal and vertical axes mean azimuth angle ϕ and zenith angle θ. The color brightness means equivalent magnetic field amplitude of θ component. Here, as in the case of the Cartesian coordinate system, the equation is solved considering not only J_θ but also J_ϕ. In the case of using single measurement sphere, the inverse estimation result is disturbed by the reflected wave incident from the outside, whereas using the dual measurement planes reduces the disturbance on the estimation surface. Inverse estimation results when strong interference wave incidents to the measurement sphere by feeding all scatterers as the same amplitude and phase are

shown in Figure 5.9. Estimated distribution using only single measurement sphere is disturbed greatly, it is impossible to speculate internal source condition from this result. The disturbance is reduced by using dual measurement surface; donut shape radiation field of half wavelength dipole has been reproduced.

Relation between SIR and error norm in spherical source reconstruction is shown in Figure 5.10. Horizontal chained line presents the error norm without interference. The effectiveness of the proposed method in spherical coordinates is obvious. In the case of the spherical reconstruction under the environment where many strong interference waves are incident, it is impossible to strictly decompose the inherent distributions as in the case of the Cartesian coordinates. It because, electromagnetic waves incident to the s1R from the outside re-emerge through the interior sphere, overlap measurements on s_{1M} and s_{2M}, and to misrecognize as radiation from the internal source. However, the size of omnidirectional antenna in which spherical measurement is particularly effective is small, and it is possible to measure in a shield room in many cases. The proposed method is sufficiently effective for spherical source distribution, since it is difficult to consider an environment in which many strong interference waves are incident, it is sufficient to remove only reflected waves from the surroundings.

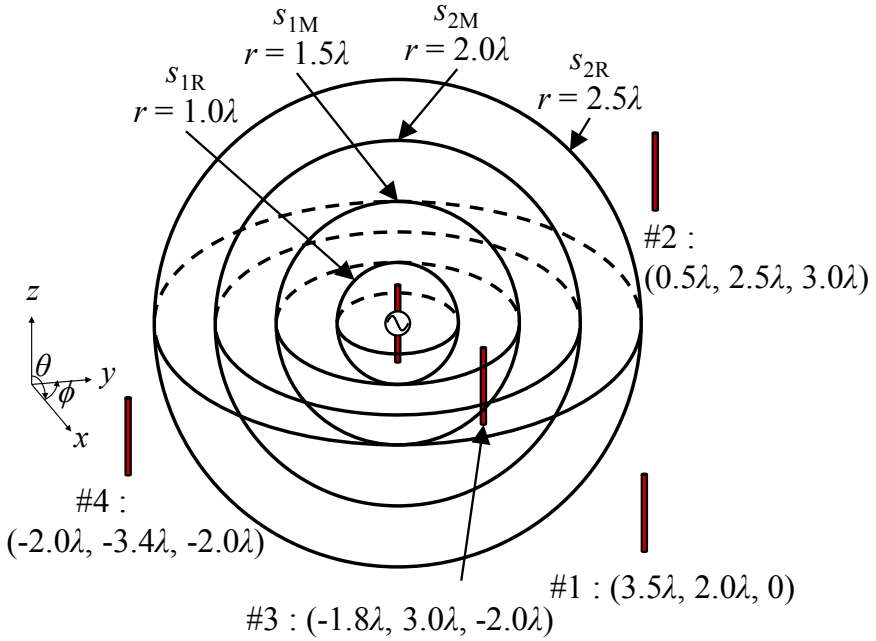

Figure 5.7: Source arrangement in spherical coordination.

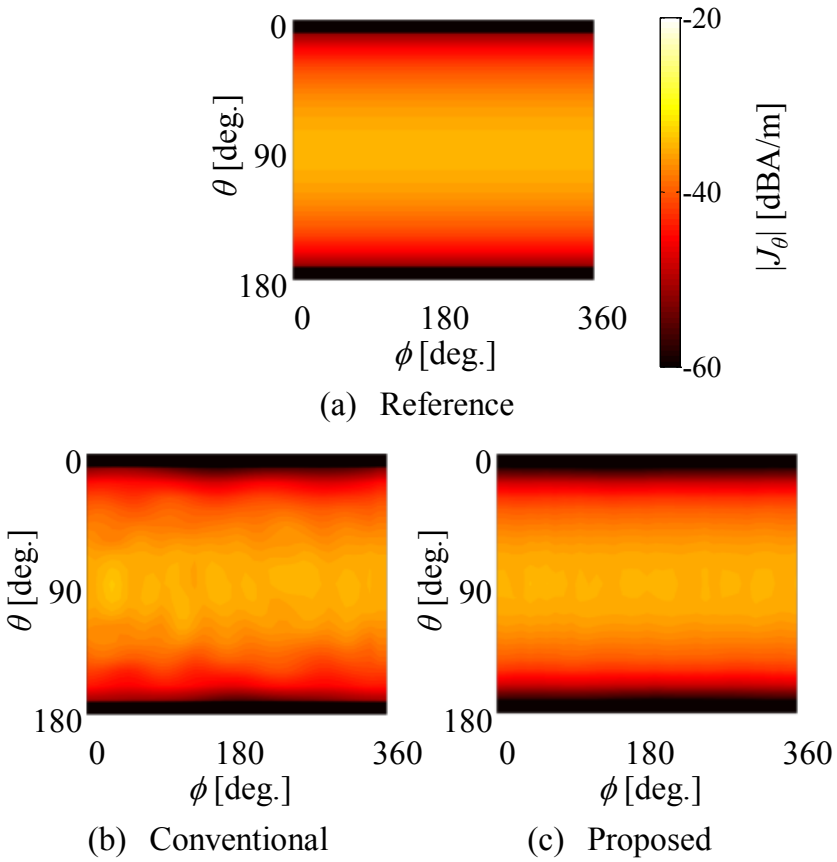

Figure 5.8: Decomposition inverse estimation of spherical source distribution.

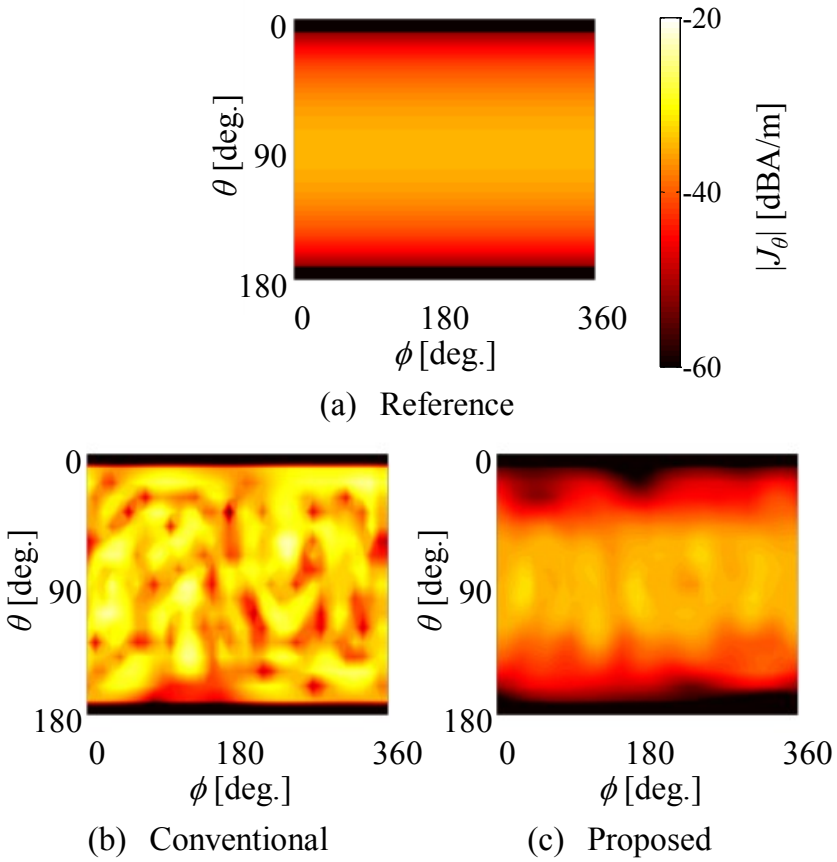

Figure 5.9: Elimination of interference waves on sphere.

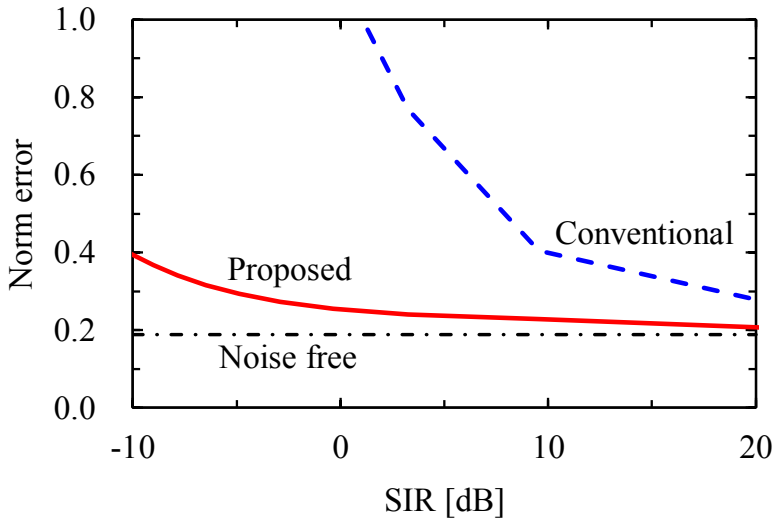

Figure 5.10: Relation between SIR and error norm in spherical coordination.

5.4 Experiment

The effectiveness of the proposed method was clarified numerically in the above section, the internal wave source distribution is separately estimated based on actually measured electromagnetic field information, and the validity of the calculation will mentioned. The overview of the measurement system is shown in Figure 5.11, and measurement specifications are shown in Table 5.1 and 5.2. We use a 2.45 GHz standard dipole antenna as an internal source, and square copper plates the size of 65 mm #1 and 40 mm #2 are placed surround the internal source as scatterer. 4 situations are measured in this experiment. Figure 5.11 (a) is measurement scene of the case 1 and Figure 5.11 (b) is deformed the case 4. When the measurement, the location of the measurement probe is constant on the other hand, the internal source and scatterers are synchronously rotating. For minimize disturbance of electromagnetic field by the probe, non-resonance 5 GHz standard dipole is used as the probe. Coupling between the internal source and probe cannot be eliminated by the proposed method, thus it is desirable to use a measurement probe that is electrically as small as possible. According to (5.1), we can obtain equivalent magnetic distribution as a reference distribution, since electric field affords equivalent magnetic field. Therefore, we estimate equivalent electric equivalent current using magnetic field in numerical analysis, whereas estimate equivalent magnetic current in experiment. In this experimental system, using the symmetry of the radiation of the source, we try to simplify the measurement by orthogonal product approximation of the spherical distribution. Circular measurements in the vertical and horizontal plane are executed and to acquire $\boldsymbol{E}(\theta, \phi = 0°)$ and $\boldsymbol{E}(\theta = 90°, \phi)$, electric field on an arbitrary point $\boldsymbol{E}(\theta' \neq 90°, \phi' \neq 0°)$ is approximated as follows

$$\begin{aligned} E_\theta(\theta',\phi') &= E_\theta(\theta',\phi = 0^\circ)E_\theta(\theta = 90^\circ,\phi') \\ E_\phi(\theta',\phi') &= E_\phi(\theta',\phi = 0^\circ)E_\phi(\theta = 90^\circ,\phi') \end{aligned} \tag{5.12}$$

Incidentally, the dynamic range of the measurement system is about 35 dB, as mentioned above; the influence of random noise is sufficiently negligible.

Equivalent magnetic current amplitudes of ϕ component reconstructed from measured electric field are shown in Figure 5.12. Figure 5.12 (a) is the reference distribution with electric field measured on position 120 mm away from the internal source replaced by equivalent magnetic current. The all figures are normalized by the maximum value of the reference value. Figures in the left side column are reconstructed distributions using electric field only s_{1M}, and in the right side column are using both of s_{1M} and s_{2M}. The estimated distribution is disturbed in single surface reconstruction, when only the scatterer #1 is placed, and each field can be estimated separately by the dual surface measurement. On the other hand, since the scatterer # 2 is electrically small relative to the wavelength of the measurement frequency and the reflected wave intensity is weak, only the

internal field can sufficiently be estimated even with single surface measurement. The two scatters are placed close to the $\theta = 180°$ side in Figure 5.12 (f), (g), and are arranged to shoot sandwiching the source on $\theta = 0°$ と $\theta = 180°$in (h) and (i). Also in these cases, in the measurement using only one surface, the estimated distribution is disturbed, and it is impossible to estimate only the internal field; however the reference value can be well reproduced by using the proposed method. Table 5.3 shows the average amplitude in the $\theta = 90°$ plane in each case when the average amplitude in the horizontal plane of Figure 5.12 (a) is assumed as 0 dB. In all cases, the estimation accuracy of the average amplitude is improved by the proposed method, and the validation of the proposed method was experimentally revealed.

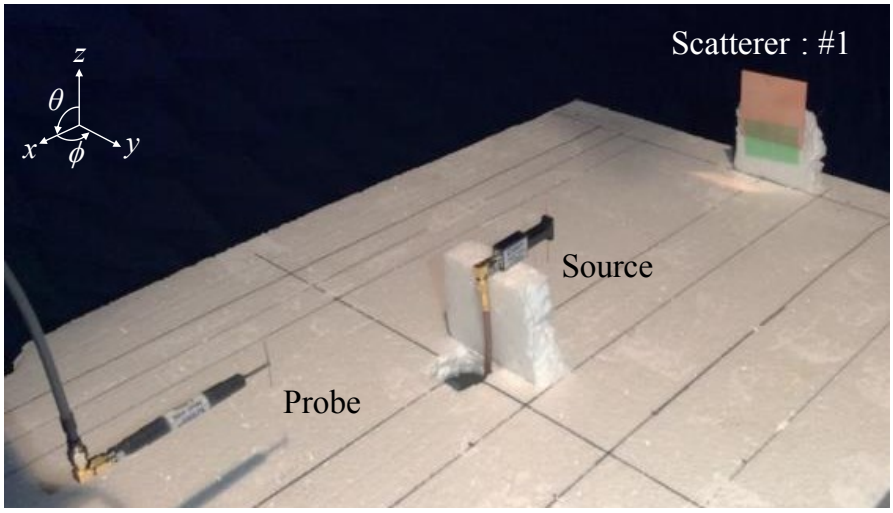

(a) Measurement overview @ case 1

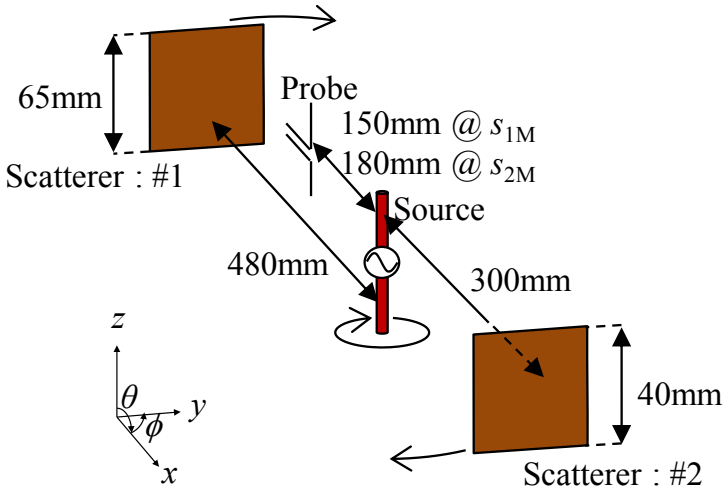

(b) Schematic diagram @ case 4

Figure 5.11: Measurement overview

Table 5.1 Sphere conditions

Case 1	Radius of	s_{1R}	120 mm
		s_{1M}	180 mm
		s_{2M}	240 mm
		s_{2R}	300 mm
Case 2 Case 3 Case 4	Radius of	s_{1R}	120 mm
		s_{1M}	150 mm
		s_{2M}	180 mm
		s_{2R}	210 mm

Table 5.2 Scatter position

Case 1	Position of	#1	(-480 mm, 0 mm, 0 mm)
		#2	NA
Case 2	Position of	#1	NA
		#2	(-480 mm, 0 mm, 0 mm)
Case 3	Position of	#1	(-480 mm, 200 mm, 0 mm)
		#2	(-480 mm, -200 mm, 0 mm)
Case 4	Position of	#1	(-480 mm, 0 mm, 0 mm)
		#2	(300 mm, 0 mm, 0 mm)

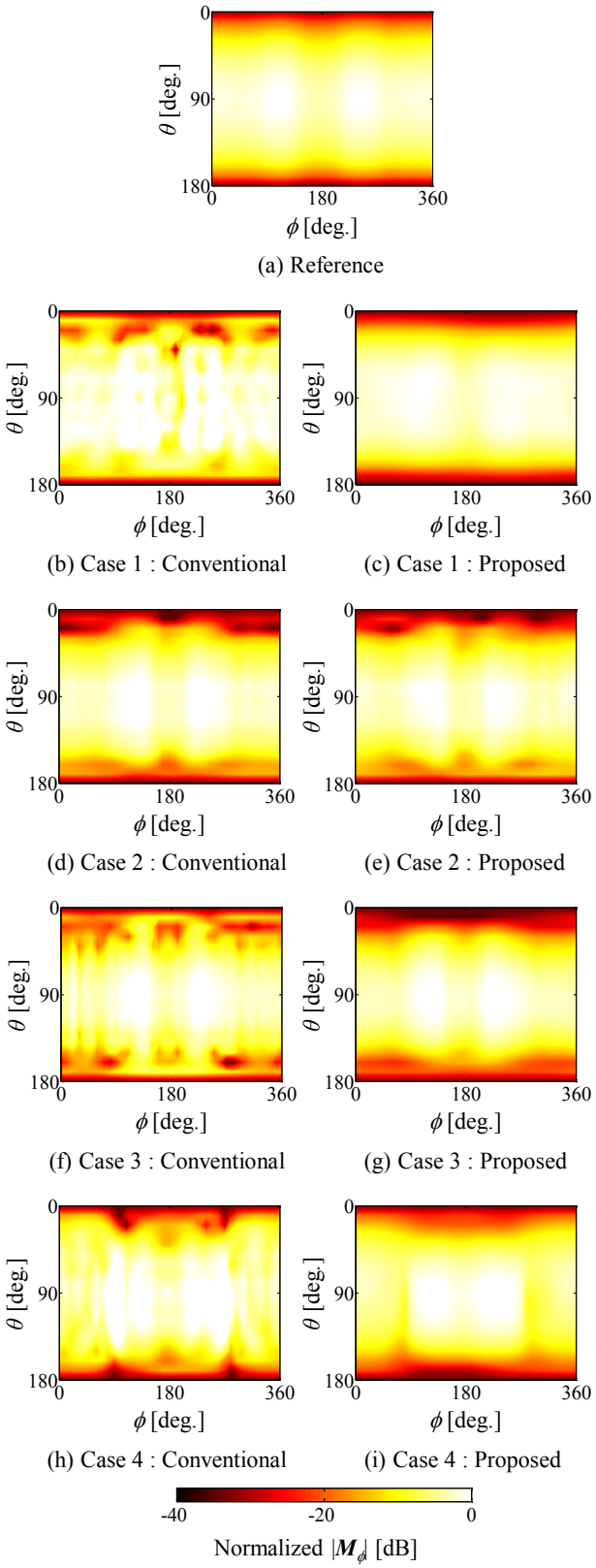

Figure 5.12: Measurement results.

Table 5.3 Average amplitude on horizontal cut plane

Case	Conv. [dB]	Prop. [dB]
Case 1	-0.21	-0.01
Case 2	-0.12	-0.02
Case 3	0.09	-0.06
Case 4	0.54	-0.31

5.5 Summary

A source reconstruction method using dual surface measurements under interference wave conditions was proposed. Introduction, we formulated the inverse problem under interference wave environment using two electromagnetic fields and described the theoretical basis of the proposed method. Subsequently, the proposed method was applied to the source distribution in the Cartesian coordinate plane and the spherical surface in numerical analysis, and the effectiveness of the developed method was clarified. Furthermore, we showed that by approximating the spherical electric field distribution using the circular electric field distribution on two orthogonal planes, it is possible to decompose only internal source distribution from the measured electric field distributions under multi reflection wave environments.

Reference

[1] Y. Álvarez, F. L. Heras and M. R. Pino, “Reconstruction of equivalent currents distribution over arbitrary three-dimensional surfaces based on integral equation algorithms,” *IEEE Trans., Antennas and Propag*., vol. 55, no. 12, pp. 3460-3468, Dec. 2007.

[2] A. J. Devaney and G. C. Sherman, “Nonuniqueness in inverse source and scattering problems,” *IEEE Trans.. Antennas and Propag*., vol. 30, no. 5, pp. 1034-1037, Sept. 1982.

[3] K. Hirota and Y. Kuwahara, “Estimation of current distribution on the plate with complex 3 dimensional shape by the inverse problem,” *IEICE Trans. Commun.*, vol. J98-B, no. 5, pp. 425-432, May 2015.

[4] J. L. A. Quijano and G. Vecchi, “Improved-accuracy source reconstruction on arbitrary 3-D surfaces,” *IEEE Antennas and Wireless Propag. Lett*., vol. 8, pp. 1046-1049, Sept. 2009.

[5] T. K. Sarkar and A. Taaghol, “Near-field to near/far-field transformation for arbitrary near-field geometry utilizing an equivalent electric current and MOM,” *IEEE Trans.. Antennas and Propag*., vol. 47, no. 3, pp. 566-573, March 1999.

[6] Y. Álvarez, M. Rodríguez, F. L. Heras and M. M. Hernando, “On the use of the source reconstruction method for estimating radiated EMI in electronic circuits,” *IEEE Trans., Instrum. Meas*., vol. 59, no. 12, pp.3174-3183, Dec. 2010.

[7] 岩崎, “電磁波の散乱・吸収計測技術の現状と課題,” 電学論 A, vol. 117-A, no. 5, pp. 450-455, 1997.

[8] M. A. Qureshi, C. H. Schmidt and T. F. Eibert, “Comparative probe parameter error analysis with a novel approach for reduced probe-AUT interaction,” *Proc. Annual Meeting and Symposium of the Antenna Measurement Techniques Association.*, Oct. 2012.

[9] G. E. Hindman and A. C. Newell, “Reflection suppression in a large spherical near-field range,” *Proc. Annual Meeting and Symposium of the Antenna Measurement Techniques Association*, Oct. 2005.

[10] S. Gregson, A. C. Newell and G. Hindman, “Reflection suppression in cylindrical near-field antenna measurement system –cylindrical mars,” *Proc. Antennas & Propag. Conference LAPC*, Nov. 2009.

[11] J. A. Kong, *Electromagnetic wave theory 2nd ed*., John Wiley & Sons, 1990.

[12] J. A. Stratton, *Electromagnetic theory*, McGraw-Hill, 1941.

[13] S. Omi, T. Uno and T. Arima, “A study about inverse equivalent current estimation,” *IEICE Technical Report*, A・P2016-98, Sept. 2016.

[14] M. R. Hestenes and E. Stiefel, “Methods of conjugate gradients for solving linear systems,” *Journal of Research of the National Bureau of Standards*, vol. 45, no. 6, pp. 409-436, Dec. 1952.

[15] Y. Saad, *Iterative methods for sparse linear systems 2nd ed.*, SIAM, 2003.

[16] W. C. Gibson, *The method of moments in electromagnetics*, Chapman & Hall/CRC, 2008.

[17] EEM-MOM, http://www.e-em.co.jp/

[18] D. Slater, *Near-field antenna measurements*, Artech House, 1991.

[19] J. L. A. Quijano and G. Vecchi, "Near- and very near-field accuracy in 3-D source reconstruction," *IEEE Antennas and Wireless Propag. Lett*., vol. 9, Sept. 2010.

6 A Method to Estimate Far-Field Using Phaseless Planar Near-Field Measurements with Probe-Positioning Errors Compensation

6.1 Introduction

Near-field measurement that can characterize the radiation performance of antenna under test (AUT) using an area close to the source has great benefits in evaluating the far-field for reducing the cost of measurement systems [1]. With the recent trend toward developing of higher-frequency communication, an increasing attention is given to techniques measuring planar near-field to evaluate manufactured electrically large aperture antennas.

Near-field to far-field transformation methods require both amplitude and phase distributions in a near-field region [2]. In high-frequency bands, accurate vectorial measurements are difficult due to the uncertainty of the measurement phase. The removal of phase measurements in phaseless techniques is an economically challenging topic for near-field measurements [3], [4]. Phase resurrection techniques using various phaseless near-field measurement techniques are studied due to the effectiveness in high-frequency measurements [5]. These methods measure over two surfaces of amplitude-only data to estimate the exact phase distribution by initializing phase some arbitrary distribution and iteratively performing the forward/backward propagation between the measured two surfaces [6], [7]. The far-field estimation method that incorporated these phase resurrection techniques is very effective for high-frequency near-field measurements, in which, it is usually difficult to avoid phase uncertainty.

Measurement errors caused by probe misaligned are unavoidable in high frequency measurements. In high-frequency bands, misalignment can cause serious errors in the measured values because even a slight physical misalignment of the probe is regarded as unacceptable technical error. Probe-positioning error is indicated as among the most predominant kind of error in near-field measurements [8]-[10]. The probe-positioning error in near-field measurements can be studied in depth when the error values are known [11], [12]. With the introduction of devices for obtaining error information, the cost of measurement system will increase. In addition, amplitude-only measurements have better resilience to probe-positioning errors than the amplitude-phase measurements; however, the estimated far-field will certainly deteriorate due to positioning errors. Moreover, probe-positioning errors occur due to misalignments of the probe and due to discrepancy in the probe jig. If higher-frequency band measurements become mainstream in the future, positioning-error tolerance beyond the conventional phaseless measurement will be required. Thus, techniques that can numerically compensate the probe-positioning errors are required

to estimate far-field pattern and also to distribute correct phase.

This chapter proposes a probe-positioning error compensation method for planar phaseless near-field measurements; also, this paper proposes a far-field estimation method that implements these correction techniques. We have classified the positioning error as errors that occur in random in each measurement point due to the displacement of the probe, and the errors that occur in the depth direction in each measuring surface has been found to be due to the positional displacement of the jig. In the proposed method, the random error in each measurement point is reduced by adding a low-pass filter at wave number space. Depth-direction errors in measurement planes are iteratively compensated using the residual error between measured values and estimated values in the measurement planes. The iteration process captures the exact measured position between measurement planes and presents accurate phase distributions. We evaluate the effectiveness of the proposed method by calculated far-field using measured amplitude distribution and estimated phase distribution.

The chapter is organized as follows. 6.2 introduces the phase resurrection scheme. Following the introduction, the next section models the probe-positioning error and describes the proposed compensation method. 6.3 shows the numerical results of compensation method for planar array antennas. The estimated far-field patterns of simulations with uniform excitation and electrical beam-tilt antenna are demonstrated in this section. 6.4 illustrates phaseless near-field measurement results for planar array antenna in 60 GHz bands. Following 4.4, a conclusion section is provided.

6.2 Method

6.2.1 Phaseless Measurement

In this section, we mention the phaseless measurements techniques. The proposed method resurrects the phase over the measurement surfaces by iterative forward/backward propagation based on the equivalent principle [1], [13]. A phaseless measurements system diagram is shown in Figure 6.1. We assume a closed surface in front of the aperture of the AUT, and two measurement surfaces are placed in front of the aperture. From the equivalent theorem, fields over the aperture plane are replaced with equivalent sources as,

$$\begin{aligned} \boldsymbol{J} &= \hat{\mathbf{n}} \times \boldsymbol{H} \\ \boldsymbol{M} &= \boldsymbol{E} \times \hat{\mathbf{n}} \end{aligned} \tag{6.1}$$

$\hat{\mathbf{n}}$ is normal vector of the aperture surface. The electric field on an arbitrary point $\boldsymbol{E}(\mathbf{r})$ in measurement surface is given by equivalent currents on arbitrary points $\mathbf{r'}$ as

$$\begin{aligned} \boldsymbol{E}(\mathbf{r}) &= -jk_0\eta\int_{S_A}\left\{\boldsymbol{J}(\mathbf{r}')+\frac{1}{k_0^2}\nabla\nabla\cdot\boldsymbol{J}(\mathbf{r}')\right\}G(\mathbf{r},\mathbf{r}')dS_A \\ &\quad -\int_{S_A}\nabla\times\boldsymbol{M}(\mathbf{r}')G(\mathbf{r},\mathbf{r}')dS_A \end{aligned} \tag{6.2}$$

where η is the characteristics impedance in free space and k_0 is the free space wavenumber. $G(\mathbf{r}, \mathbf{r}')$ is the free space Green's function as

$$G(\mathbf{r},\mathbf{r}')=\frac{e^{-jk_0|\mathbf{r}-\mathbf{r}'|}}{4\pi|\mathbf{r}-\mathbf{r}'|}. \tag{6.3}$$

Where in region of $z < 0$ is assumed as Perfect Electric Conductor (PEC), radiation from equivalent electric current on the aperture plane can be assumed to be zero from image theory. Thus we can obtain the electric field distribution over measurement surfaces to consider only equivalent magnetic current on the aperture plane. Let us consider image theory, equivalent magnetic current over an infinite PEC radiate the same fields as twice the magnetic current in free space [13], [14]. Due to these simplifications applying to (6.2) we obtain

$$\boldsymbol{E}(\mathbf{r}) = -2\int_{S_A}\nabla\times\boldsymbol{M}(\mathbf{r}')G(\mathbf{r},\mathbf{r}')dS_A \tag{6.4}$$

We can obtain equivalent magnetic current distribution on the aperture plane by solve this equation with magnetic current. Providing some arbitrary phase distribution on the measurement surface (e.g. uniform distribution), and to iterate forward propagation from aperture plane to measurement planes and backward propagation from measurement planes to aperture plane. Exact phase distribution can be resurrected by doing this iteration while overwriting the amplitude distribution with measured value.

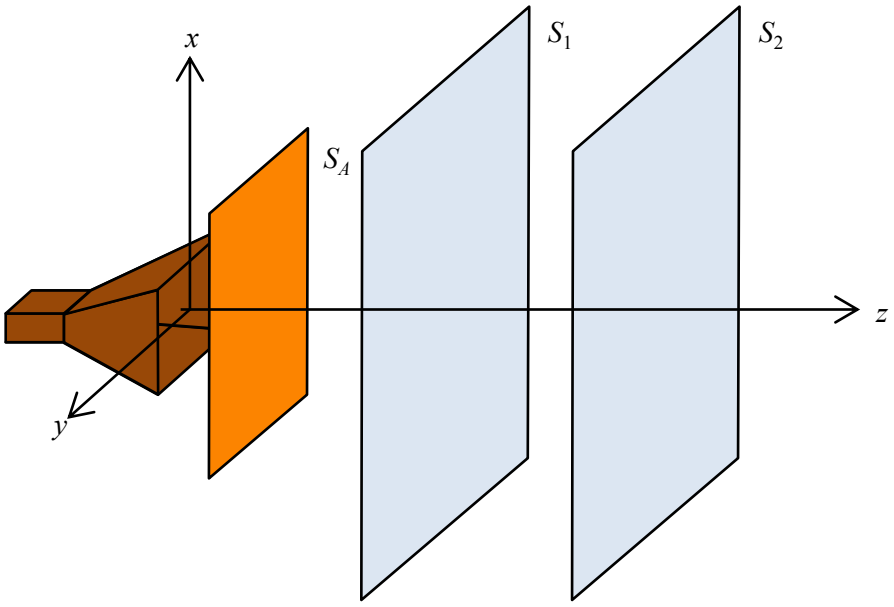

Figure 6.1: Planar near-field measurement system. The electric fields amplitude of the x and y components are measured over S_1 and S_2. The equivalent magnetic currents are reconstructed on aperture plane S_A.

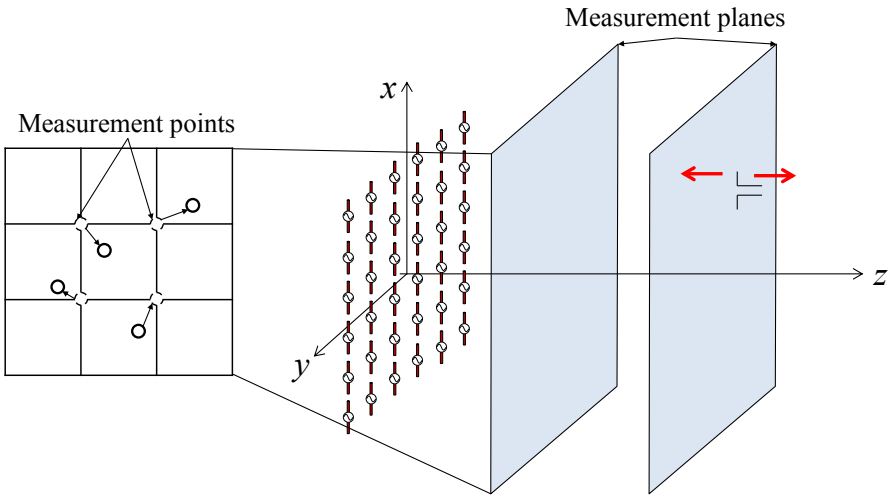

Figure 6.2: Schematic view of Probe positioning error occurrence scenario on the planar near-field measurement domain.

6.2.2 Probe Positioning Error Compensation

In near-field measurements, negative impact by misalignment of measurement devices are inevitable regardless of whether phase measurement is performed or not. The higher measurement frequency the electrically positioning deviation is larger, error of estimated phase distribution and far-field will

increases. The factor of generating the positioning misalignment error is caused by various reasons. For accurate far-field estimation with phaseless near-field measurements, it is important to distinguish error cause and do appropriate compensation. We predict the probe positioning misalignment is occurred due to two factors as shown in Figure 6.2.

The first class of reason is errors occurring randomly in all of the measurement points. It can consider to be occurring by probe vibration when scanning the probe. As a premise of near-field measurements, sampling interval satisfy the Nyquist sampling criteria. If a misalignment vector occurs in parallel to *xy*-plane and uniformly random, its spatial frequency is much higher than electrical field spatial frequency. Focusing on this fact, to 2D Fourier transform the measured distribution thus multiplying a low-pass filter in reciprocal lattice space. In this paper, we assume the cycle of minimum spacial frequency K_s of random error is the same as sampling frequency. Filter characteristics that bandlimits the higher frequency components in reciprocal lattice space are given as follows;

$$F(u,v) = \begin{cases} 1 & (\sqrt{u^2+v^2} < K_s) \\ 0 & (otherwise), \end{cases} \tag{6.5}$$

where u and v are space frequency in x and y directions.

The second class of error cause is related to deviation of measurement plane position. On multi surface measurement of the planar measurement domains, we measure second plane by moving the probe to the depth direction after measured the first plane. When moving the probe to depth direction, it is assumed that an error occurs in the moving distance. If measurement domain included depth error of plane position, phase resurrection term cannot obtain exact phase distribution because mismatch between Green's function for phase resurrection and measured electrical field is arises. This is due to the fact that the distance ratio of forward propagation and backward propagation is incorrect. In brief, essence of negative impact by depth direction misalignment is misrecognized the distance between measurement surfaces when calculate the Green's function. We can compensate enough accurately the depth positioning error without some process with measured data if we know correct distance between two surfaces.

We consider the case that the distance between two measured planes false recognized as narrower than exact distance. Amplitude over S_2 transformed from S_1 after phase retrieval is smaller than the measured one, on the other hand over amplitude of S_1 reconstructed from S_2 is larger than the measured one. Under broad misrecognized situation, estimated amplitude will be inverse relation. Using these facts, to update the depth direction location of two planes $z(S_1)$, $z(S_2)$ iteratively after phase resurrection process as follows;

$$z_{i+1}(S_1) = \{(1-a)+(1+b)\}\frac{z_i(S_1)}{2} \tag{6.6}$$

$$z_{i+1}(S_2) = \{(1+a)+(1-b)\}\frac{z_i(S_2)}{2} \tag{6.7}$$

where i is iteration counter, a and b is given by

$$a = \frac{\left\|\boldsymbol{E}_{meas.}(S_1)\right\| - \left\|\boldsymbol{E}_{Est.}(S_1)\right\|}{\left\|\boldsymbol{E}_{meas.}(S_1)\right\|} \tag{6.8}$$

$$b = \frac{\left\|\boldsymbol{E}_{meas.}(S_2)\right\| - \left\|\boldsymbol{E}_{Est.}(S_2)\right\|}{\left\|\boldsymbol{E}_{meas.}(S_2)\right\|}. \tag{6.9}$$

$\boldsymbol{E}_{\text{meas.}}(S_1)$ and $\boldsymbol{E}_{\text{est.}}(S_1)$\$ is measured amplitude distribution and reconstructed amplitude distribution after phase retrieval process over the S_1. The exact distance between two planes is derived by iterate the phase resurrection process including above plane location update. Additional information is not unnecessary for applying (6.5) and (6.6), furthermore this techniques will converged under finite attempt.

This paper supposes the planar measurement domain, thus truncation error arise in edge region of each planes. Truncation error has adverse effect to iterative compensation, we restrict the calculation area of (6.7) and (6.8) to the same size as aperture plane. With the restriction, we compensate the plane position while reducing negative impact of truncation of measurement planes.

The total error of estimated far-field is evaluate quantitatively as [7]

$$total \quad error = \frac{\left\|\left|\boldsymbol{E}_{FF}(Ref.)\right| - \left|\boldsymbol{E}_{FF}(Est.)\right|\right\|}{\left|\boldsymbol{E}_{FF}(Ref.)\right|} \tag{6.10}$$

where $\boldsymbol{E}_{\text{FF}}(Ref.)$ is the true far-field electric field and $\boldsymbol{E}_{\text{FF}}(Est.)$ is the far-field computed using phase reconstruction and neaf to far-field transformation from two amplitude distribution with probe compensation error.

6.3 Simulation

We demonstrate validity of the proposed method from numerical results simulated a planar measurement domain. This paper adopts 8 × 8 dipoles planar array as AUT. The center of AUT is placed on the origin, the first measurement plane S_1 is placed at 10 mm to z direction from the origin and the second measurement plane S_2 is placed at 20 mm. Size of each planes are 100 mm^2, and the sampling resolution is 4 mm (approximately 0.4λ). The coplanar random error is generated

uniformly as range in $\sqrt{\left(\Delta x^2 + \Delta y^2\right)} < 4\,\text{mm}$, where Δx and Δy is positioning deviation in x- and y-axis direction. Aperture plane the size of 60 mm^2 is placed on coplanar of the AUT, and the calculation frequency is 30 GHz. The maximum iteration number of phase resurrection is constant as 500, initial phase distribution is given as uniform distribution.

The first case, all elements are excited as uniform amplitude and phase. The relationship between iteration number of proposed compensation technique and recognized distance of measurement planes is shown in Figure 6.3. As the number of corrections increases, the distance between the two planes approaches the exact distance and finally it is asymptotically to the exact value. It does not match perfectly with the reference value, because the truncation error cannot be ignored and sampling points on the aperture plane are discrete. Even taking it into consideration, it can be corrected with sufficiently good accuracy; we can see the proposed method is working properly. Figure 6.4 shows the amplitude distribution and phase distribution over the S_1 after 20th iterative compensation. The amplitude distribution of the proposed side is multiplied the low-pass filter to eliminate the random error. If the probe positioning error including to measured data, both of amplitude and phase distribution has difference with exact distributions. By the proposed methods, these disturbances are removed and it accurately reproduced the reference distributions. The adverse effect of random error mainly appears on amplitude distribution, on other hand depth error affects to phase distribution. Therefore the low-pass filter is effective to amplitude compensation; the iterative compensation is effective to accurate phase resurrection. Estimated far-field patterns by near-field to far-field transformation using these electric field distributions are shown in Figure 6.5, and relative estimation errors in each cut planes are shown in Figure 6.6. As mentioned above, the electric field is not accurately obtained without the proposed compensations, thus estimated far-field pattern is markedly different with the reference far-field. The pattern with the proposed method is good agreement with the reference patterns because the accurate electric field can be obtained. The mean value of relative error with the proposed method in H-plane and E-plane is -35.8 dB and -50.1 dB, without the compensation is -22.4 dB and -31.0 dB. As shown in table 6.1, total error is sufficiently reduced; it is clear the effectiveness of proposed method for the uniformly excited array.

Table 6.1 Total errors in estimated far-field of uniform excited antenna

	Total error
Compensated	0.042
Misaligned	0.194

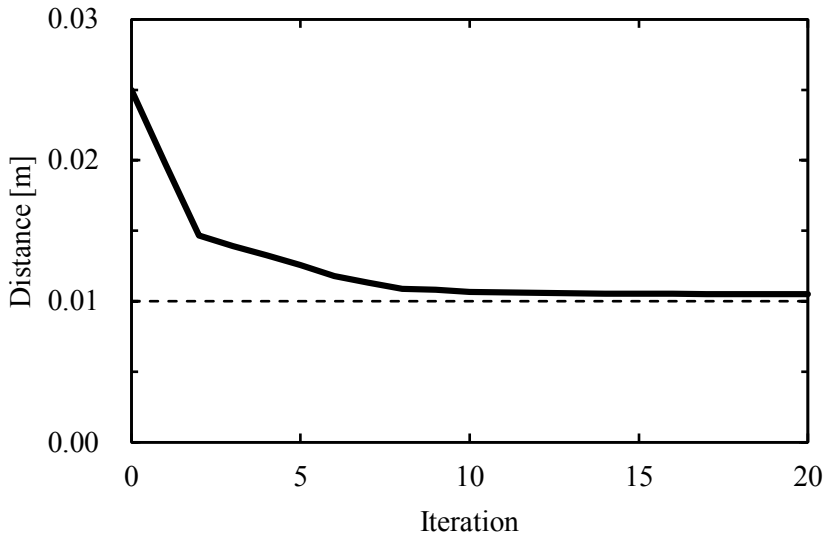

Figure 6.3: Convergence circumstances of distance between two planes recognized by phase resurrection process, the horizontal dotted line is the exact distance.

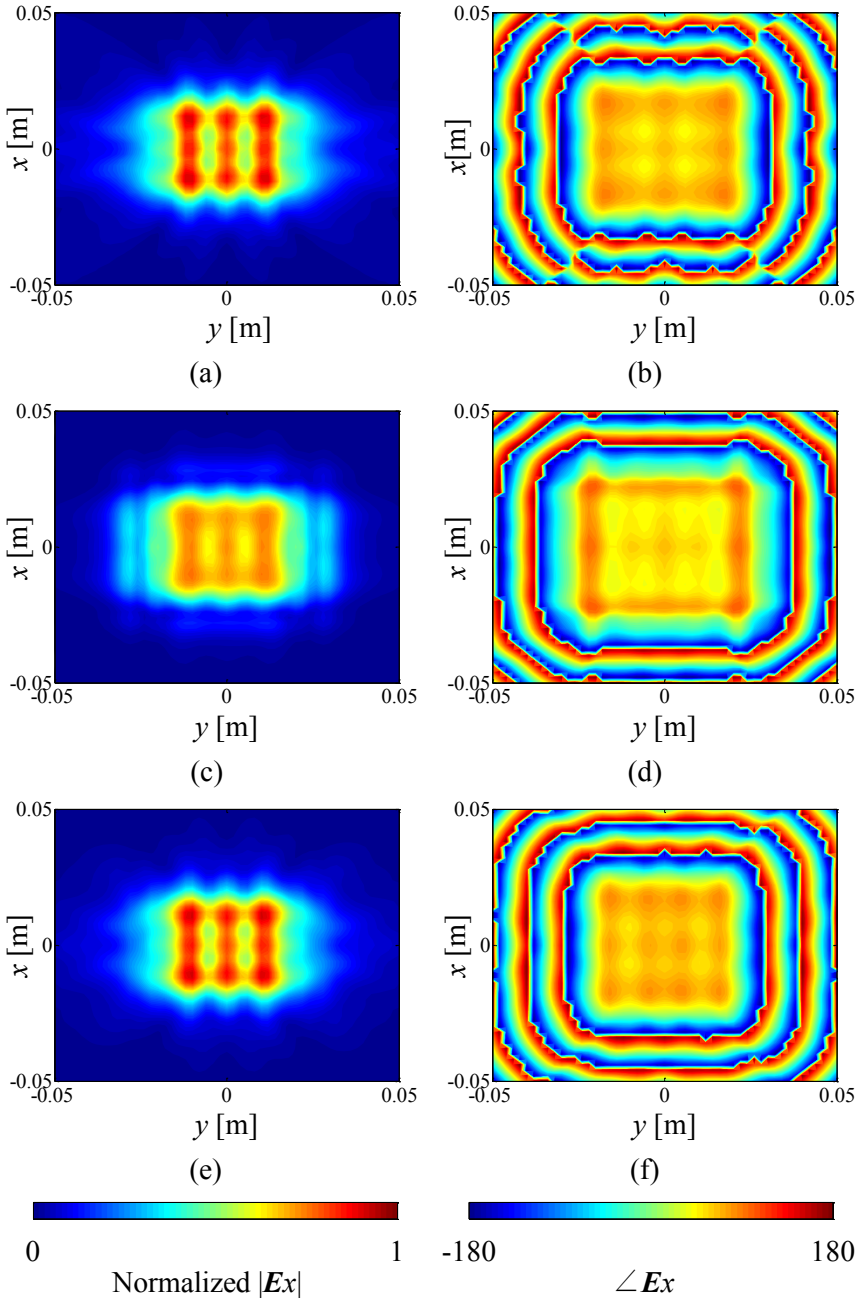

Figure 6.4: Simulated x component electric distribution of uniform excited array over the S_1; (a) and (b) are references; (c) and (d) are without compensation; (e) and (f) are compensated by the proposed method. The left side is the normalized amplitude distribution, and the right side is the phase distribution.

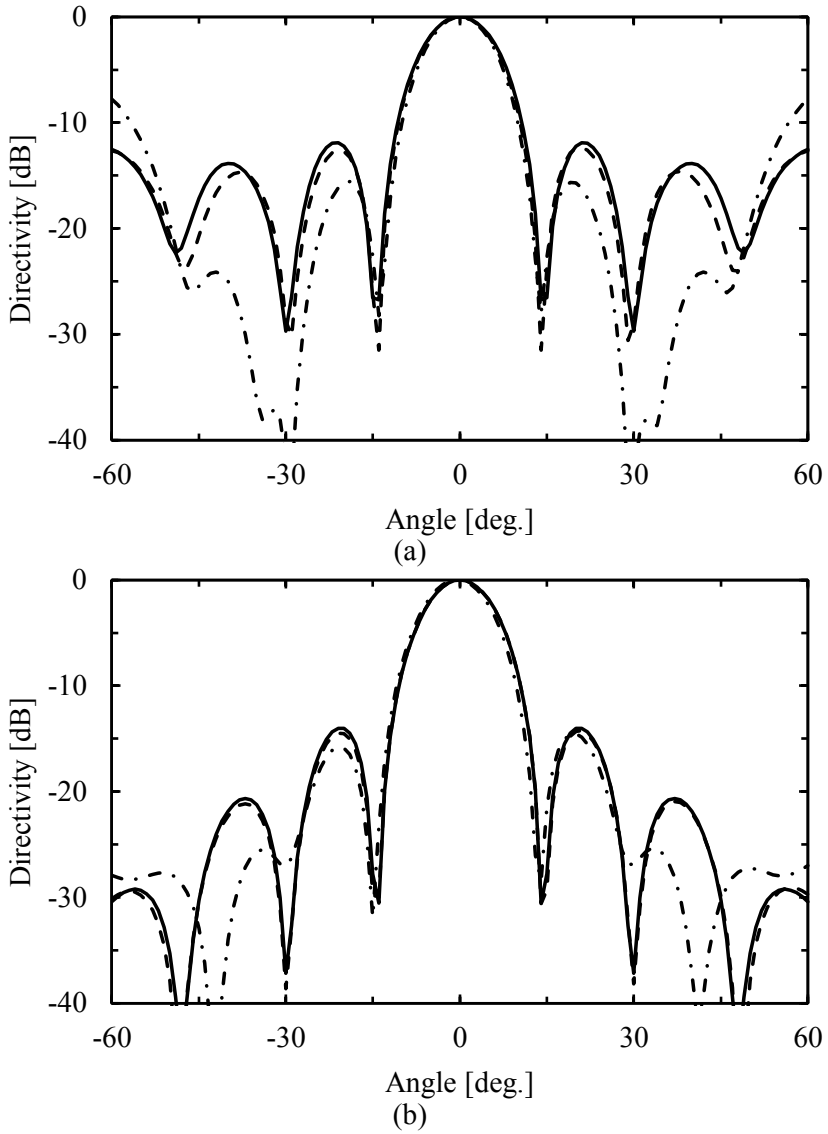

Figure 6.5: Estimated far-field pattern (a) is H-plane and (b) is E-plane. Solid line is reference pattern, dotted line is proposed and chain is without compensation.

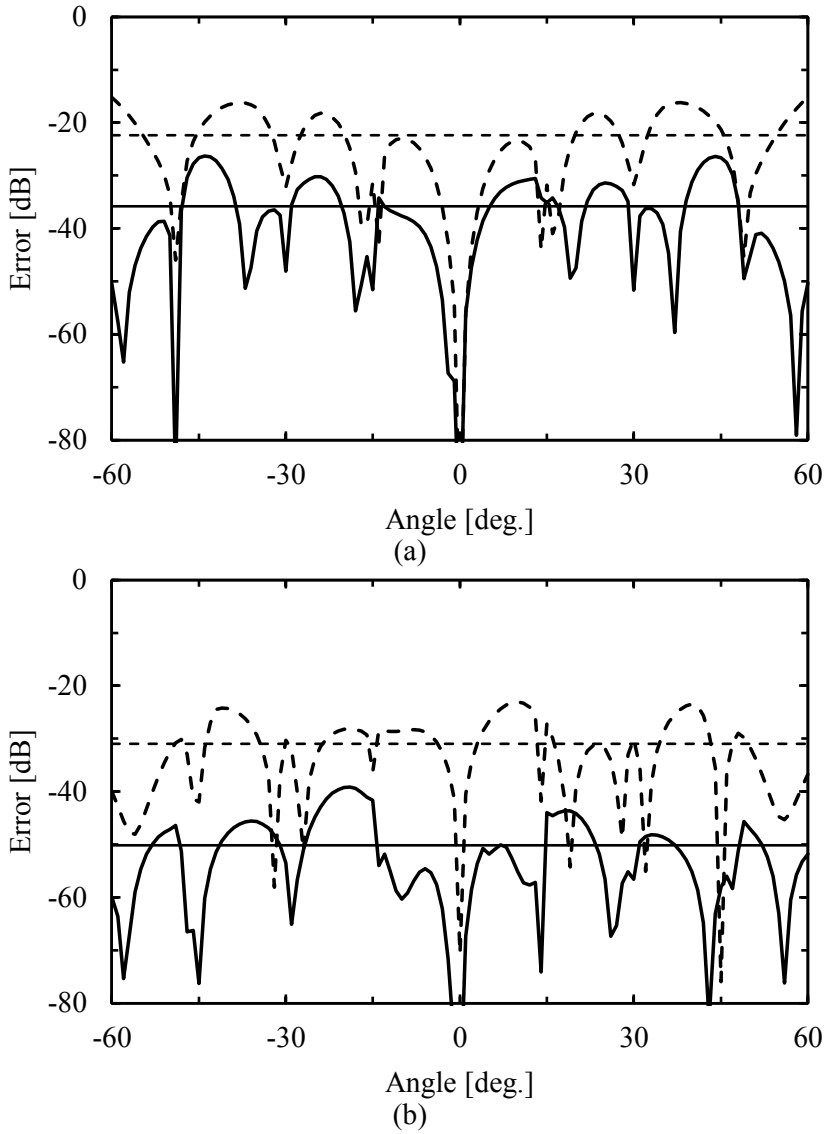

Figure 6.6: Relative error of estimated far-field pattern; (a) presents H-plane; (b) presents E-plane. The solid line represents the results from the proposed method, and the dotted line represents the conventional method; the horizontal lines represent the mean value.

The next situation of the AUT is beam-tilted pattern. We tilted the main beam direction in E-plane by changes the feeding phase of each dipole elements. The relationship between iteration number of proposed compensation technique and recognized distance of measurement planes is shown in Figure 6.7. It shows the estimated distance is approaches the exact distance, the proposed method is available to beam tilted antenna. The truncation error is reduced by restricting the region of calculating norm within the iteration formula, and the distance between the two planes is accurately obtained. We illustrate the reconstructed electric field distribution over the S_1 in Figure

6.8. It is definite that the reconstruction accuracy used the proposed method is better than the without compensation, especially phase distribution has superior improvement. The probe positioning errors cause enormous phase reconstruction errors in the case of beam-tilted antenna, due to the mismatch between exact distance and the Green's function. Estimated E-plane far-field pattern and its error are shown in Figure 6.9. In case of without the compensation, the estimated maximum radiation direction disagrees with the reference value since the phase gradient cannot be reconstructed. The maximum direction is one of the most important parameters to evaluate beam-tilted antenna. However, the maximum direction cannot be accurately estimated; this becomes a fatal drawback to the estimation method for beam-tiled antennas. This weakness is overcome using the proposed method to accurately estimate the maximum direction and pattern. The estimated far-field without compensation has a maximum direction error of 3°. The derived error around the main beam is extremely small; the mean value of the proposed method is -48.6 dB and without compensation, it is -22.7 dB. Amount of improvement more than 20 dB is achieved, and the error shown in table 6.2 indicates that the present methods are effective for probe-positioning error compensation in beam-tilt antenna measurements.

Table 6.2 Total error in estimated far-field of beam-tilt antenna

	Total error
Compensated	0.066
Misaligned	0.287

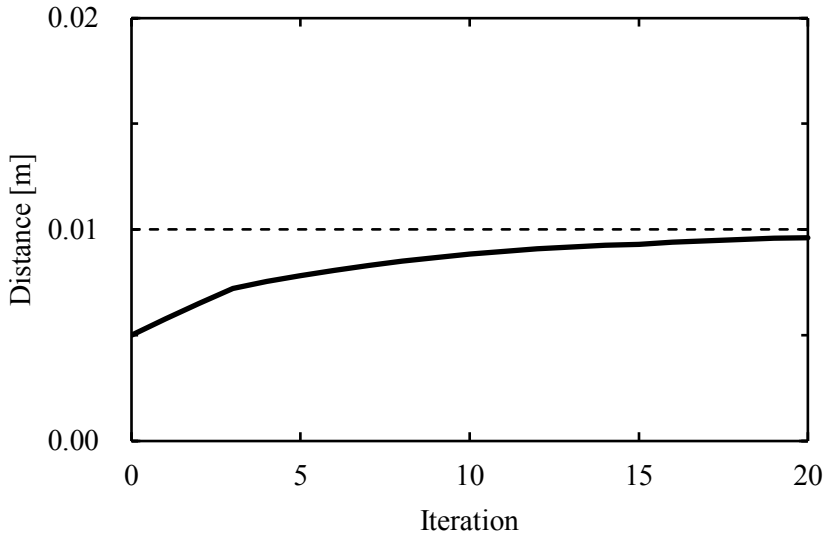

Figure 6.7: Convergence circumstances of beam tilt antenna, the horizontal dotted line is the exact distance.

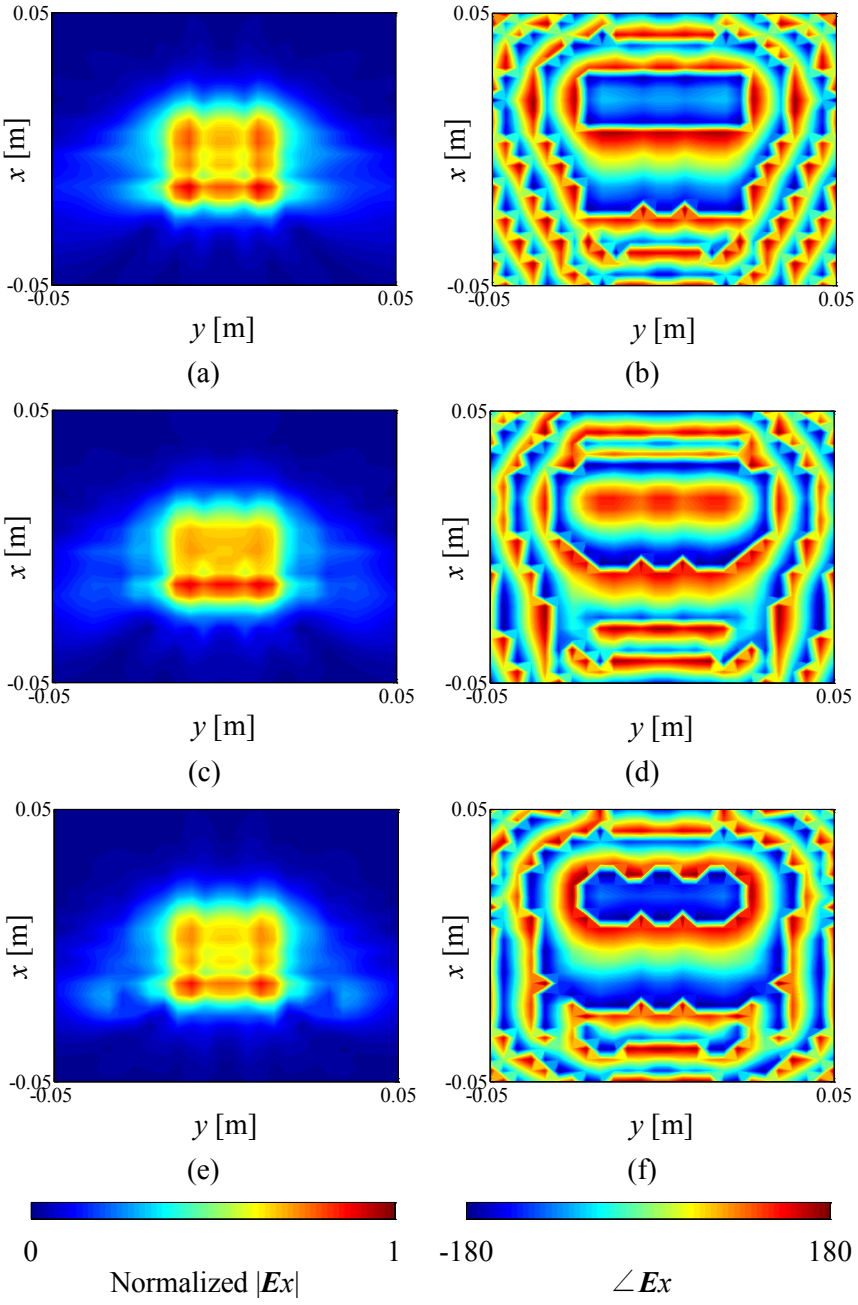

Figure 6.8: Simulated x component electric distribution of beam tilted array over the S_1; (a) presents H-plane; (b) presents E-plane. The solid line represents the results from the proposed method, and the dotted line represents the conventional method; the horizontal lines represent the mean value.

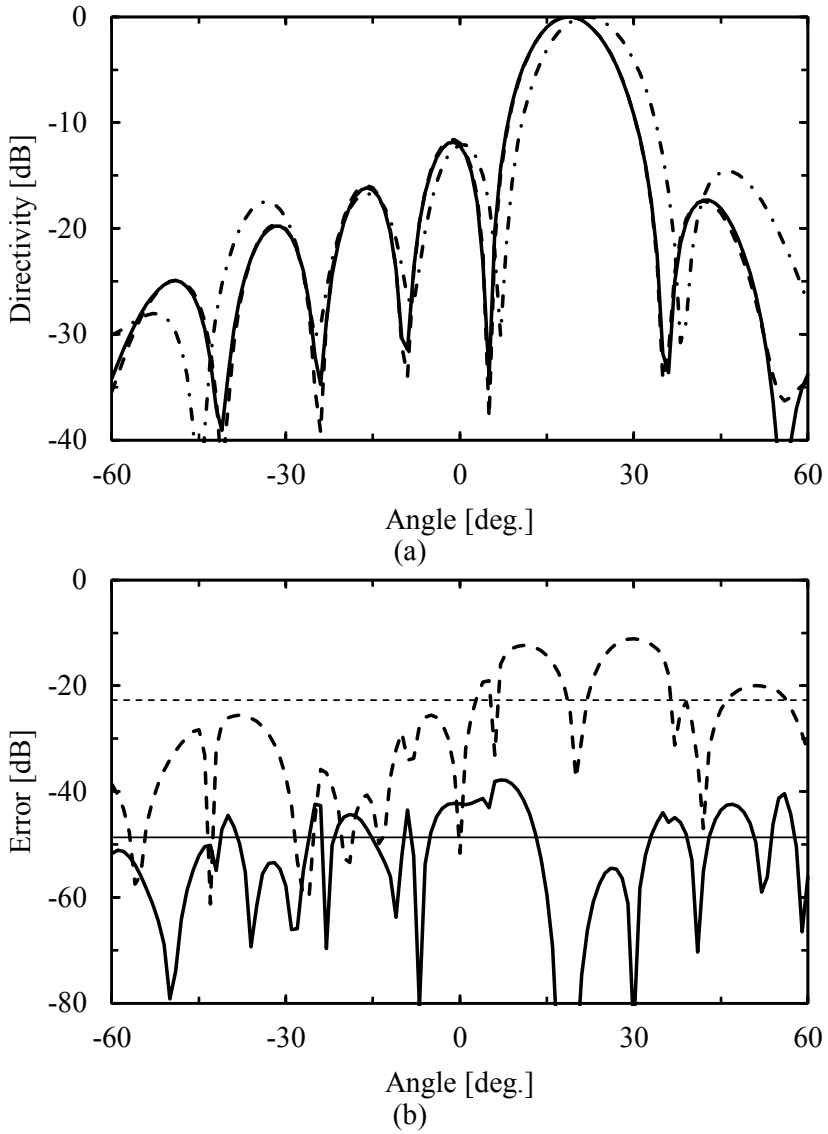

Figure 6.9: Estimated far-field pattern and its relative error of beam-tilt antenna; (a) presents far-field pattern solid line shows reference pattern, dotted line shows proposed method and chain shows without compensation techniques. (b) presents error the solid line represents proposed method and the dotted line represents without compensation techniques, and horizontal line represent the mean value.

6.4 Experiment

To further evaluate the developed synthetic far-field estimation system, experimental tests were performed. Figure 6.10 shows the AUT using measurements. The AUT is operated in 61 GHz and is a linearly polarized planar slot array. The physical aperture size is 120 mm^2, and the numerical aperture for phase reconstruction is 150 mm^2. The measurement planes are located at distances of 25 mm and 50 mm from the AUT. The measurement data is acquired over two rectangle of size 200 mm × 200 mm , and the sampling resolution is 2.2 mm (approximately 0.45λ). The coplanar random error is given as range in $\sqrt{\left(\Delta x^2 + \Delta y^2\right)} < 2$ mm. The phase resurrection process is performed under misrecognized situation that the measured planes are set at 10 and 50 mm. Estimation accuracy is evaluated by far-field pattern, and the reference pattern for evaluation is obtained from planar near-field far-field transformation using measured amplitude and phase distribution. The distance between two planes after applying the compensation methods is shown in Figure 6.10. Finally converged value is slightly different to the reference value, solution is enough well accurate. The obtained distance is 26.1 mm and that error is less than 5%. The far-field pattern and its relative error using reconstructed near-field distribution are shown in Figure 6.11 and Figure 6.12. The error included in estimated far-field is greater reduced by incorporate the proposed methods, and accurate far-field pattern can be obtained. Difference occurs in null level since the low-pass filter is used, however the amount of error is very small and does not becomes problem in terms of estimation accuracy. The mean value of relative error with the proposed method in H-plane and E-plane is -36.6 dB and -34.0 dB, without the compensation is -25.2 dB and -18.7 dB. The amount of improvement is over than 10 dB, it is clear the effectiveness of proposed method for the measurement tests. Also from the total error shown in table 6.3, the effectiveness is sufficient.

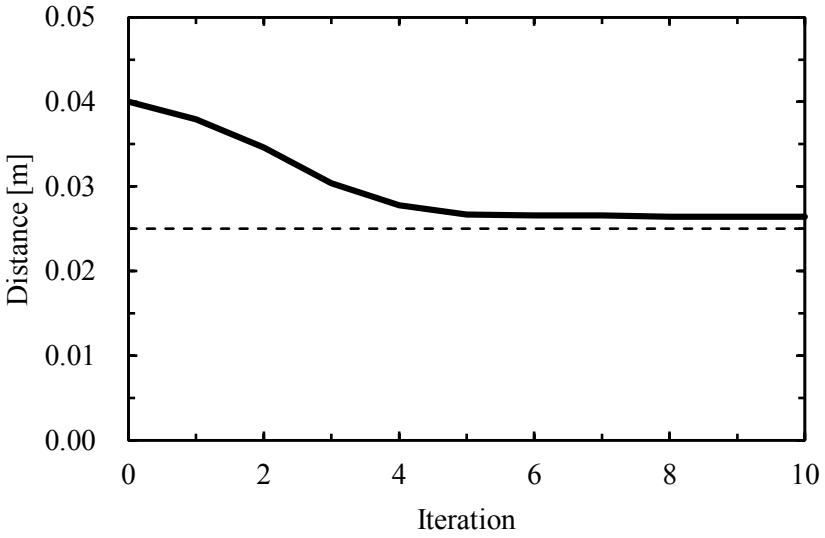

Figure 6.10: Convergence of recognized distance.

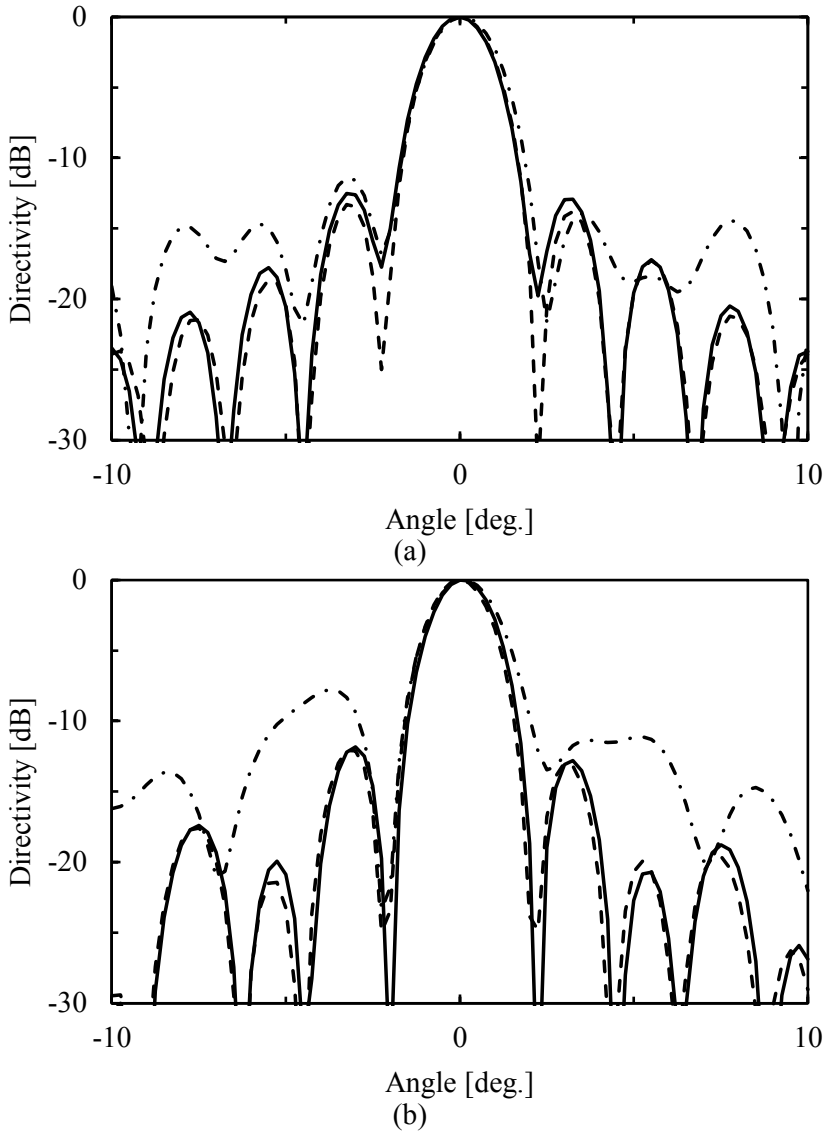

Figure 6.11: Estimated far-field pattern. (a) is H-plane, (b) is E-plane; the solid line represents using planar near-field amplitude-phase measurement, the dotted line represents the results obtained using the proposed method and chain line represents without compensation case.

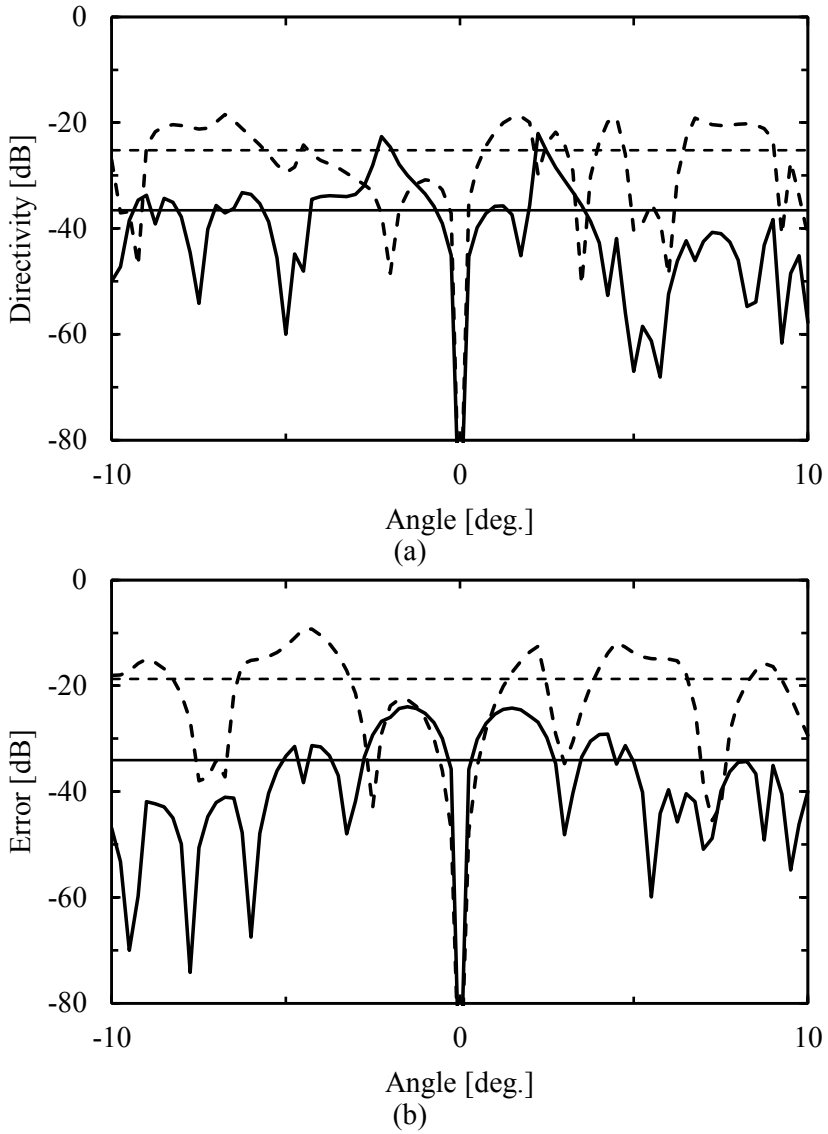

Figure 6.12: Relative error of estimated far-field patterns. (a) is H-plane and (b) is E-plane; solid line represents the results obtained using proposed method and the dotted line represents the results using conventional method. Horizontal lines are mean value.

Table 6.3 Total error in estimated far-field of measurement

	Total error
Compensated	0.066
Misaligned	0.287

6.5 Summary

A probe positioning error compensation method for near-field phaseless measurements was proposed. We classified the probe positioning error is contained by probe vibration random error and depth direction misalignment of probe jig. The random error was reduced by adding the 2D low-pass filter to the measured amplitude distribution. The depth error was compensated by an iterative trial that used the norm difference between measured and reconstructed planes during the phase reconstruction process. The proposed method was applied to the numerical simulation that included the uniform excitation and beam-tilted arrays. The numerical results showed that the accuracy of the proposed compensation method agreed with the far-field pattern. The error included in the measured planes is eliminated by the proposed method, and the distribution of amplitude and phase was accurately reconstructed. Results using experimentally collected measurement data were presented for the planar slot array antenna, and the effectiveness of the proposed techniques in controlling the measurement errors has been described herein. The proposed method can be compensates compensate the measured amplitude data without adding information related to the probe-positioning error.

Reference

[1] D. Slater, *Near-field antenna measurements*, Artech House, 1991.

[2] A. D. Yaghjian, "An overview of near-field antenna measurements," *IEEE Trans., Antennas and Propag*., vol. AP-34, no. 1, pp. 30-45, Jan. 1986.

[3] S. F. Razavi and Y. Rahmat-Samii, "A new look at phaseless planar near-field measurements: Limitations, simulations measurements and a hybrid solution," *IEEE Antennas Propag. Mag*., vol. 49, no. 2, pp.170-178, Apr. 2007.

[4] R. G. Yaccarino and Y. Rahmat-Samii, "Progress in phaseless near-field antenna measurement research at the University of California, Los angeles," in *Proc. IEEE Antennas and Propagation Society Int. Symp*., July 2001.

[5] L. S. Taylor, "The phase retrieval problem," *IEEE Trans. Antennas and Propag*., vol. 29, no.2, pp.386-391, Mar. 1981.

[6] O. M. Bucci, G. D'Eila, G. Leone and R. Pierri, "Far-field pattern determination from the near-field amplitude on two surfaces," *IEEE Trans. Antennas and Propag*., vol.38, no. 11, pp.1772-1779, Nov. 1990.

[7] T. Brown, I. Jeffrey and P. Mojabi, "Multiplicatively regularized source reconstruction method for phaseless planar near-field antenna measurements," *IEEE Trans. Antennas and Propag*., vol. 65, no. 4, pp.2020-2031 Apr. 2017.

[8] V. Schejbal , J. Pidanic, V. Kovarik and D. Cermak, "Accuracy analyses of synthesized-reference-wave holography for determining antenna radiation characteristics," *IEEE Antennas Propag. Mag*., vol. 50, no.6, pp.89-98, pp.89-98, Dec. 2008.

[9] A. C. Newell, "Error analysis techniques for planar near-field measurements," *IEEE Trans. Antennas and Propag*., vol. 36, no. 6, pp.754-768, June 1988.

[10] S. F. Razavi and Y. Raj,at-Samii, "Resilience to probe-positioning errors in planar phaseless near-field measurements," *IEEE Trans. Antennas and Propag*., vol. 58, no. 8, pp.2632-2640, Aug. 2010.

[11] L. Corey and E. Joy, "Far-field antenna pattern calculation from near-field measurements including compensation for probe positioning errors," in *Proc Antennas and Propagation Society Int. Symp*., June 1979.

[12] O. M. Bucci, G. Schirinzi and G. Leone, "A compensation technique for positioning errors in planar near-field measurements," *IEEE Trans. Antennas and Propag*., vol. 36, no. 8, pp.1167-1172, Aug. 1988.

[13] S. R. Rengarajan and Y. Rahmat-Samii, "The field equivalence priciple: Illustration of the establishment of the non-intuitive null fields," *IEEE Antenna Propag. Mag*., vol. 42, no. 4, pp.122-128, Aug. 2000.

[14] T. P. Sakar and A. Taaghol, "Near-field to near/far-field transformation for arbitrary near-field

geometry utilizing an equivalent electric current and MoM," *IEEE Trans. Antennas and Propag*., vol. 47, no. 3, pp. 566-573. March 1999.

7 A Far-Field Estimation Method of Antenna Above the Earth Using Hemispherical Near-Field Measurements

7.1 Introduction

Antennas for land mobile communications are affected from the earth, the radiation pattern under practical use conditions are different from the radiation characteristics in the free space [1], [2]. General antenna measurement is done in an anechoic chamber; the measured result of Antenna Under Test (AUT) is assumed the same as the characteristics in the free space. In order to evaluate correctly antenna performance in practical environment, it is necessary to discuss about far-field pattern above the earth [3]. However, direct measurement of the antenna pattern above the earth is realistically difficult because an expensive economic cost is required to construct measurement facilities. Conventionally, its radiation performance has generally been evaluated using the far-field in the free space measured in an anechoic chamber.

The method to compute the radiated electromagnetic field in the vertical plane when there is an infinite conducting plate under the radiation source has been studied for a long time. The method to calculate a rigorous far-field above the earth was developed by Sommerfeld [4]. This method finds the radiation electromagnetic field by solve the integral equation by considering the image current below the earth. The exact solution including the mutual coupling between the surface current and the image current can be obtained. The other technique is the method to consider reflection wave from the earth. There is another method to use reflection coefficient which introduced by Wise [5]. This method is called as Reflection Coefficient Method (RCM). If the current distribution on the AUT surface is known, it is clarified that by considering the reflected wave from the earth, the antenna far-field above the earth can be obtained with good precision. The RCM cannot to take into account mutual coupling with image current and it requires known current distributions. However it has great advantage that the far-field pattern can be calculate from the current distributions in the free space. Since it is not easy to directly measure the current distribution on the AUT surface, we are necessary to estimate the current distribution on the surface based on the electromagnetic field measured in near-field of the AUT.

We obtain the surface current on the AUT using source reconstruction method [6]-[8]. Source reconstruction method can be acquired current distribution by solve integral equation from measurement near-field including the AUT. Here, when the AUT size is physically large, that has difficulty to measure spherical near-field distribution. The area of the near-field that can be measured is limited by the durability limit of the measurement equipment. In addition, a jig for rotating the AUT always exists under the AUT. In this case, the inverse problem will be ill-posed conditions due to physical overlap of the AUT and the jig as seen from the measurement point, and then the current

distribution on the AUT surface cannot be reconstructed accurately. We are impossible to estimate the accurate far-field even if calculate the far-field using RCM, because the current distribution itself is not obtained correctly. In order to estimate the far-field of the AUT above the earth, we must to avoid ill-posed conditions of the inverse problem due to lack of the measurement area and reconstruct the correct surface current distribution.

In this chapter, we supplement the above-mentioned missing of the measurement area, not only use the inverse source reconstruction but also use the forward near-field to near-field transformation. The hemispherical near-field at the bottom of the measurement field is regenerated using the current distribution on the AUT surface that was pre-reconstructed. We construct a full-spherical near-field combined a measured upper hemispherical near-field and regenerated lower hemispherical near-field. The current distribution on the AUT and the jig surfaces are reconstruct using this supplemented full-spherical near-field. The far-field pattern when the AUT is placed on the earth is estimated applying the RCM based on the obtained current distribution.

This chapter is organized as follows. 7.2 introduces the self-supplemented spherical source reconstruction method, and the far-field estimation method using reconstructed surface current. 7.3 shows the numerical results of estimation method for a monopole antenna and a dipole antenna with reflector cases. The estimated far-field patterns of simulations with uniform excitation and electrical beam-tilt antenna are demonstrated in this section. This section also shows the effectiveness of the proposed method against to the earth with arbitrary electrical constants. 7.4 illustrates hemispherical near-field measurement result. Following 7.4, a conclusion section is provided.

7.2 Method

7.2.1 Source Reconstruction Using Hemispherical Near-Field

This section mentions a method to estimation of current distribution on the AUT surface using hemispherical measured near-field. We define measurement scenario as shown in Figure 7.1 to obtain electrical near-field. In this system, rotation table under the AUT realizes rotation in azimuth direction, to measure the near-field in the vertical plane by moving the probe in the zenith angle direction. It is assumed that the jig is made of a metal such as a copper plate. The AUT is physically large and it is impossible to measure the lower hemispherical near-field by inverting the AUT in the vertical plane. Thus, we can only obtain the near-field distribution of the upper hemisphere.

The electric field on an arbitrary point $\boldsymbol{E}(\mathbf{r})$ in measurement surface is given as [9]

$$\boldsymbol{E}(\mathbf{r}) = -jk_0\eta\int_{S_A}\left\{\boldsymbol{J}(\mathbf{r}') + \frac{1}{k_0^2}\nabla\nabla\cdot\boldsymbol{J}(\mathbf{r}')\right\}G(\mathbf{r},\mathbf{r}')dS_A \tag{7.1}$$

where $\boldsymbol{J}(\mathbf{r}')$ is complex surface current on the surface of AUT or jig, η is the characteristics

impedance in free space and k_0 is the free space wavenumber. $G(\mathbf{r},\mathbf{r'})$ is the free space Green's function as

$$G(\mathbf{r},\mathbf{r}') = \frac{e^{-jk_0|\mathbf{r}-\mathbf{r}'|}}{4\pi|\mathbf{r}-\mathbf{r}'|}. \tag{7.2}$$

Let us consider to reconstruct surface current using measured electric field distribution. We reform the integral equation of (1) from known measurement electric field vector $\boldsymbol{E}$, coefficient matrix $\boldsymbol{A}$ and unknown current vector $\boldsymbol{J}$, and we acquire following matrix equation

$$\begin{bmatrix} E_\theta \\ E_\phi \end{bmatrix} = \begin{bmatrix} A_{x\theta} & A_{y\theta} & A_{z\theta} \\ A_{x\phi} & A_{y\phi} & A_{z\phi} \end{bmatrix} \begin{bmatrix} J_x \\ J_y \\ J_z \end{bmatrix}. \tag{7.3}$$

By solving this matrix equation for the current vector, it is possible to acquire the surface current on the AUT and the jig.

However as mentioned above, we spend attention that we only have upper hemispherical near-field distribution. In such measurement environment, the matrix equation almost certainly becomes an ill-posed problem due to the lack of near-field information at the low elevation part and the physical overlap between the AUT and the jig as seen from the measurement surface. Electric current component on the AUT and the jig cannot be accurately separated under this condition. If we obtain least square solution by solve this matrix equation and to perform far-field estimation using acquired current, in many cases the far-field level in the low elevation angle direction decreases and an accurate far-field cannot be estimated.

It is effective to approximately compensate the electric field distribution of the lower hemispherical surface to improve the above problem. Therefore, we propose a source reconstruction method from self-supplemented full-spherical near-field distribution. The flowchart of the proposed method is shown in Figure 7.2. Firstly, the electric field distribution on the upper hemispherical surface ($0° \leqq \theta \leqq 90°$) near the AUT and the jig is measured (step 1). Then, current distributions on the AUT and the jig surface are reconstructed using measured hemispherical electric field $\boldsymbol{E}_m$ (step 2). The surface current distribution reconstructed at this step falls into the ill-posed condition described above, and accurate surface current distribution is not obtained. In the step 3, we calculate the lower hemispherical surface ($90° \leqq \theta \leqq 180°$) near-field with the same radius as the measurement surface using the current distribution only on the AUT surface reconstructed at step 2. The calculated near-field is normalized using the highest elevation angle point (i.e. $\theta = 90°$) of the calculation near-field $\boldsymbol{E}_c$ and the lowest elevation angle point (i.e. $\theta = 90°$) of the measurement

near-field $\boldsymbol{E}_m$ as follows;

$$\boldsymbol{E}_s(\theta > 90^\circ, \phi) = \boldsymbol{E}_c(\theta, \phi) \frac{\boldsymbol{E}_m(90^\circ, \phi)}{\boldsymbol{E}_c(90^\circ, \phi)}. \tag{7.4}$$

The lower part of the measurement near-field is complemented using the regenerated lower hemispherical near-field as mentioned; then we obtain a virtual full-spherical near-field distribution (step 4). The AUT and the jig are set as the estimation surfaces, and to reconstruct its current distribution using generated full-spherical near-field (step 5). In the next section, to remove the jig from the surface current distributions derived in step 5, and the far-field is estimated when the AUT is placed on the earth by RCM using only the current distribution on the AUT surface.

In this proposed method, we regenerate lower hemispherical near-field in step 3 only using the AUT surface current. If the current distribution on the jig is also used for regeneration, the current distribution to be reconstructed in step 5 will be the equal to the least square solution reconstructed in step 2. For this reason, the lower hemispherical near-field is regenerating using only the AUT surface current. Further, for suppressing numerical divergence in step 5, regenerated near-field is normalized by measured value at $\theta = 90°$ and calculated value at $\theta = 90°$ in step 4.

7.2.2 Far-Field Estimation with Reflection Coefficient Method

A method of estimating the far-field of AUT above the earth using the surface current distribution obtained in the previous section will be described. Since the proposed method reconstructs the surface current distribution in the free space, we adopt RCM to calculate the far-field. The proposed method, it is impossible take into account the coupling between AUT and image current below the earh, however it is known that a sufficiently accurate radiation field above the earth can be obtained even with only RCM. In addition we assuming few radiations to the ground direction, the coupling with the image currents are not a big problem.

The RCM consider the following reflection coefficient for each of TM wave and TE wave incident to the ground.

$$\begin{aligned} \Gamma_{TM} &= \frac{\varepsilon_r \cos\theta - \sqrt{\varepsilon_r - \sin^2\theta}}{\varepsilon_r \cos\theta + \sqrt{\varepsilon_r - \sin^2\theta}} \\ \Gamma_{TE} &= \frac{\cos\theta - \sqrt{\varepsilon_r - \sin^2\theta}}{\cos\theta + \sqrt{\varepsilon_r - \sin^2\theta}} \end{aligned}, \tag{7.5}$$

where ε_r is complex effective dielectric constant derived from relative dielectric constant of the earth ε_s, and conductivity σ given as

$$\varepsilon_r = \varepsilon_s - j\frac{\sigma}{\omega\varepsilon_0} \tag{7.6}$$

ε_0 is dielectric constant of the free space.

By introducing these reflection coefficients, we can assume the image current below the earth as shown in Figure 7.3. We performing radiation integration from these currents, we derive the far-field in the vertical plane of the AUT above the earth as follows [5];

$$\begin{aligned} FF_\theta(\theta,\phi) &= FF_\theta^v(\theta,\phi) + FF_\theta^h(\theta,\phi) \\ &\quad \sum_{n=1}^{N} J_n l_n \sin\theta\left(e^{jk_0 d} + \Gamma_{TM} e^{jk_0 d'}\right) \\ &\quad + \sum_{n=1}^{N} J_n l_n \cos\theta\cos\phi\left(e^{jk_0 d} - \Gamma_{TM} e^{jk_0 d'}\right), \end{aligned} \tag{7.7}$$

$$FF_\phi(\theta,\phi) = \sum_{n=1}^{N} J_n l_n \left(\hat{\boldsymbol{l}}_n \cdot \hat{\boldsymbol{\phi}}\right)\hat{\boldsymbol{l}}_n\left(e^{jk_0 d} + \Gamma_{TE} e^{jk_0 d'}\right). \tag{7.8}$$

where J_n is discretized complex current on the AUT, and l_n is the length of line current element.

In this chapter, we use far-field by Sommerfeld integral equation obtained from FEKO [10] as a theoretical pattern. The estimation accuracy of the far-field is evaluated using the following evaluation formula;

$$Error = \frac{\left\| \left|\boldsymbol{E}_{FF}(Ref.)\right| - \left|\boldsymbol{E}_{FF}(Est.)\right| \right\|}{\left|\boldsymbol{E}_{FF}(Ref.)\right|}. \tag{7.9}$$

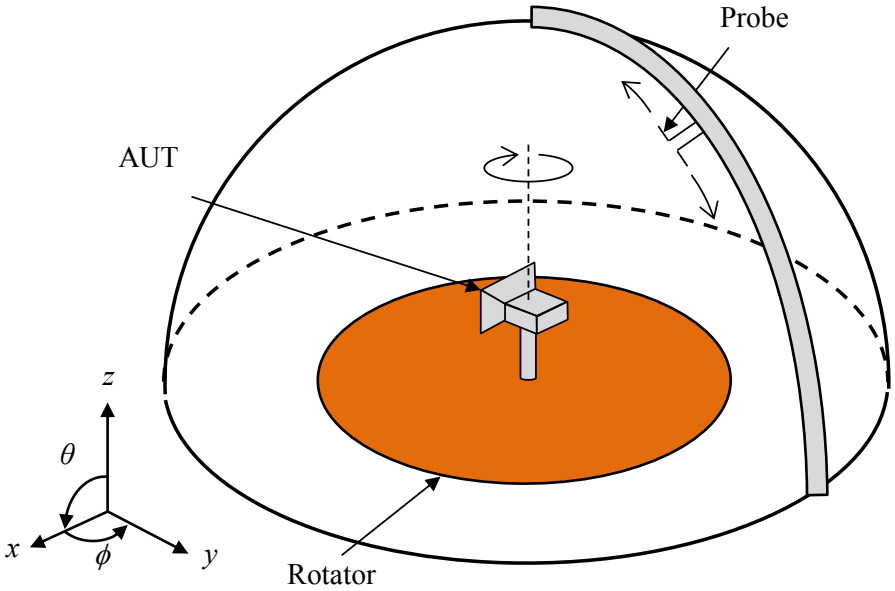

Figure 7.1: Measurement equipment of hemispherical scan.

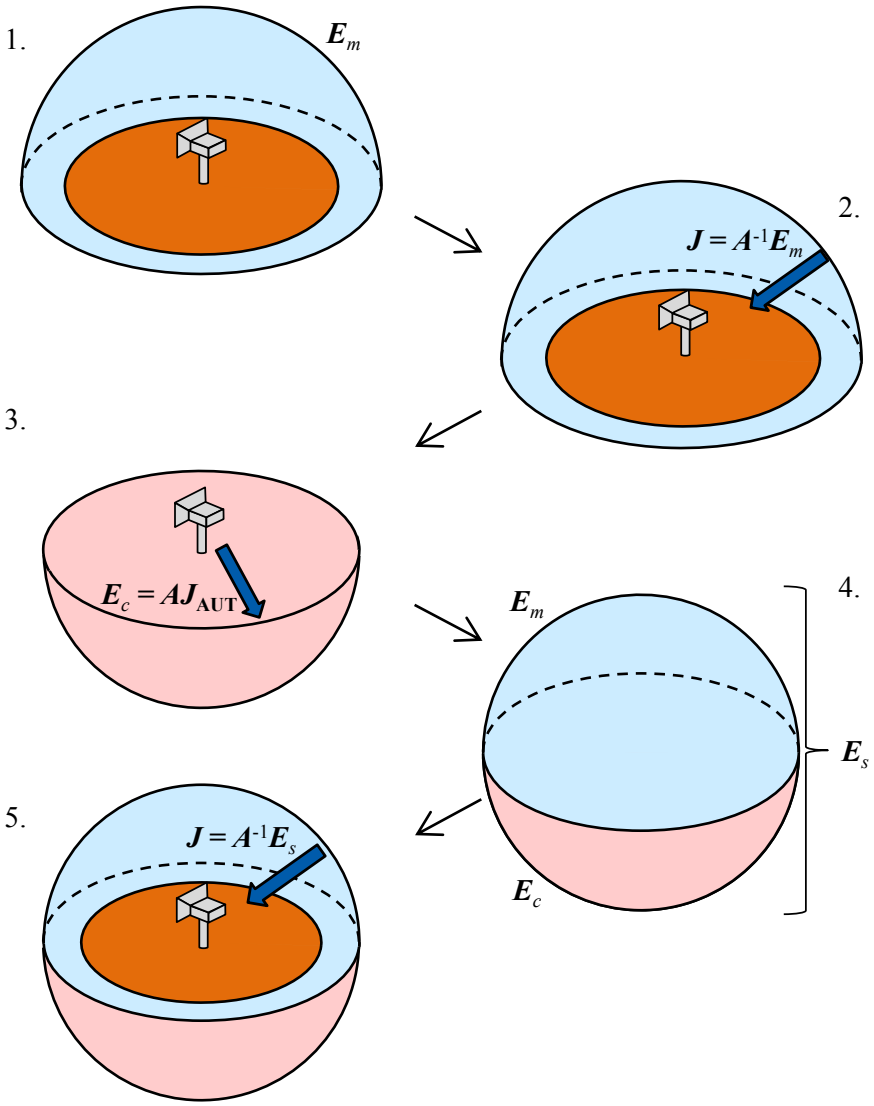

Figure 7.2: Procedure of self-supplemented spherical source reconstruction.

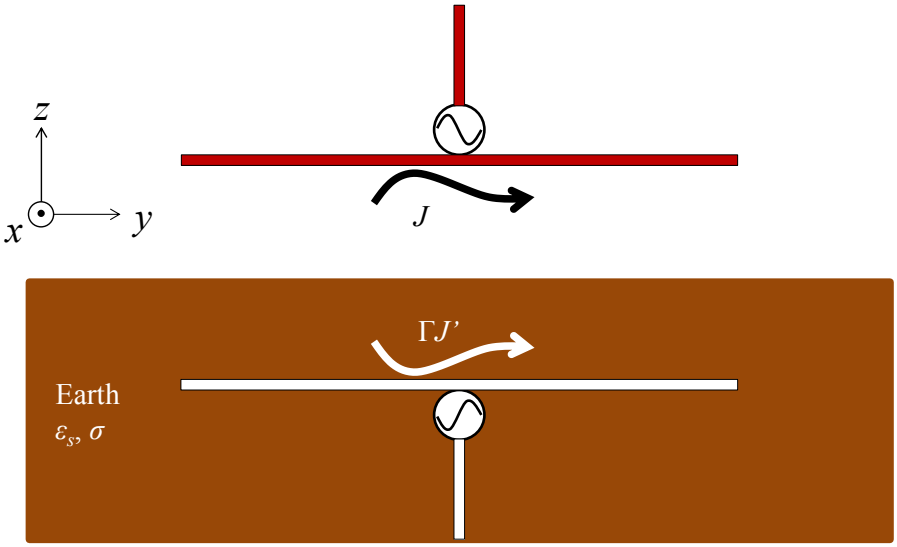

Figure 7.3: Antenna above the earth and image antenna below the earth.

7.3 Simulation

This section mentions that effectiveness of the proposed method. We use a monopole antenna and a dipole antenna with circular reflector as AUT shown in Figure 7.4. A circular PEC plate simulating the rotating table is set under the AUT, the center of the PEC plate placing on the axis origin. The distance between the AUT and the PEC plate is 2 m. We acquired upper near-field distribution including the AUT and the jig as measurement electric field. The radius of measurement hemisphere is 5 m and the sampling intervals of θ and f direction are $\Delta\theta = \Delta\phi = \Delta 5°$. If the number of measurement points in the near-field is less than number of discretization point on the AUT surface, the inverse problem also becomes ill-posed condition. Thus the number of sampling points in the near-field is sufficiently larger than the number of reconstruction points. Calculating frequency band is UHF band. From the hemispherical near-field acquired these measurement environment, we estimate the vertical plane far-field such as shown in Figure 7.4 (b).

A normalized electric field distribution of the monopole AUT supplemented by the proposed method is shown in Figure 7.5. The lower hemisphere distribution does not completely reproduce the exact distribution because the near-field is calculated only using the reconstructed source of the AUT in step 3, nevertheless the regenerate distribution is well reproduced the exact distribution in unmeasured region at $\theta > 90°$. This is because the estimated near-field was normalized by the measurement near-field at the step 4.

A normalized surface current amplitude distribution reconstructed using the virtually regenerated full-spherical near-field is shown in Figure 7.6. We can see that accurate current distribution cannot be reproduced even if source reconstruction is performed by using hemispherical near-field for either AUT. The amplitude on the radiating elements is reconstructed smaller than the

exact amplitude, and the far-field level in the low elevation angle direction is estimated to be significantly smaller if the far-field is estimated using this distribution. On the other hand, we can see that the accuracy of the estimated current distribution is greatly improved by performing the source reconstruction using the proposed method. The amount of improvement of monopole AUT is larger than the dipole AUT. Because of the proposed method is especially for improving the estimation accuracy of the current distribution on the AUT surface, the proposed method is effective for the monopole than the dipole which the radiation tangential component of AUT coincides with the PEC surface tangent component.

Figure 7.7 shows the result of estimating the far-field in the vertical plane by RCM using only the current distribution on AUT surface obtained as described above. The electrical constants of the earth are defined as $\varepsilon_s = 4$, $\sigma = 10^{-3}$. We are assuming that the AUT is placed above a dry ground [12]. Figure 7.7(a) is far-field in vertical plane of the monopole AUT, the first quadrants of Figure 7.7(b) is far-field in H-plane of the dipole AUT and the second quadrants of Figure 7.7(b) is far-field in E-plane. As mentioned above, when the proposed method is not used, deterioration of the estimated pattern is observed in the radiation level at the low elevation angle. It is a fatal drawback as a test method of antennas for land mobile communications that cannot estimate the pattern in the low elevation angle because the radiation of horizontal direction is particularly important for land mobile antennas. On the other hand, the far-field estimated using the proposed method the estimated pattern has good agreement with the reference pattern.

We consider that the effectiveness for arbitrary electric constant of the earth. Estimated far-field of when changing the electric constant of the earth is shown in Figure 7.8. The AUT is the monopole in Figure 7.4, and $\varepsilon_s = 10$, $\sigma = 10^{-1}$. These electric constants were determined assuming wet ground. We can see from Figure 7.8, the far-field of the proposed method has good agreement with the reference pattern, indicating that the estimation accuracy of the far-field does not depend on the electrical constants of the earth. This is because of the TCM can derive the far-field above the earth if current distribution in the free space is obtained accurately. Therefore, the most important point to estimate far-field is how accurately the current distribution on the AUT surface is to be obtained. Obviously, the proposed method plays an extremely important role to achieving above.

For further evaluate the proposed method, we introduce additional parameter that measurement angle θ_m as shown in Figure 7.9(a), and discuss of estimation accuracy of the far-field. For example, when acquiring the upper hemispherical surface as shown in Figure 7.4, $\theta_m = 90°$. The relation between measurement angle θ_m and accuracy of estimated far-field pattern is shown in Figure 7.9(b). Where the electric constants of the earth are same as the case of Figure 7.7 and the AUT is monopole antenna as Figure 7.4. As can be seen from Figure 7.9 (b), when using the normal source reconstruction method, the estimation accuracy decreases when $\theta_m < 120°$. The reason for accuracy deterioration is the inaccuracy of the reconstructed current distribution due to the missing of the

measurement region. On the other hand, when the proposed method is used, the estimation accuracy of the far-field is greatly improved, and it can be seen that the far-field can be estimated sufficiently accurately if $\theta_m \geqq 80°$.

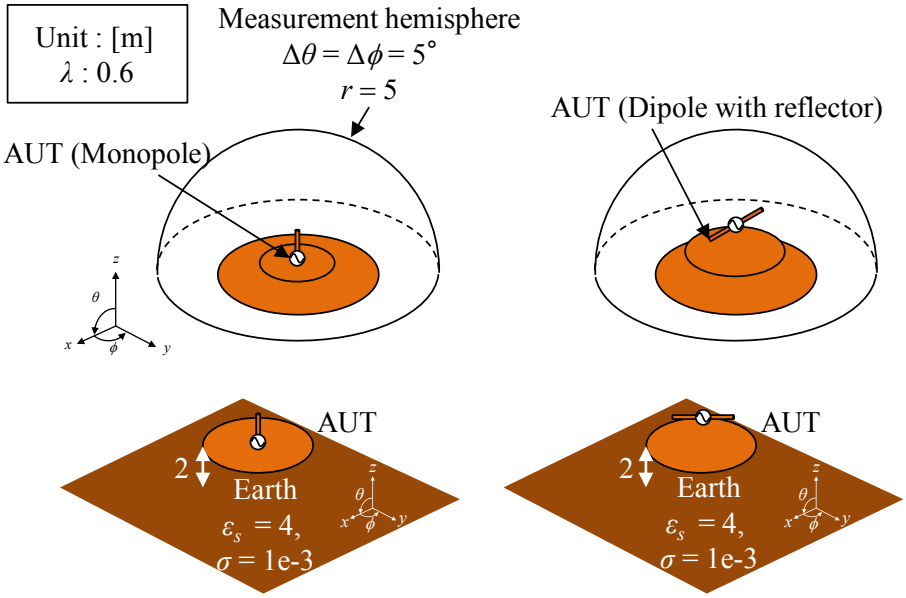

Figure 7.4: Structure of AUT and simulating situation.

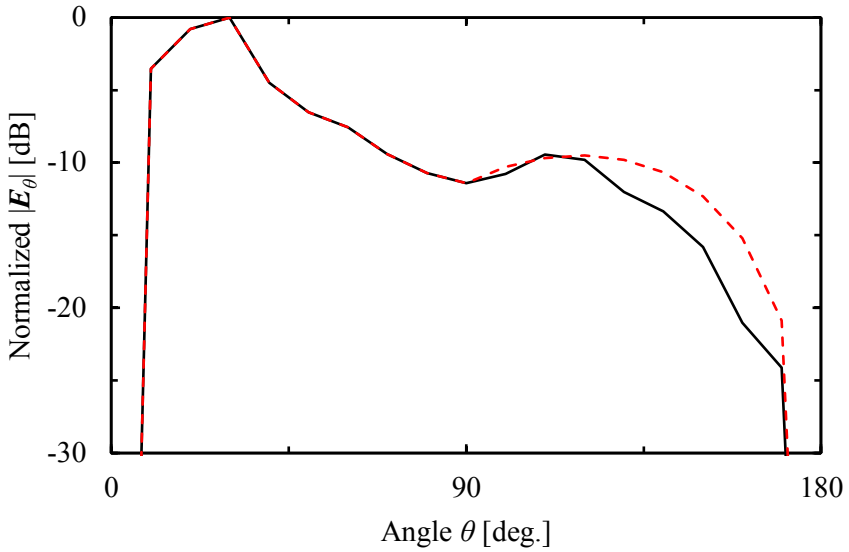

Figure 7.5: Compensated full spherical near-field distribution. The solid line represents the exact distribution and the dotted line is the reconstructed result.

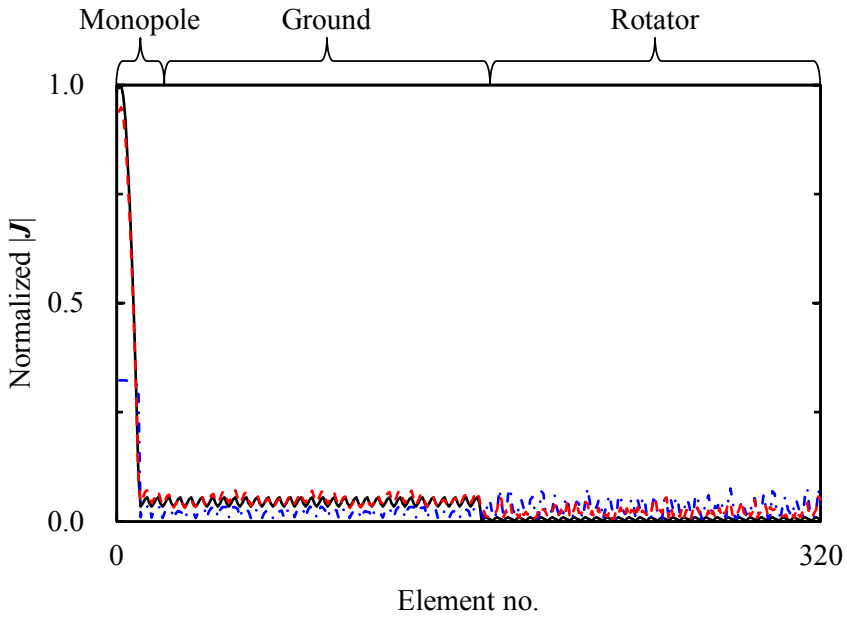

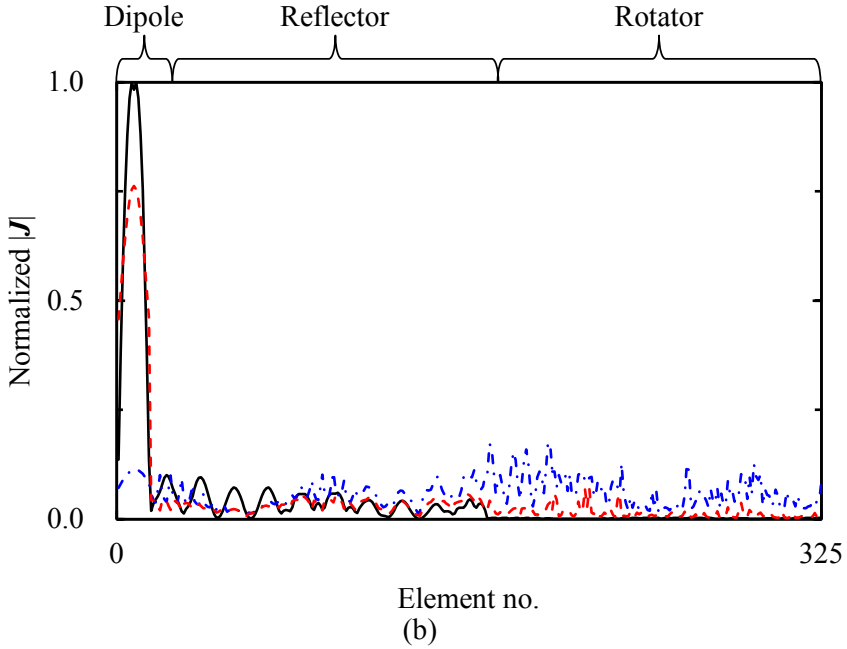

Figure 7.6: Reconstructed current distribution. (a) presents the monopole case and (b) presents the dipole with reflector case. The solid lines represent the exact distribution, the dotted lines are reconstructed results using proposed method, and the chain lines are reconstructed using conventional reconstruction technique.

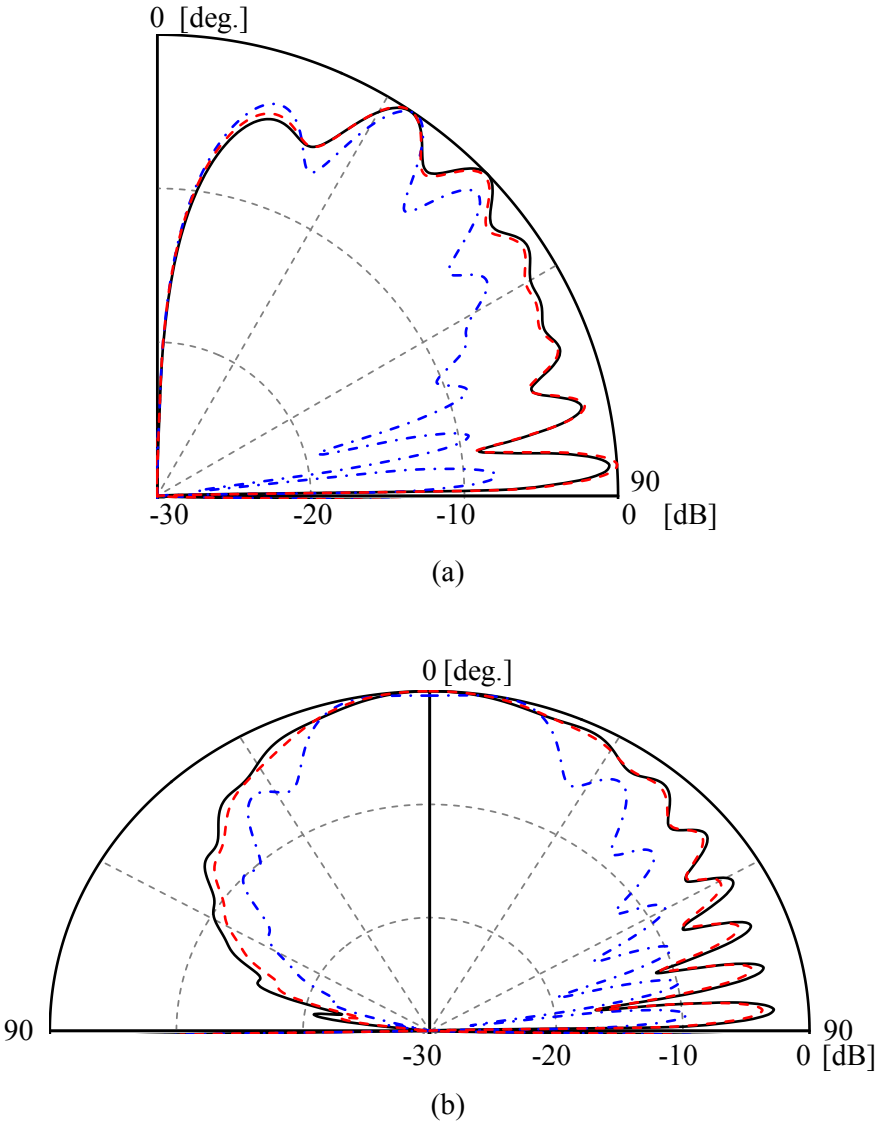

Figure 7.7: Estimated far-field pattern above the earth. (a) presents the monopole case and (b) presents the dipole with reflector case. The solid lines represent the theoretical pattern, the dotted line represent estimated pattern using the proposed method and the chain lines are estimated pattern using conventional reconstruction technique.

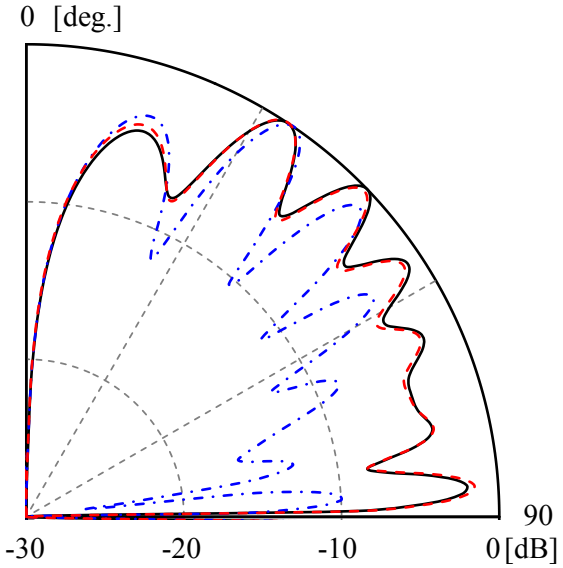

Figure 7.8: Estimated far-field pattern above the earth of monopole antenna. The solid lines represent the theoretical pattern, the dotted line represent estimated pattern using the proposed method and the chain lines are estimated pattern using conventional reconstruction technique.

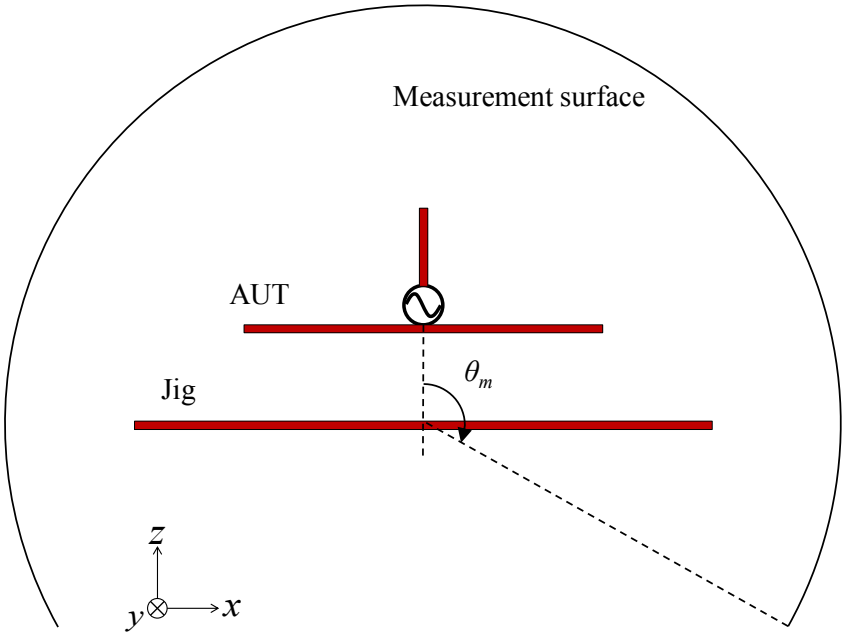

(a)

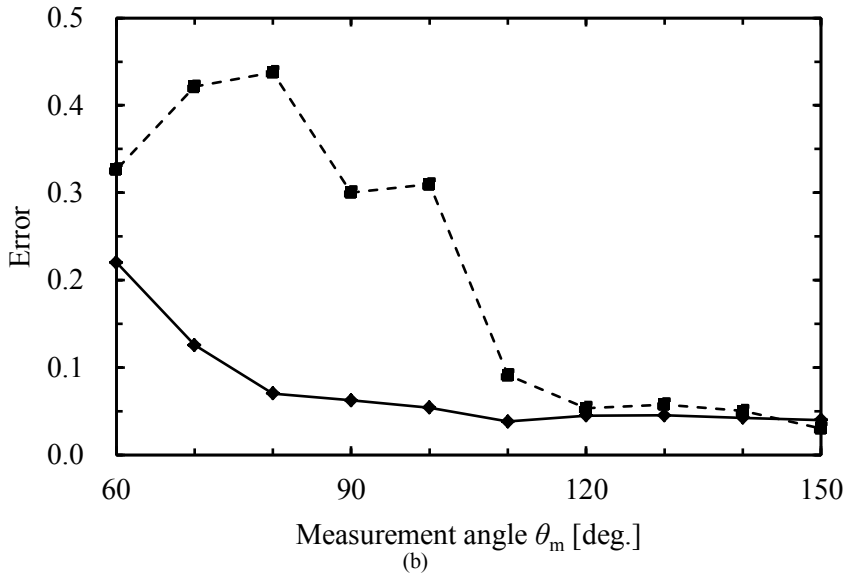

(b)

Figure 7.9: Definition of measurement angle θ_m and relation between the measurement angle θ_m and error of estimated far-field. (a) presents section of near-field sampling, (b) presents the effect of measurement angle. The solid line represents the case of using the proposed method and the dotted is conventional method case.

7.4 Experiment

We clarify the validity of the calculation using measurement near-field data in this section. It is impossible to measure the far-field pattern above the earth with the known electric constant to a make a reference pattern, from the viewpoint of measuring equipment. Therefore, in this section we reconstruct the current distribution on the AUT surface from the hemispherical near-field distribution by the proposed method and discuss the far-field in the free space obtained from reconstructed surface current as a reference value. As mentioned in the previous section, if the surface current distribution of AUT can be accurately obtained, it is a reasonable comparison since the far-field assuming the earth of arbitrary electric constant is accurately obtained by RCM.

The overview of measurement system is shown in Figure 7.10. We used a monopole antenna AUT. Measurement frequency is 2.5 GHz, and we place a copper plate under the AUT assuming a rotation jig. The AUT is rotating synchronously with the copper plate. The distance between the AUT and copper plate is 75 mm. The center of copper plate is placed on the origin, measurement radius is 600 mm, sampling interval is $\Delta\theta = \Delta\phi = 5°$. A standard dipole for 5 GHz is used as a non-resonant probe. Estimated far-field using measured electric field is shown in Figure 7.11. The reference pattern is far-field pattern of this measurement system when removed the copper plate. The level around the low elevation angle region of estimated pattern using the normal reconstruction method is much lower than the reference value. It can be inferred that the surface current distribution is not accurately obtained. The estimation accuracy is improved by applying the proposed method. It is considered that the current distribution on the AUT surface is also accurately obtained. Therefore, by applying the RCM to the reconstructed current distribution, we can estimate the far-field when the AUT is placed on an arbitrary earth.

The validity of the calculation in the previous chapter was proved. As mentioned above, it is possible to estimate the antenna far-field from the insufficient measurement near-field using the proposed method and it can be expected that the proposed method can be an effective technique to test antenna radiation characteristics in practical use condition.

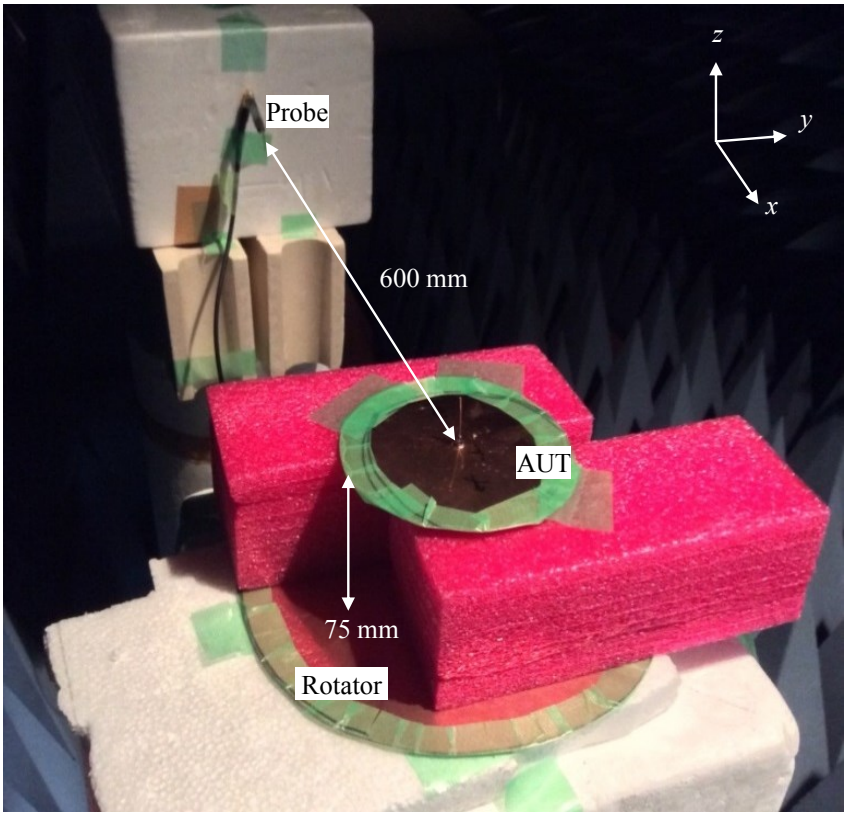

Figure 7.10: Measurement results.

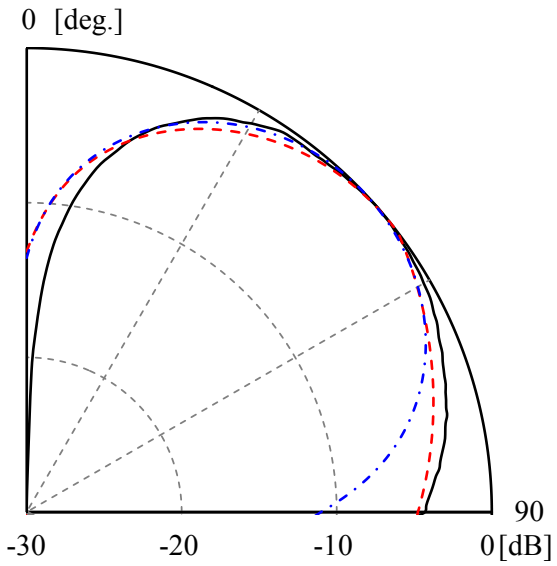

Figure 7.11: Estimated far-field pattern using measurement data. The solid line represents the theoretical pattern, the dotted line represents estimated pattern using the proposed method and the chain line are estimated pattern using conventional reconstruction technique.

7.5 Summary

The method for estimation of antenna far-field above the earth using hemispherical near-field distribution was proposed. The proposed method is composed from source reconstruction using hemispherical near-field and estimating far-field using the RCM. First, we mentioned that the surface current of the AUT cannot be reconstructed accurately because the near-field around the AUT can measure only the upper hemisphere due to the measurement equipment restriction, and the inverse problem becomes ill-posed condition. We showed that the accuracy of the reconstructed surface current distribution on the AUT surface can be improved by using the regenerated full-spherical near-field using a part of reconstructed current. In the proposed method, RCM was applied to the AUT surface current distribution reconstructed imaginary full-spherical near-field to estimate the far-field above the earth. It is clarified that the reconstruction accuracy of AUT surface current distribution was greatly improved by using the proposed method. In addition, we showed that the proposed method is not restricted by the value of electric constant of the earth, and we can estimate far-field above arbitrary earth. Furthermore, the validity of the calculation is demonstrated by experiments, and the fact that the proposed method is effective for evaluating the antenna radiation performance assuming actual use environment.

Reference

[1] K. Nishikawa and Y. Asano, "Vertical radiation patterns of mobile antenna in UHF band," *IEEE Trans., Vehicular Tech*., vol. 35, no. 2, May 1986.

[2] D. C. Chang and J. B. Wait, "Theory of a vertical tubular antenna located above a conducting half-space," *IEEE Trans., Antennas and Propag*., vol. AP-18, no. 2, pp. 182-188, Mar. 1970.

[3] R. Ehmann, B. Wagner and T. Weiland, "Farfield calculations for car antennas at different locations," *IEEE Trans., Magnetics*, vol. 33, no. 2, Mar. 1997.

[4] A. Sommerfeld, "Über die ausbreitung der wellen in der drahtlosen telegraphie," *Ann. Physik(4)*, 28, pp. 665, 1909.

[5] W. H. Wise, "Asymptotic dipole radiation formulas," *Bell System Tech. Journal*, Oct. 1929.

[6] T. K. Sarkar and A. Taaghol, "Near-field to near/far-field transformation for arbitrary near-field geometry utilizing an equivalent electric current and MOM," *IEEE Trans.. Antennas and Propag*., vol. 47, no. 3, pp. 566-573, March 1999.

[7] Y. Álvarez, F. L. Heras and M. R. Pino, "Reconstruction of equivalent currents distribution over arbitrary three-dimensional surfaces based on integral equation algorithms," *IEEE Trans., Antennas and Propag*., vol. 55, no. 12, pp. 3460-3468, Dec. 2007.

[8] J. L. A. Quijano and G. Vecchi, "Improved-accuracy source reconstruction on arbitrary 3-D surfaces," *IEEE Antennas and Wireless Propag. Lett*., vol. 8, pp. 1046-1049, Sept. 2009.

[9] D. Slater, *Near-field antenna measurements*, Artech House, 1991.

[10] FEKO Suite 7.1, http://www.feko.info/

[11] W. R. Scott and G. S. Smith, "Measured electrical constitutive parameters of soil as functions of frequency and moisture content," *IEEE Trans., Geosci. Remote Sensing*, vol. 30, no. 3, pp.621-623, May 1992.

8 Conclusion

In this dissertation, we focused on the near-field measurement of the electromagnetic source, and a new methodology of electromagnetic field analysis and estimation method based on the equivalent field principle and inverse problem analysis was presented.

Chapter 1 mentioned the background surrounding the electromagnetic measurement and measurement technique of electromagnetics especially near-field measurements.

Chapter 2 described the handling of the electromagnetic field in the space by the equivalent source theorem and the reconstruction method of the wave source distribution from the measured electromagnetic field by the inverse problem. This dissertation was numerical processed to measurement electromagnetic field according to the principle introduced in this chapter.

Chapter 3 proposed the fast far-field estimation method of electrically long antenna in compact measurement space. The presented method estimated far-field pattern on orthogonal cut plane from the linear equivalent electric current and circular current distribution. The equivalent electric current data was measured in reactive near-field region using a small loop probe. In the horizontal plane, the far-field pattern was calculated from circular equivalent electric and magnetic distribution approximating equivalent magnetic current with equivalent electric current. We confirmed the validity of the proposed method from the numerical simulation and measurements results. The noteworthy contribution of this chapter is that the proposed method was achieved the fast far-field estimation method by reduction of measurement data dimension. The method allowed directivity measurement accurately in a small space measurement in about a few minutes.

Chapter 4 further developed the contents of chapter 3, and described the electromagnetic field regeneration method in the non-measured area. It was shown that the proposed method corrects the radiation field from reconstructed partial source, regenerates the near-field distribution the same size as the AUT aperture. The linear array antenna with various distributions was taken up as an example of numerical analysis and the effectiveness of this method was shown. The noteworthy contribution of this chapter is possible to measure the far-field in the vertical plane of the linear array antenna by near field measurement in a quite small space. The proposed method was achieved the fast far-field estimation method by reduction of measurement area.

Chapter 5 proposed the method of decomposition inverse estimation for under interference wave conditions using dual surface. The proposed method could reconstruct the current unique to each equivalent surface to solve inverse problem using dual measurement surface distribution. The noteworthy contribution of this chapter was bringing the method for electromagnetic field elimination from contaminated distribution without prior information for each field. It is expected to realizing stable measurement under outdoor environment by applicable the proposed method in

future.

Chapter 6 proposed the method to compensate the measurement errors caused by misalignment of the probe and its jig. We had classified the cause of the positioning errors in measurement as random errors occurring at each measurement points due to minute misalignments of the probe; also we had classified depth errors occurring at each measurement surfaces as errors caused by improper setting of the probe jig. The random positioning error was eliminated by adding a low-pass filter in wavenumber space, and the depth positioning error is iteratively compensated based on the relative residual obtained in each plane. The validity of the proposed method was demonstrated by estimating the far-field patterns using the results from numerical simulation and was also demonstrated using measurements of probe-positioning errors. The noteworthy contribution of this chapter is a method that can self-correct errors that cannot avoid in near field measurements.

Chapter 7 proposed the far-field estimation method when an antenna is placed above the earth. The proposed method estimated far-field using current distribution on the antenna surface that is reconstructed from hemispherical near-field information. We mentioned that the surface current of the AUT cannot be reconstructed accurately because the near-field around the AUT can measure only the upper hemisphere due to the measurement equipment restriction, and the inverse problem becomes ill-posed condition. We showed that the accuracy of the reconstructed surface current distribution on the AUT surface can be improved by using the regenerated full-spherical near-field using a part of reconstructed current. In the proposed method, RCM was applied to the AUT surface current distribution reconstructed imaginary full-spherical near-field to estimate the far-field above the earth. It is clarified that the reconstruction accuracy of AUT surface current distribution was greatly improved by using the proposed method. In addition, we showed that the proposed method was not restricted by the value of electric constant of the earth, and we can estimate far-field above arbitrary earth. The noteworthy of this chapter is that brought a method to accurately estimate the behavior of the antenna in a practical environment.

Acknowledgements

I am deeply grateful to my supervisor, Professor Hiroyuki Arai for providing me this precious study opportunity as Ph.D student in his laboratory.

I would like to express my appreciation to the committee members of Professor Takehiko Adachi, Professor Toshihiko Baba, Associate Professor Koichi Ichige, and Associate Professor Nobuhiro Kuga.

Especially, I would like to offer my special thanks to Professor Toshikazu Hori, for his outstanding guide as a supervisor in University of Fukui undergraduate and master courses. Professor Hori gave me very keenly instruction from the basic knowledge of electromagnetism and the essential thinking in research. And also, I am deeply grateful to Professor Mitoshi Fujimoto, for his advice as an assistant supervisor in University of Fukui undergraduate and master courses. Professor Fujimoto gave me polite guidance on how to draw clear figures and know-how of presentation. I received from Professor Hori and Professor Fujimoto very valuable guidance.

I am thankful to Professor Nobuyoshi Kikuma and Profesor Kunio Sakakibara of Nagoya Institute of Technology for their insightful comments in joint seminar between laboratories of University of Fukui and Nagoya Institute of Technology, also they gave me warm encouragement when I going on to doctoral course. I appreciate also the kindness of Professor Keizo Cho of Chiba Institute of Technology, Dr. Masayuki Nakano, Associate Professor Naobumi Michishita of National Defense Academy and Associate Professor Takuji Tachibana of University of Fukui for their advice when I going on to doctoral course. I am also indebt to Dr. Satoru Kurokawa and Dr. Masanobu Hirose of National Institute of Advanced Industrial Science and Technolog whose comments made enormous contribution to my work. I would like to thank everyone at NAZCA Ltd., Huawei Co. Ltd. and all of Microwave Factory Co. Ltd. who provided measurement data.

I would like to thank JSPS for a grant that made it possible to complete this study. This work was supported by JSPS KAKENHI Grant Number 17J11623.

Associate Professor Yasutaka Murakami of Tokyo University of Agriculture and Technology, and Associate Professor Ryuji Kuse of Kumamoto University give me constructive comments and warm encouragement. Mr. Koushi Amano, Mr. Shinya Ito, Mr. Kazuhiro Uchida, Ms. Hiroko Ohara, Mr. Kenichi Yamamoto and Me. Toshihiro Watanabe of 11th grader of Hori-Fujimoto Lab. offered their precious friendship to me and also honor 11th grader of Hori-Fujimoto Lab. Member Mr. Homare Morita supported me spiritually. During my work at Yokohama National University, Associate Professor Rohani Bakar, Dr. Takuya Ookura and Akira Kon offered me insightful comments and suggestions.

Finally, most of all I extend my gratitude to my beloved family for their various spiritual support and warm encouragement.

Publications

Related Works

Journal Paper

[1] Yoshiki Sugimoto and Hiroyuki Arai, “A method of decomposition inverse estimation for surface current under interference wave conditions using dual surface electromagnetic field,” *IEICE Trans. Commun*., vol. J100-B, no. 9, pp.817-825, Sept. 2017 (in Japanese).

International Conference

[1] Yoshiki Sugimoto, Eriko Ohashi and Hiroyuki Arai, “Far-field pattern estimation on long array antennas by 1D equivalent electric current distribution,” *Proc. 2015 IEEE International Conference on Antenna Measurement & Applications*, Chiang Mai, Thailand, Dec. 2015.

[2] Yoshiki Sugimoto and Hiroyuki Arai, “Adjacent point thinning sampling for cylindrical far-field estimation method,” *Proc. 2016 IEEE International Workshop on Electromagnetics*, Nanjing, China, May 2016.

[3] Yoshiki Sugimoto and Hiroyuki Arai, “Decomposition reconstruction of internal source using dual surface electromagnetic field,” *Proc. 2017 IEEE International Symposium on Antennas and Propagation*, San Diego, USA, July 2017.

[4] Yoshiki Sugimoto and Hiroyuki Arai, “Dual surface source reconstruction on arbitrary shape for interference elimination,” *Proc. 39th Annual Meeting and Symposium of the Antenna Measurement Techniques Association*, Atlanta, USA, Nov. 2017.

[5] Yoshiki Sugimoto and Hiroyuki Arai, “Far-field estimation of antennas above the earth using hemispherical source reconstruction,” *Proc. 2017 International Symposium on Antennas and Propagation*, Phuket, Thailand, Nev. 2017.

Technical Report

[1] Yoshiki Sugimoto, Hiroyuki Arai, Toshiyuki Maruyama, Masahiko Nasuno, Masanobu Hirose and Satoru Kurokawa, “Far-field estimation method of array antenna by simple near-field measurement,” *IEICE Technical Report*. AMT2015-16, Dec. 2015 (in Japanese).

[2] Yoshiki Sugimoto and Hiroyuki Arai, “Decomposition reconstruction of internal source under interference wave conditions using dual surface electromagnetic field,” *IEICE Technical Report*, AMT2016-3, Dec. 2016 (in Japanese).

[3] Yoshiki Sugimoto and Hiroyuki Arai, “Far-field estimation of antenna above the earth by source reconstruction from hemispherical near-field,” *IEICE Technical Report*, AP2017-81, Aug. 2017 (in Japanese).

Domestic Conference

[1] Yoshiki Sugimoto and Hiroyuki Arai, “Estimation method of spherical far-field for large array antenna using cylindrical current distribution,” *IEICE Society Conference*, B-1-157, Sept. 2015 (in Japanese).

[2] Yoshiki Sugimoto and Hiroyuki Arai, “Cylindrical far-field estimation method by adjacent point thinning sampling,” *IEICE General Conference*, B-1-224, Mar. 2016 (in Japanese).

[3] Yoshiki. Sugimoto and Hiroyuki Arai, “Decomposition reconstruction of internal source using dual surface electromagnetic field,” *IEICE General Conference*, BI-1-6, Mar. 2017 (in Japanese).

[4] Yoshiki Sugimoto and Hiroyuki Arai, “Far-field estimation by planar phaselss near-field measurement with positioning error compensation of measurement surfaces,” *IEICE Society Conference*, B-1-158, Sept. 2017 (in Japanese).

The Other Works

Journal Paper

[1] Yoshiki Sugimoto, Toshikazu Hori and Mitoshi Fujimoto, “Dual-band dipole antenna with dual flat reflectors,” *IEICE Trans. Commun*., vol. J98-B, no. 7, pp.672-680, July 2015 (in Japanese).

[2] Yoshiki Sugimoto, Toshikazu Hori, Mitoshi Fujimoto and Yoshio Ebine, “Dipole antenna with side reflector for utilizing orthogonal polarization,” *IEICE Trans. Commun*., vol. J99-B, no. 2, pp.45-52, Feb. 2016 (in Japanese).

International Conference

[1] Yoshiki Sugimoto, Toshikazu Hori and Mitoshi Fujimoto, “Dual-band dipole antenna with dual flat reflectors,” *Proc. 2014 International Symposium on Antennas and Propagation*, Kaohsiung, Taiwan, Dec. 2014.

[2] Yoshiki Sugimoto Toshikazu Hori, Mitoshi. Fijimoto, Shinya Iwanaga and Satoshi Hori, “Broadband characteristics of T-shaped planar monopole antenna,” *Proc. 2015 International Workshop on Antenna Technology,* Seoul, Korea, March 2015.

Technical Report

[1] Yoshiki Sugimoto, Toshikazu Hori and Mitoshi Fujimoto, “Design of dual-band dipole antenna with dual flat reflectors,” *IEICE Technical Report*, AP2014-12, Apr. 2015 (in Japanese).

[2] Yoshiki Sugimoto, Toshikazu Hori and Mitoshi Fujimoto, “Dual-band dipole antenna with dual

flat reflectors," *Proc. 2014 Asian Workshiop on Antennas and Propagation*. Kanazawa, Japan, May 2014.

[3] Yoshiki Sugimoto, Toshikazu Hori, Mitoshi Fujimoto and Yoshio Ebine, "Design method of dipole antenna with metal reflector for utilizing orthogonal polarization," *IEICE Technical Report*, AP2014-104, Sept. 2015 (in Japanese).

Domestic Conference

[1] Yoshiki Sugimoto, Toshikazu Hori and Mitoshi Fujimoto, "Broadband characteristics of rectangular planar monopole antenna," *IEICE General Conference*, B-1-115, March 2013 (in Japanese).

[2] Yoshiki Sugimoto, Toshikazu Hori and Mitoshi Fujimoto, "Broadband characteristics of cross triangular planar monopole antenna," *IEICE Society Conference*, B-1-168, Sept. 2013 (in Japanese).

[3] Yoshiki Sugimoto, Toshikazu Hori and Mitoshi Fujimoto, "Broadband orthogonal planar monopole antenna with triangular feeding element," *Joint conference of Hokuriku chapters of Electrical Societies 2013*, C-28, Sept. 2013 (in Japanese).

[4] Yoshiki Sugimoto, Toshikazu Hori and Mitoshi Fujimoto, "Dual band dipole antenna with two layer flat recrector," *IEICE General Conference*, B-1-156, March 2014 (in Japanese).

[5] Yoshiki Sugimoto, Toshikazu Hori and Mitoshi Fujimoto, "Dipole antenna with side and dual reflectors," *IEICE Society Conference*, B-1-32, Sept. 2014 (in Japanese).

[6] Yoshiki Sugimoto, Toshikazu Hori and Mitoshi Fujimoto, "Dual-band dipole antenna with dual structure side reflectors for orthogonal polarization," *IEICE General Conference*, B-1-148, March 2015 (in Japanese).